

UNCLASSIFIED

AD NUMBER: AD0842604

LIMITATION CHANGES

TO:

Approved for public release; distribution is unlimited.

FROM:

Distribution authorized to US Government Agencies and their Contractors; Export Control; 1 Jan 1968. Other requests shall be referred to Space and Missile Systems Organization, Norton AFB, CA, 92408.

AUTHORITY

Per SAMSO (AFSC) ltr dtd 28 Feb 1972

AD842604

FINAL REPORT
MATERIAL RESPONSE STUDIES (MARS I)

Volume II

HIGH STRAIN-RATE RESPONSE OF THREE
HEAT-SHIELD MATERIALS AT
ELEVATED TEMPERATURES

by
S. G. Babcock
R. D. Perkins

Materials & Structures Laboratory
Manufacturing Development
General Motors Corporation

Technical Report SAMSO TR 68-71-Vol. II
1968, January

Prepared For
Space and Missile Systems Organization
Deputy for Ballistic Missile Reentry Systems
Air Force Systems Command
Norton Air Force Base, California
Contract No. FO4694-67-C-0033

This document may be further distributed by any holder only
with specific prior approval of Space and Missile Systems
Organization (██)

(SMSD) L.A. AFS, Cal 90045

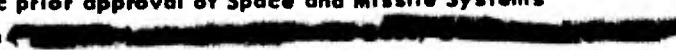
FINAL REPORT
MATERIAL RESPONSE STUDIES (MARS I)

Volume II

**HIGH STRAIN-RATE RESPONSE OF THREE
HEAT-SHIELD MATERIALS AT
ELEVATED TEMPERATURES**

by
S. G. Babcock
R. D. Perkins

Materials & Structures Laboratory
Manufacturing Development
General Motors Corporation

This document may be further distributed by any holder only
with specific prior approval of Space and Missile Systems
Organization 

This report was prepared by the Applied Mechanics Section of the Materials and Structures Laboratory, Manufacturing Development, General Motors Technical Center, Warren, Michigan, under Air Force Contract F04694-67-C-0033. The work was administered by the Air Force Space and Missile Systems Organization, Air Force Systems Command, with Major N. J. Azzarita as technical administrator. Mr. R. B. Mortensen, Mr. R. A. Needham, Dr. F. A. Field and Dr. W. Barry of the Aerospace Corporation served as principal technical monitors for the Air Force.

Because of the different types of work performed in this study, the report is divided into seven separately bound volumes listed below. The present volume is one of these parts.

- Volume I: Summary
- Volume II: High Strain-Rate Response of Three Heat Shield Materials at Elevated Temperatures
- Volume III: Development of Multiaxial Stress High Strain Rate Techniques
- Volume IV: Dynamic Mechanical Properties at Ablative Temperatures - Techniques
- Volume V: Dynamic Behavior of Polymers and Composites
- Volume VI: Mechanical Properties of Beryllium at High Strain Rates
- Volume VII: Ablation Test Specimen Environment at High Temperature

The work was performed under the supervision of Dr. C. J. Maiden. Program Manager and Principal Investigator was Mr. S. J. Green. Other project scientists included:

S. G. Babcock, Dr. A. Kumar, R. G. Kumble, J. D. Leasia, W. F. Dais, R. D. Perkins, F. L. Schierloh.

This report is UNCLASSIFIED. This document may be further distributed by any holder only with specific prior approval of Space and Missile Systems Organization (~~SMYSE~~), ~~Wright Air Force Base, Dayton, Ohio 45433.~~

This technical report has been reviewed and is approved.

Nicholas J. Azzarita
Major, USAF
Project Officer
SAMSO/SMYSE

ABSTRACT

This report presents the results of an experimental study to determine the high strain-rate behavior of typical ablative reentry-vehicle heat shield materials at temperatures up to 600°F. Characterizations of quartz, silica, and carbon phenolic are presented where the effect of rate of loading, temperature, direction of loading to the fiber layup, and specimen size were investigated. In addition the material behavior after two types of impulsive loadings, a uniaxial strain preshock and a uniaxial stress preload, is presented.

TABLE OF CONTENTS

	Page
FOREWORD	ii
ABSTRACT	iii
INTRODUCTION	1
SECTION I STRAIN-RATE BEHAVIOR AT ELEVATED TEMPERATURE	4
Loading Normal and Parallel to Fiber Layup	5
Loading at Intermediate Fiber Layup Angles	31
SECTION II STRAIN-RATE BEHAVIOR AFTER IMPULSIVE LOADING	45
Uniaxial-Strain Preshock	45
Uniaxial-Stress Preload	58
SUMMARY	72
REFERENCES	74
APPENDIX A - MATERIAL DESCRIPTION	77
APPENDIX B - EQUIPMENT DESCRIPTION	80
APPENDIX C - STATISTICAL TREATMENT	89
APPENDIX D - PRELIMINARY DATA ON TWO "3-D" QUARTZ ANTENNA WINDOW MATERIALS	93
DD FORM 1473 - DOCUMENT CONTROL DATA - R & D	103

LIST OF ILLUSTRATIONS

Figure	Title	Page
1	Temperature Profile in Quartz Phenolic	6
2	Compression Tests on Quartz Phenolic, Layup Normal to Loading Axis - Stress vs. Temperature	8
3	Compression Tests on Quartz Phenolic, Layup Parallel to Loading Axis - Stress vs. Temperature	9
4	Compression Tests on Quartz Phenolic, Layup Normal to Loading Axis - Stress vs. Strain	10
5	Compression Tests on Quartz Phenolic, Layup Parallel to Loading Axis - Stress vs. Strain	11
6	Tension Tests on Quartz Phenolic, Layup Parallel to Loading Axis - Stress vs. Strain	12
7	Tension Tests on Quartz Phenolic, Layup Normal to Loading Axis - Stress vs. Strain	13
8	Compression Tests on Silica Phenolic, Layup Normal to Loading Axis - Stress vs. Strain	15
9	Compression Tests on Silica Phenolic, Layup Parallel to Loading Axis - Stress vs. Strain	16
10	Tension Tests on Silica Phenolic, Layup Parallel to Loading Axis - Stress vs. Strain	17
11	Tension Tests on Silica Phenolic, Layup Normal to Loading Axis - Stress vs. Strain	18
12	Compression Tests on Carbon Phenolic, Layup Normal to Loading Axis - Stress vs. Strain	21

Figure	Title	Page
13	Compression Tests on Carbon Phenolic, Layup Parallel to Loading Axis - Stress vs. Strain	22
14	Tension Tests on Carbon Phenolic, Layup Parallel to Loading Axis - Stress vs. Strain	23
15	Size Effect Study on Quartz Phenolic in Compression, Layup Normal to Loading Axis	25
16	Size Effect Study on Quartz Phenolic in Compression, Layup Parallel to Loading Axis	26
17	Size Effect Study on Quartz Phenolic in Tension, Layup Parallel to Loading Axis	27
18	Size Effect Study on Quartz and Carbon Phenolic in Tension, Layup Normal to Loading Axis	28
19	Tensile Specimen Schematic	29
20	Compressive Behavior of Quartz Phenolic at Various Layup Angles - Fracture Stress vs. Layup Angle	35
21	Tensile Behavior of Quartz Phenolic at Various Layup Angles - Fracture Stress vs. Layup Angle	36
22	Tensile Behavior of Quartz Phenolic at Various Layup Angles - Fracture Strain vs. Layup Angle	37
23	Stiffness Behavior of Quartz Phenolic at Various Layup Angles - Initial Modulus vs. Layup Angle	39
24	Compressive Behavior of Quartz Phenolic at Various Strain Rates - Fracture Stress vs. Strain Rate	40
25	Compressive Behavior of Quartz Phenolic at Various Strain Rates - Initial Modulus vs. Strain Rate	41

Figure	Title	Page
26	Compressive Strain Rate Sensitivity of Quartz Phenolic at Various Layup Angles	42
27	Photograph of Fractured Quartz Phenolic Compression Specimens	43
28	Schematic Diagram of Preshock Experimental Technique	46
29	Preshock Target and Impactor Components	48
30	Photograph of Experimental Arrangement for Preshock	50
31	Testing of Preshocked Specimens	51
32	Photomicrograph Showing Cracks in Resin Matrix in Preshocked Quartz Phenolic	54
33	Diagram of Stepped Release Wave in Target - Impactor System with Mismatched Impedances	57
34	Prefracture Damage Study on Quartz Phenolic, Compressive Loading Normal to Layup - 72°F	61
35	Prefracture Damage Study on Quartz Phenolic, Compressive Loading Parallel to Layup - 72°F	62
36	Prefracture Damage Study on Quartz Phenolic, Compressive Loading Normal to Layup - 600°F	64
37	Prefracture Damage Study on Quartz Phenolic, Compressive Loading Parallel to Layup - 600°F	65
38	Prefracture Damage Study on Quartz Phenolic, Tensile Loading Parallel to Layup - 600°F	66
39	Photomicrographs of Quartz Phenolic After Loading in Compression Normal to Fiber Layup	67
40	Photomicrographs of Quartz Phenolic After Loading in Compression Parallel to Fiber Layup	68

Figure	Title	Page
A-1	Photomicrographs of Quartz Phenolic	79
B-1	Quasi-Static Testing Machine	81
B-2	Medium Strain-Rate Machine	82
B-3	Hopkinson Bar Setup	85
B-4	Hopkinson Bar Tension Device	85
D-1	Photograph of 3-D Quartz/Ethyl Silicate	94
D-2	Compression Tests on 3-D Quartz/Ethyl Silicate - 72°F	96
D-3	Compression Tests on 3-D Quartz/Teflon-72°F	98
D-4	Schematic of 3-D Weave	100

Table	LIST OF TABLES	Page
I	Quartz Phenolic - Fiber Layup Parallel to Specimen Axis	52
II	Quartz Phenolic - Fiber Layup Normal to Specimen Axis	53
C-I	"Student T Distribution"	92

INTRODUCTION

Design of reentry vehicles requires the knowledge of the high strain-rate behavior of candidate heat shield and structural materials. Strain rates up to $10 - 10^2$ /second are produced under blast loading and as high as $10^5 - 10^8$ /second under shock loading conditions. Since little or no high strain-rate data exist for the newest candidate materials, techniques for characterizing these materials at high strain rates must be developed.

The objective of this program, MARS Task 2, was to extend and continue work initiated under previous defense contracts (1, 2, 3). This extension called for uniaxial-stress tensile and compressive characterization of candidate materials at strain rates from 10^{-3} to about 10^3 /second at temperatures up to about 600°F. In this study, techniques were developed to determine the effect of heating rate/time at temperature. Some understanding had been advanced previously (2), but only quantitative results were known. Techniques for conducting very high rate tensile tests ($>10^2$ /second) were also developed. Tensile strain measuring techniques were developed to accurately and reliably determine strain at low and intermediate strain rates and at elevated temperatures.

The inhomogeneity and anisotropy of the heat shield composites must be evaluated for design purposes. In this study sample size was considered, extending previous investigations (3), in order to assess the effect of the inhomogeneity,

or size effect. Investigations were performed with the load applied parallel and normal to the fiber layup as well as intermediate angles to the layup to evaluate the material anisotropy. The obtained results were compared to analytical calculations. Hopefully these results will provide an understanding of composite materials under generalized loading conditions.

The objective also called for extending to elevated temperatures the investigations on materials preconditioned with an impulsive load⁽³⁾, either a uniaxial-strain preshock or a uniaxial-stress preload. Techniques were developed to perform uniaxial-strain preshocks at elevated temperature and for separating the effects of the shock from those from the thermal cycle. Techniques were also developed to load a specimen in uniaxial stress and stop the test at some precise point just prior to fracture, and then reload to fracture without undergoing a thermal cycle.

Although the primary purpose of this task was to study the high strain-rate response of candidate materials, a major fallout is the evaluation of the reliability of fabrication techniques for composite materials. Indeed in some cases it was discovered that fabrication techniques were at a stage where material reliability was so poor that strength scatter far overshadowed time dependent effects such as strain rate temperature and anisotropy. On this basis, vehicle design would have to rely on highly "degraded" material properties to produce a reliable vehicle.

The outline of this report is similar to previous results.⁽³⁾ Where necessary, results from the initial work were included in this report for clarity. Appendix A describes the test

materials used in these studies. Appendix B describes the equipment used to perform the tests. The derivation and explanation of the statistical approach used to establish confidence intervals on the test results is found in Appendix C. Appendix D contains the results of a limited room temperature compression characterization of two 3-dimensional weave antenna-window materials.

SECTION I
STRAIN-RATE BEHAVIOR AT ELEVATED TEMPERATURE

The high strain-rate characterization presented here is an extension to elevated temperatures of data reported in References 3 and 4. The data from the present study are presented with the room temperature results as necessary for clarity and comparison.

The following heat shield composite materials are characterized in this section:

- Quartz Phenolic (Astroquartz)
- Silica Phenolic (Astrosil)
- Carbon Phenolic (RAD 6300)

Each of these materials is completely described in Appendix A.

Material characterization consists of uniaxial-stress tension and compression test results at strain rates from 10^{-3} to 10^3 /second and at temperatures from 72°F to 600°F. Each material is characterized in two orthogonal loading directions, normal and parallel to the fiber layup. The effect of specimen size on observed material properties is also presented in order to assist in extending controlled laboratory data to bulk material behavior. Finally, a complete study of the behavior of quartz phenolic at intermediate fiber layup angles is presented where test results are compared to an existing phenomenological theory.

The equipment used to perform the tests is described in Appendix B. Special techniques were developed to perform some of the tests and are fully described.

In order to understand and interpret the elevated temperature test results, the effect of heating rate and time-at-temperature was studied. It is well known that typical ablation heat shield materials such as quartz, silica, and carbon phenolic have relatively low thermal conductivities (compared to most metals). In order to determine the optimum heating rate for the test specimens in this study, a series of tests was conducted to measure the thermal gradient produced in the materials used in this study during heat up to test temperature. Specimens (0.375 inch diameter by 0.50 inch long) were inserted into the Medium Strain-Rate Machine radiant oven, described in Appendix B, and thermocouples were inserted at various locations in each test sample. As each sample was brought up to test temperature, temperature as a function of time was recorded for each thermocouple location. A typical time-temperature plot is shown in Figure 1. It shows that for a $10^{\circ}\text{F}/\text{second}$ heat up on quartz phenolic, nearly a 200°F maximum temperature gradient exists in the sample. This profile was similar for silica and carbon phenolic. It was found that at heating rates below about $1^{\circ}\text{F}/\text{second}$, maximum temperature gradients were reduced to near 10°F . This then was the approximate heating rate used in this entire study. Once at the test temperature, hold times were kept to less than 3 minutes in order to minimize the effect of time-at-temperature on the chemical decomposition of the composite.

LOADING NORMAL AND PARALLEL TO FIBER LAYUP

Material Characterization

Quartz Phenolic: Strain-rate characterization on quartz phenolic has been reported for room temperature^(1, 3, 4, 5) and elevated temperature⁽²⁾ testing. Each of the referenced

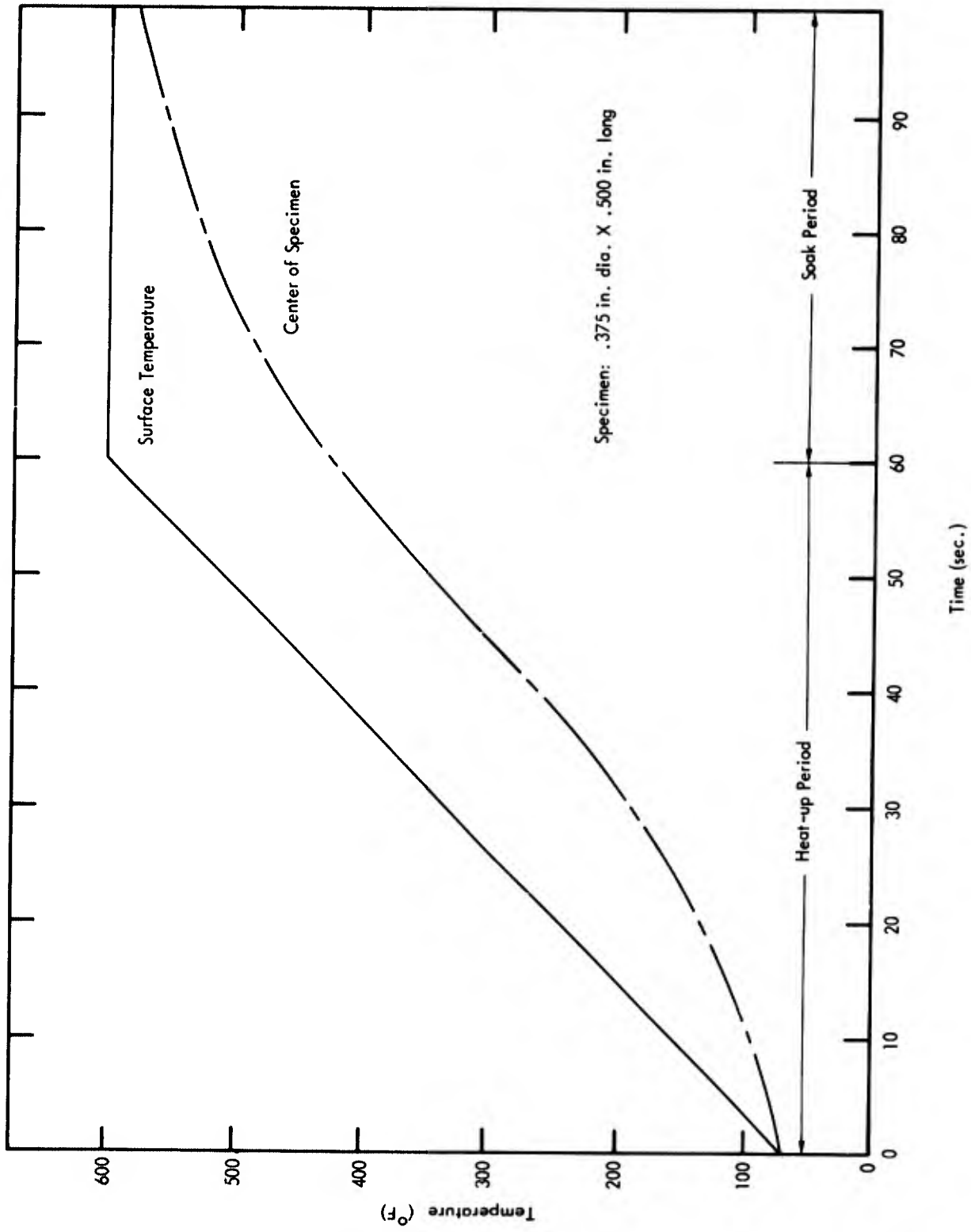


Figure 1 Temperature Profile in Quartz Phenolic

documents contains test data on different lots of material. Although characterizing another lot of quartz phenolic, this report attempts to draw on the other test results and form general observed trends. Each of the lots of quartz phenolic referenced was purchased and manufactured to identical specifications. The material purchased for this study was the first lot in the series to show drastic deviation in mechanical properties from the other lots. While the quartz phenolic in the past studies and all but one block of material used for this study had a nominal density of 1.77 gm/cm^3 , one block of this study's material had a density of 1.66 gm/cm^3 . A check of the compressive fracture strength normal to the fiber layup (at $\sim 10^{-3}$ /second) showed approximately 66,000 psi for the 1.66 gm/cm^3 block, while the 1.77 gm/cm^3 material average showed approximately a 106,000 psi fracture strength. This lower density block was not used to characterize quartz phenolic in this study.

Figures 2 through 7 show the dynamic response of quartz phenolic in uniaxial-stress compression and tension from room temperature to 600°F . Statistical confidence intervals have been determined for average fracture stress as a result of combining test results from this study and previous work. Appendix C contains computational details for determining the confidence intervals. Figures 2 and 3 show the dynamic stress versus temperature behavior of quartz phenolic when loaded in compression normal and parallel to the fiber layup. A minimum in fracture stress is observed at 400°F at all strain rates from 10^{-3} to 10^3 /second for loadings normal to the layup (Figure 2). This behavior is due to the change in fracture mode between the 400°F and 600°F tests. At temperatures up to 400°F failure is by shear where the phenolic matrix controls the nucleation of cracks to cause failure.

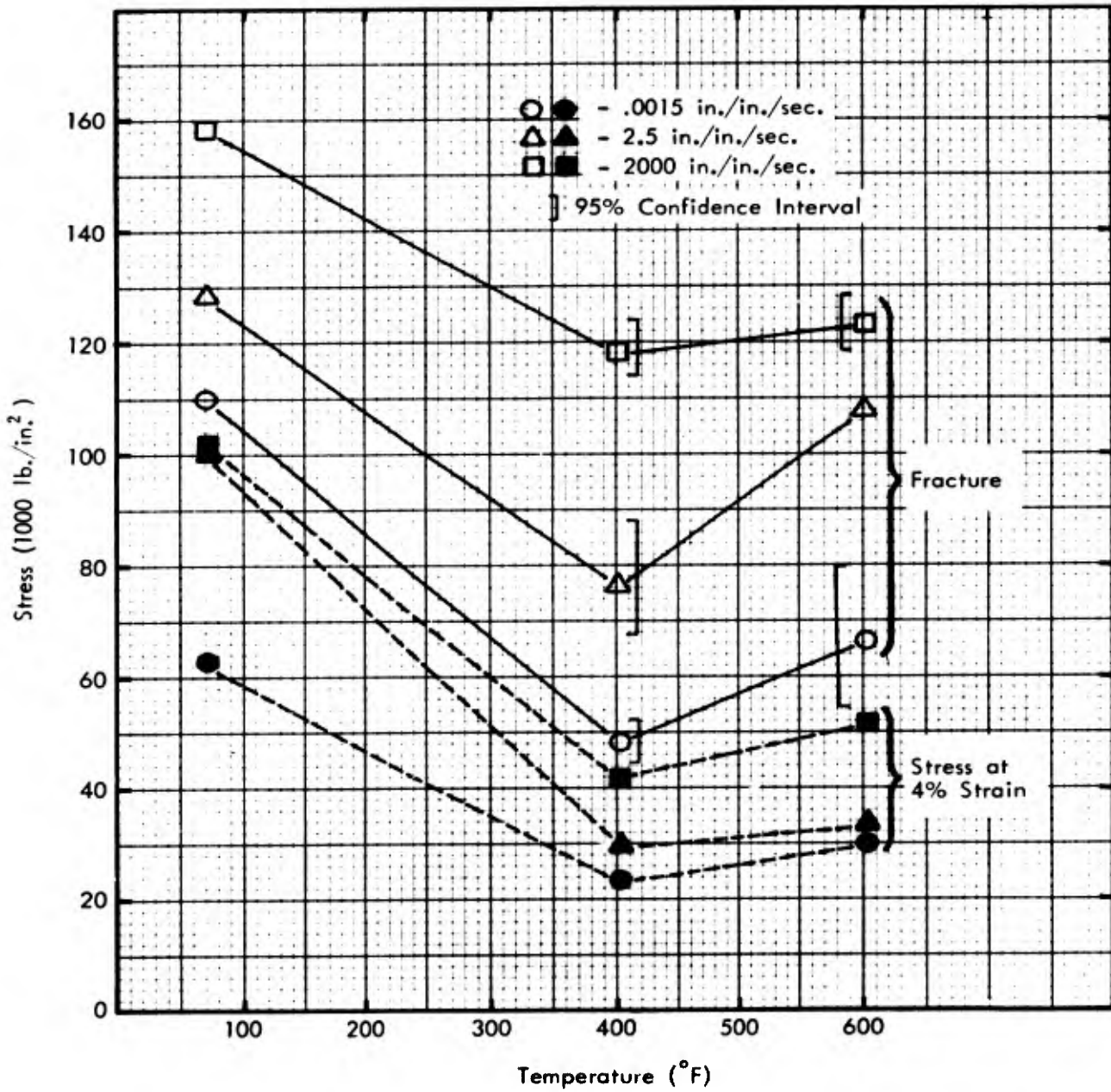


Figure 2 Compression Tests on Quartz Phenolic, Layup Normal to Loading Axis - Stress vs. Temperature

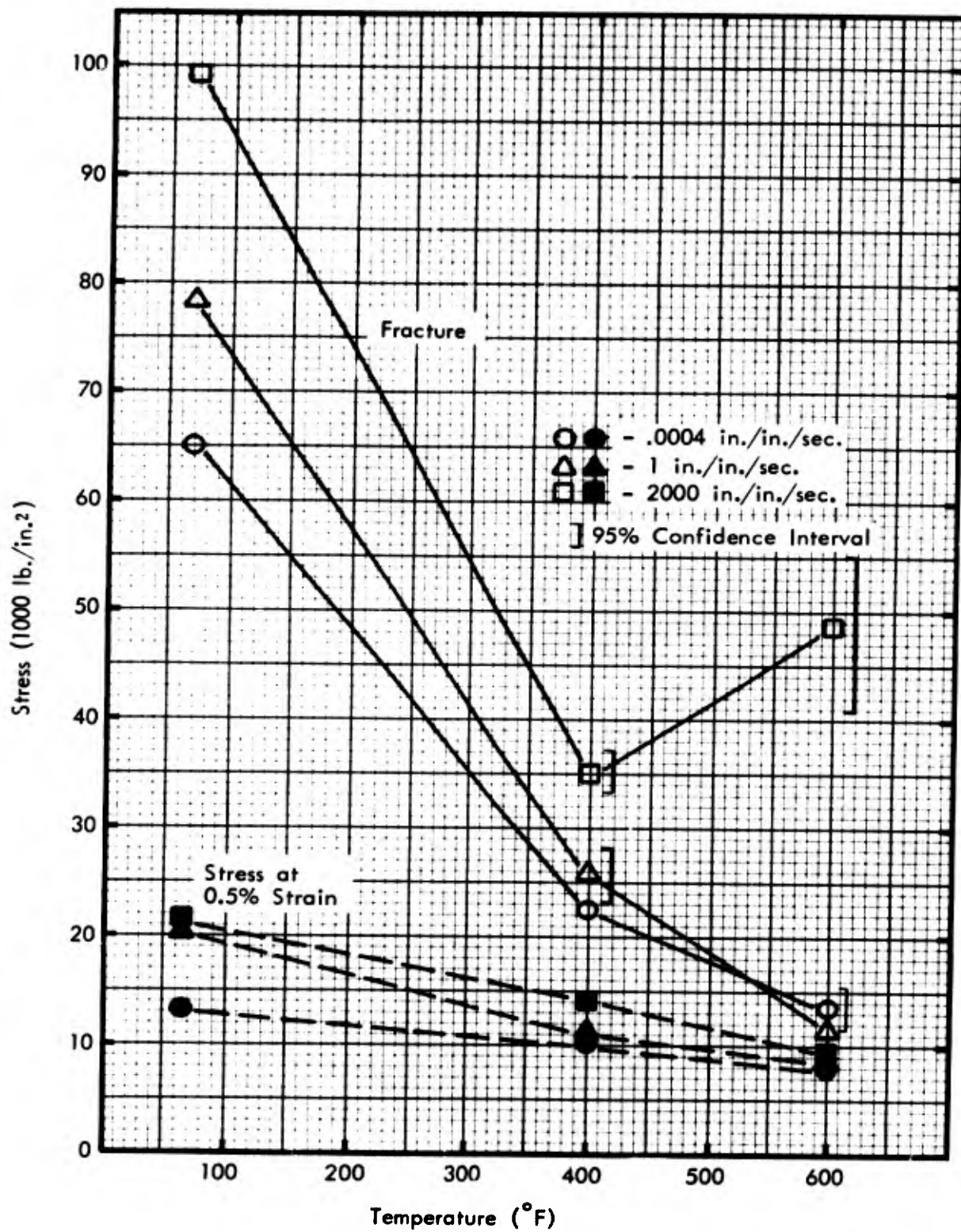


Figure 3 Compression Tests on Quartz Phenolic, Layup Parallel to Loading Axis - Stress vs. Temperature

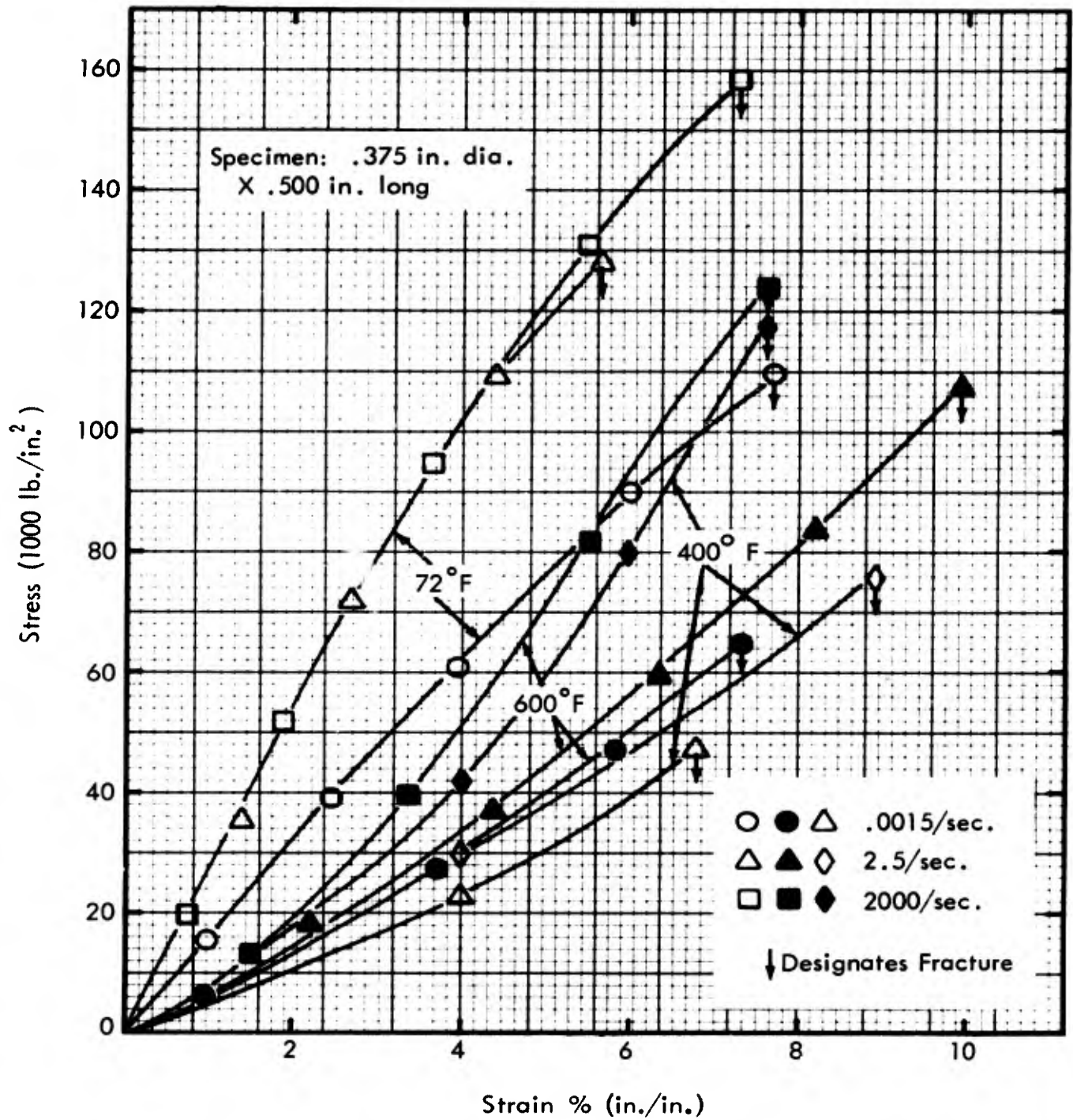


Figure 4 Compression Tests on Quartz Phenolic, Layup Normal to Loading Axis - Stress vs. Strain

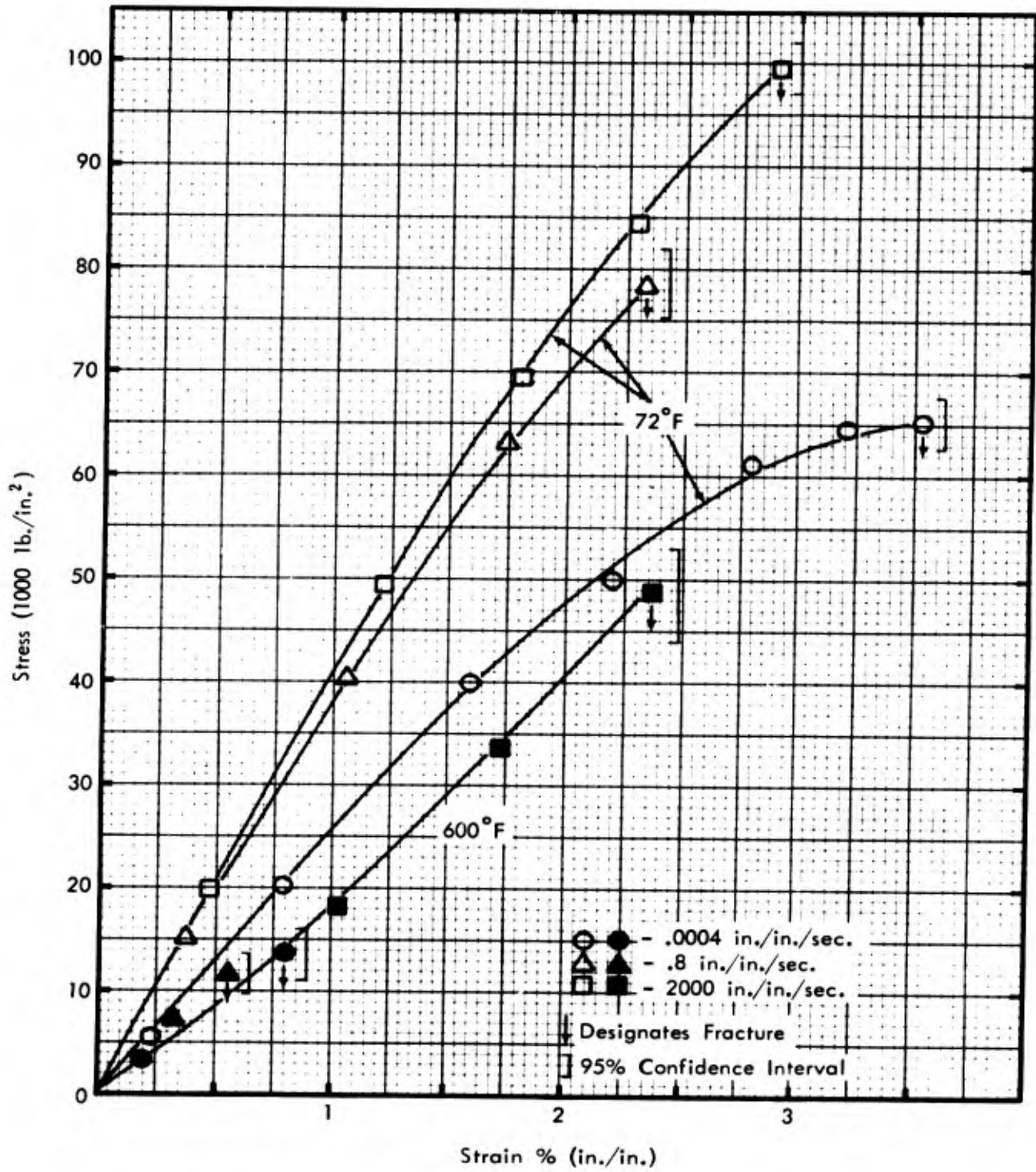


Figure 5 Compression Tests on Quartz Phenolic, Layup Parallel to Loading Axis - Stress vs. Strain

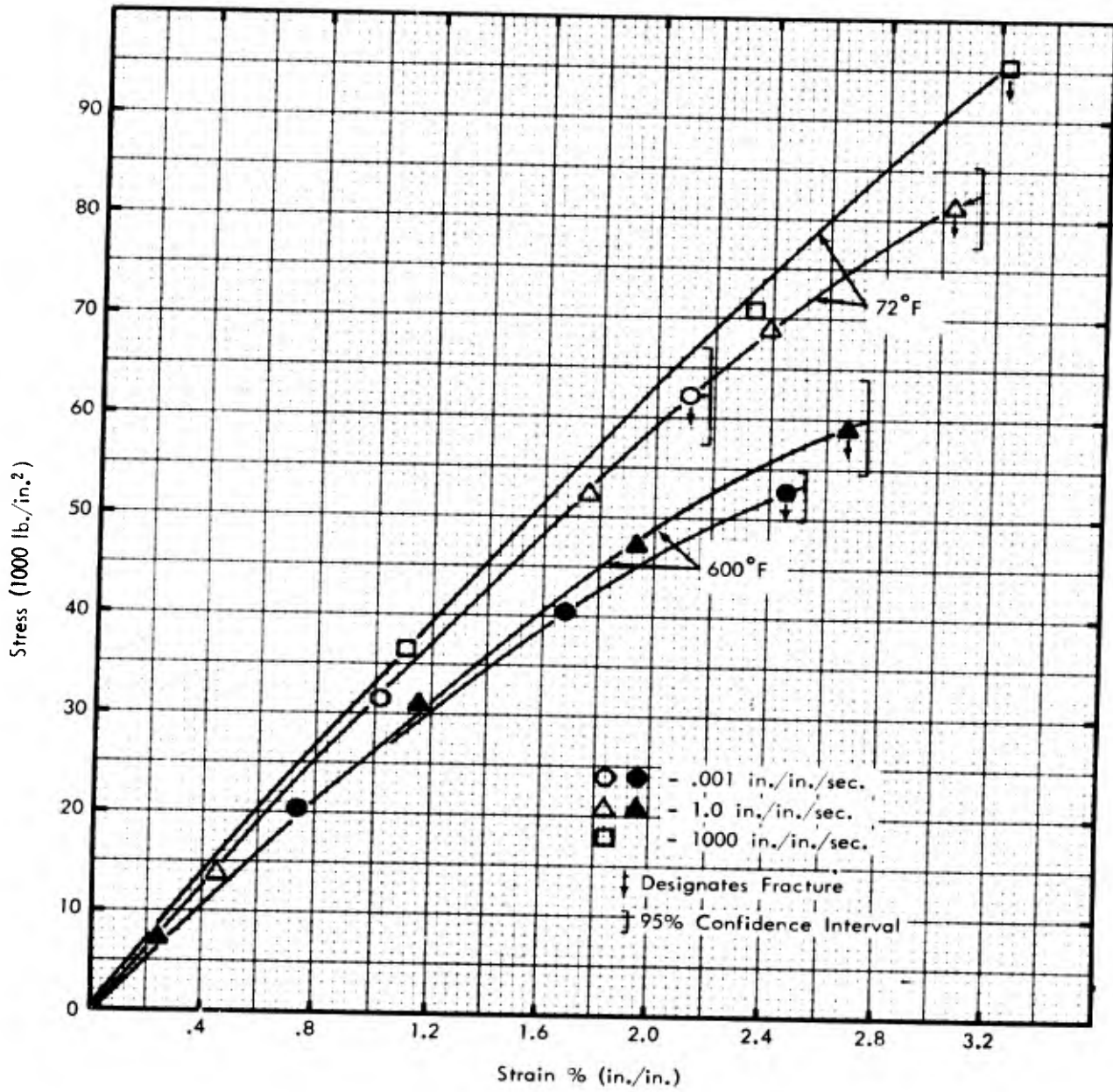


Figure 6 Tension Tests on Quartz Phenolic, Layup Parallel to Loading Axis - Stress vs. Strain

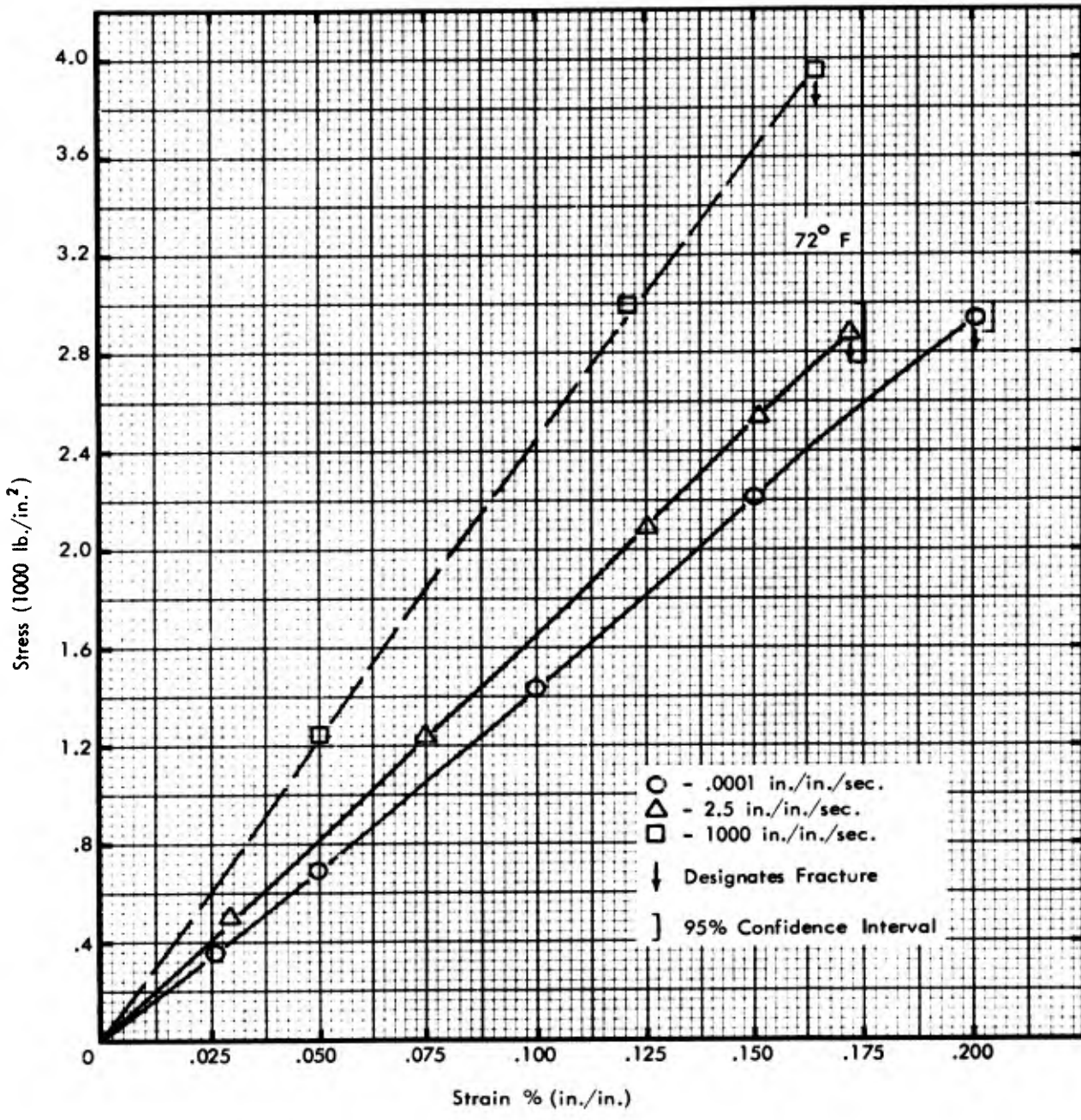


Figure 7 Tension Tests on Quartz Phenolic, Layup Normal to Loading Axis - Stress vs. Strain

At 600°F, a change in failure mode is observed. Greater resin decomposition has taken place as seen by an increase in fracture strain from 400°F to 600°F (Figure 4), and the fibers begin to control strength or crack nucleations. The fibers are actually playing a larger role in the composite strength at this temperature. For loadings parallel to the layup, a minimum in fracture stress at 400°F is observed only at the very high strain rate (Figure 3). Stiffness (stress at 4% strain) exhibits a minimum at 400°F for loadings normal to the layup (Figure 2), while it tends to decrease linearly with increased temperature up to 600°F for loadings parallel to the layup in compression. Much larger strength degradation at 600°F is seen for loadings parallel to the layup where the phenolic matrix tensile strength plays a major role in the composite strength.

Quartz phenolic dynamic tensile behavior for two orthogonal loading directions is shown in Figures 6 and 7. Test results for loading normal to the layup at 600°F are not shown because specimens were found to have been taken from the one low density block of material. In general the tensile behavior of quartz phenolic is similar to the compressive behavior for room temperature loadings at the same layup orientations. Initial stiffnesses are nearly identical but fracture stress can vary depending on the layup orientation. Elevated temperature comparison shows marked differences between similar loadings. This is due primarily to the changes in the fiber-matrix interrelationship caused by the elevated temperature. Reference 2 discusses the observed differences on quartz, silica and carbon phenolic.

Silica Phenolic: Figures 8 through 11 show the dynamic response of silica phenolic at 72°F and 600°F for compressive

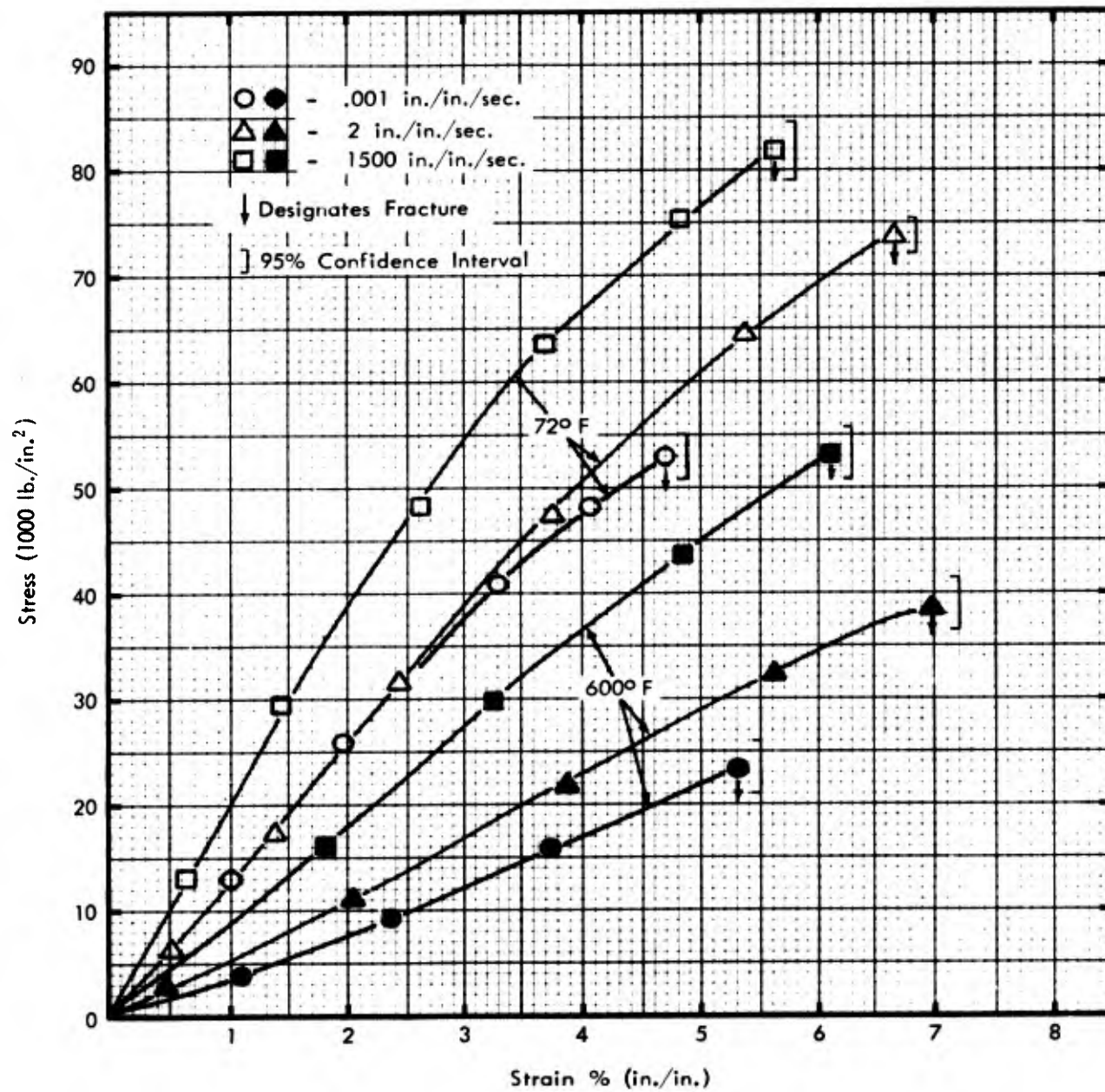


Figure 8 Compression Tests on Silica Phenolic, Layup Normal to Loading Axis - Stress vs. Strain

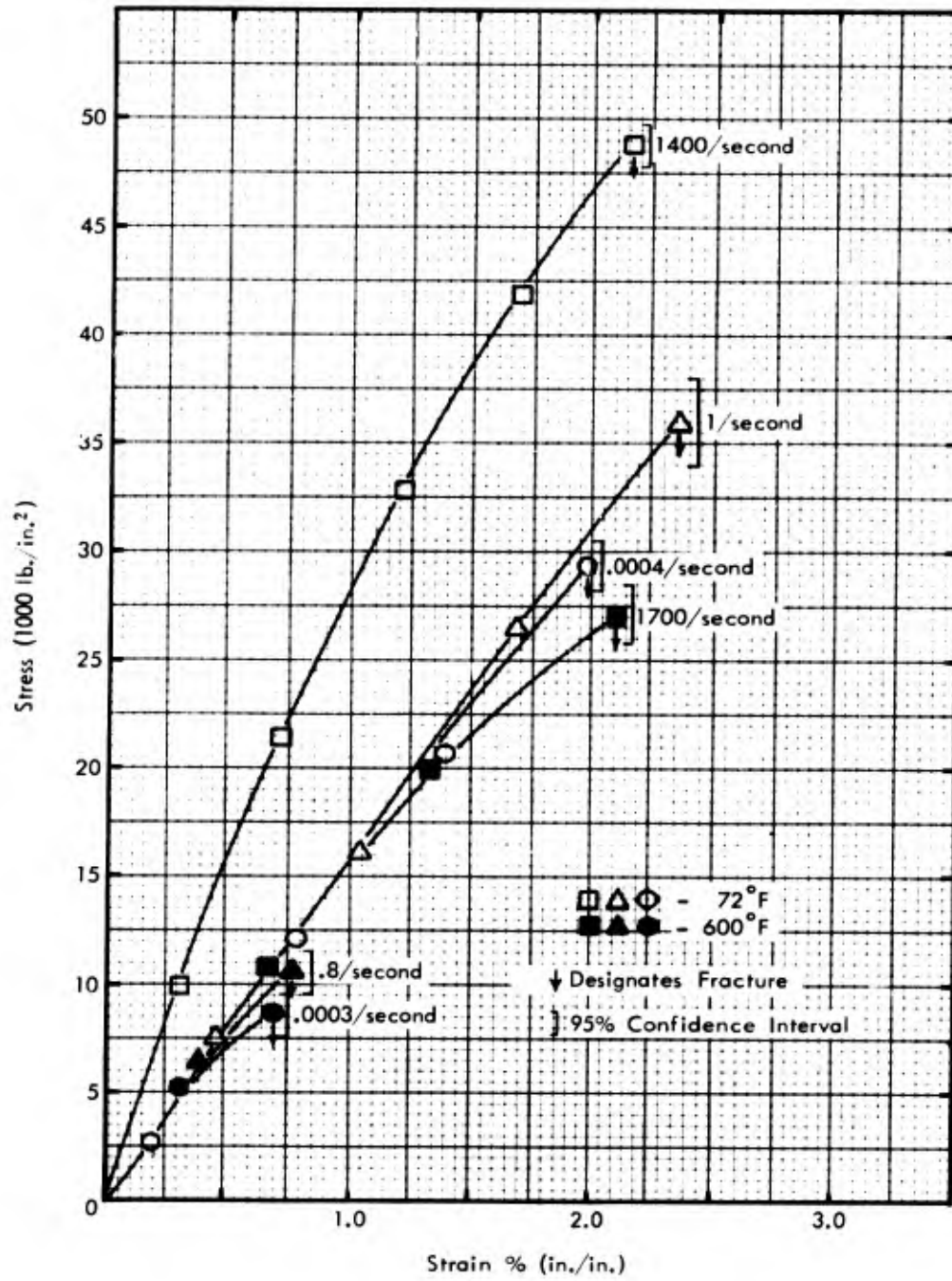


Figure 9 Compression Tests on Silica Phenolic, Layup Parallel to Loading Axis - Stress vs. Strain

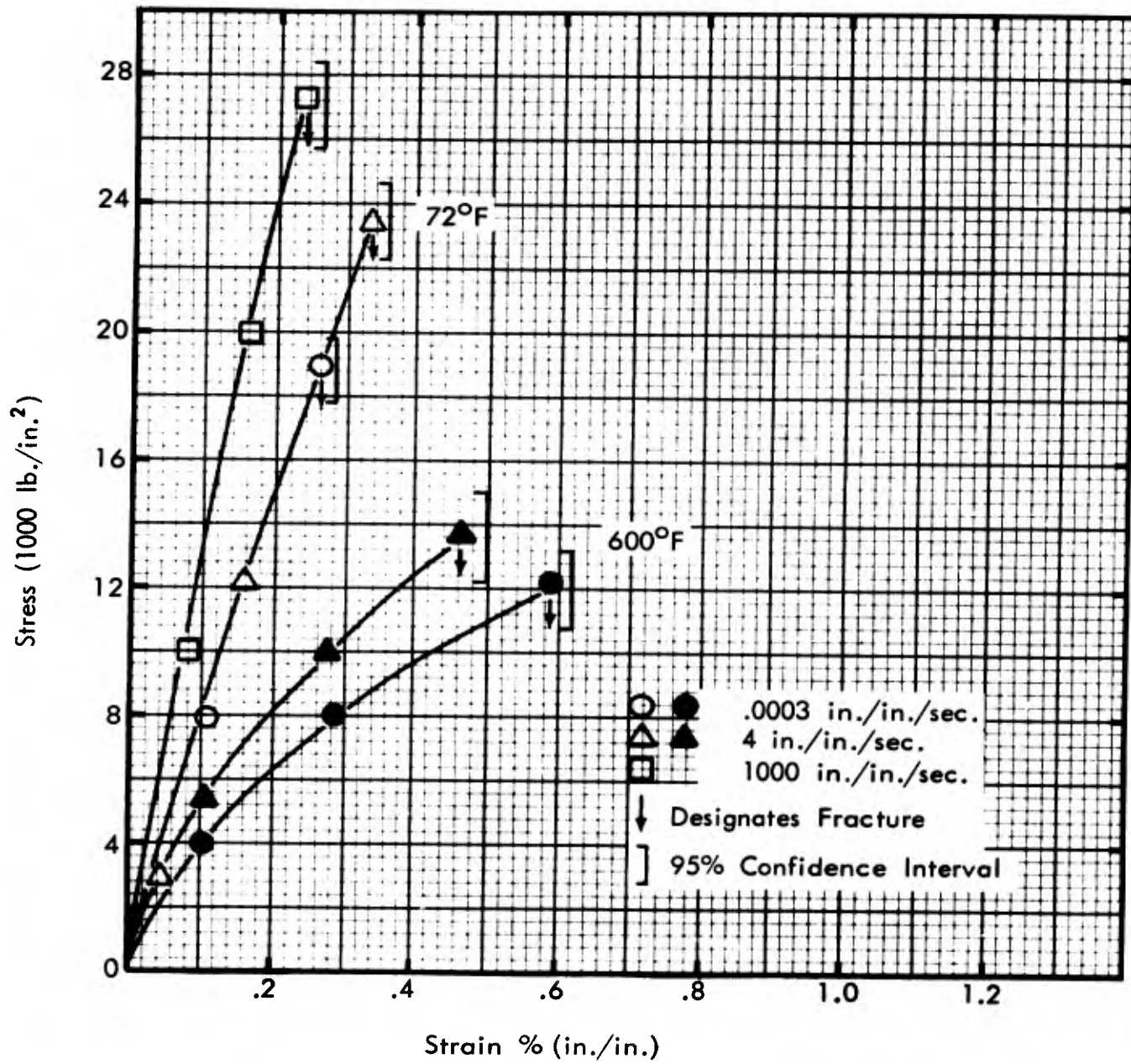


Figure 10 Tension Tests on Silica Phenolic, Layup Parallel to Loading Axis - Stress vs. Strain

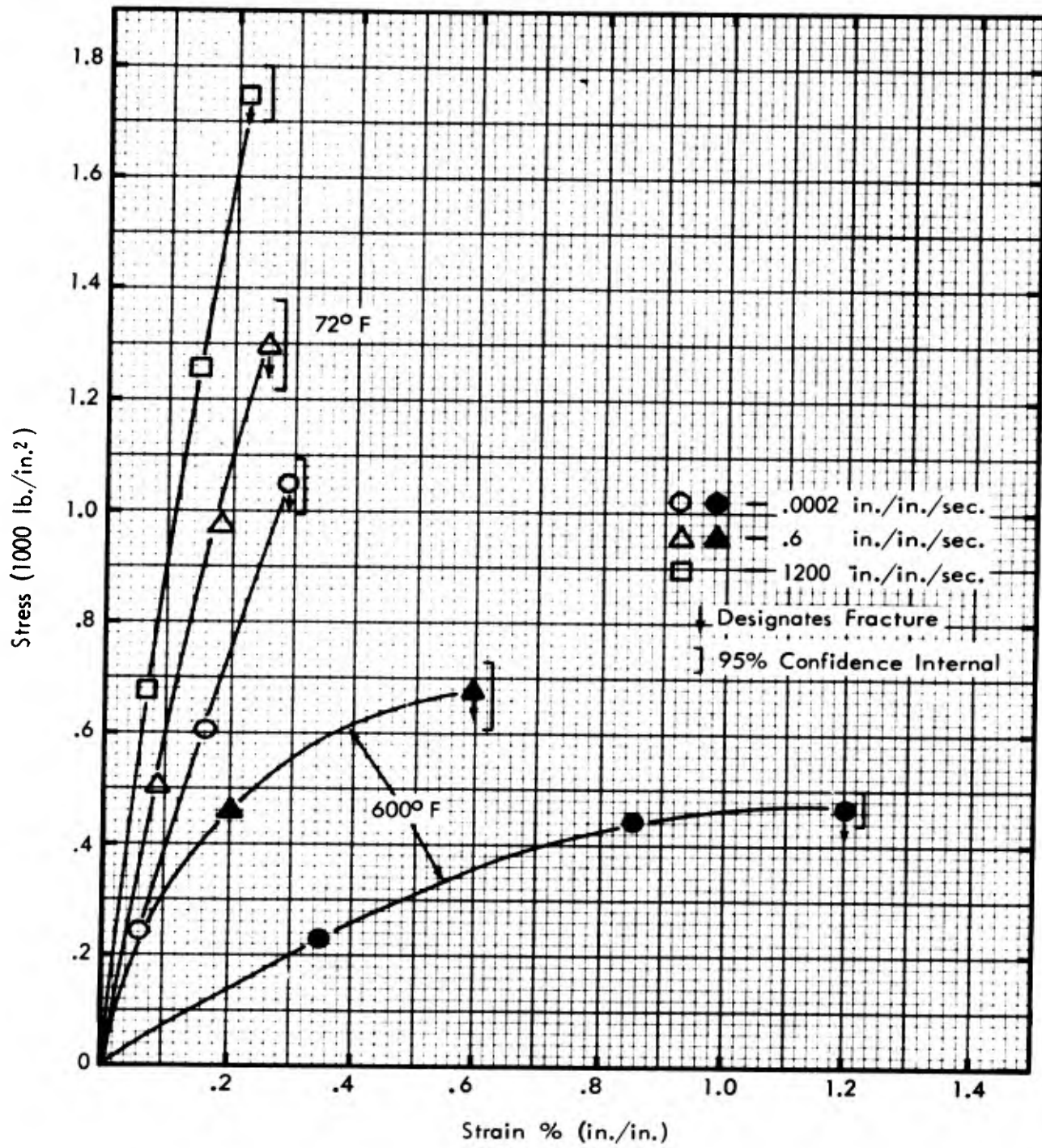


Figure 11 Tension Tests on Silica Phenolic, Layup Normal to Loading Axis - Stress vs. Strain

and tensile loadings normal and parallel to the fiber layup. For compressive loading normal to the layup (Figure 8), an increase in temperature reduces stiffness but changes strain-to-fracture little. This trend is similar to the quartz phenolic behavior at 72°F and 600°F although fracture stress for silica phenolic is only about one-half that of quartz phenolic. Although 400°F tests were not conducted, a previous report⁽²⁾ indicates that the reduced strength and stiffness observed for quartz phenolic at 400°F does not occur in silica phenolic. This can possibly be explained by the higher resin content in silica phenolic (37% versus 31% for quartz phenolic). Since heating and test times were very similar for the two materials, the higher resin content in silica phenolic means that more undecomposed resin remained at the time of test in the silica phenolic, thus having a role in the composite fracture behavior. For loadings parallel to the layup in compression (Figure 9), fracture stress and stiffness for silica phenolic is about one-half of that for quartz phenolic. At 600°F, stiffness and fracture stress are nearly the same for the two materials for this loading direction. Strain-rate sensitivity increases drastically at 600°F.

For room temperature tensile loadings parallel to the layup (Figure 10), silica phenolic fracture stress is only about one-third of quartz phenolic. Stiffness for silica phenolic is almost twice that of quartz phenolic at 72°F, while at 600°F, the difference is very small. Fracture stress at 600°F for quartz phenolic is about four times that of silica phenolic. For tensile loadings at room temperature normal to the layup, stiffness and fracture strength of quartz is about twice that of silica phenolic.

The silica phenolic test results presented in this report differ from those previously published⁽²⁾ due to the nature of the material tested. While the silica phenolic used for this study was made from J. P. Stevens Astrosil 84 fabric and SC-1008 resin, the material used in Reference 2 was HITCO Type II fabric and SC-1008 resin. In addition, fabric weave differences were large. The Astrosil 84 fabric contained fibers of approximately 0.006 to 0.008 inch diameter and spaced 0.012 to 0.015 inch apart. The Type II fabric contained fibers of approximately 0.013 to 0.015 inch diameter with 0.030 to 0.035 inch spacing.

Carbon Phenolic: Figures 12 through 14 show the dynamic response of carbon phenolic at 72°F and 600°F when loaded in compression and tension parallel to the fiber layup and compression normal to the layup. Due to the lack of proper material (see Appendix A, Section 3), elevated temperature tensile tests normal to the layup were not conducted. Room temperature results for this layup are reported in Reference 3.

Size Effect

The effect of specimen size was studied in order to aid in correlation between laboratory-obtained data and bulk material properties. Since the general observations at room temperature for quartz and carbon phenolic were nearly identical⁽³⁾, the present extension to elevated temperatures concentrated on quartz phenolic. However, both materials were studied in tension at room temperature with loading normal to the fiber layup.

In compression, three sizes of specimens were tested all with a length-to-diameter ratio of 1.33. In tension, three sizes of specimens were tested with length-to-diameter ratios of 5.

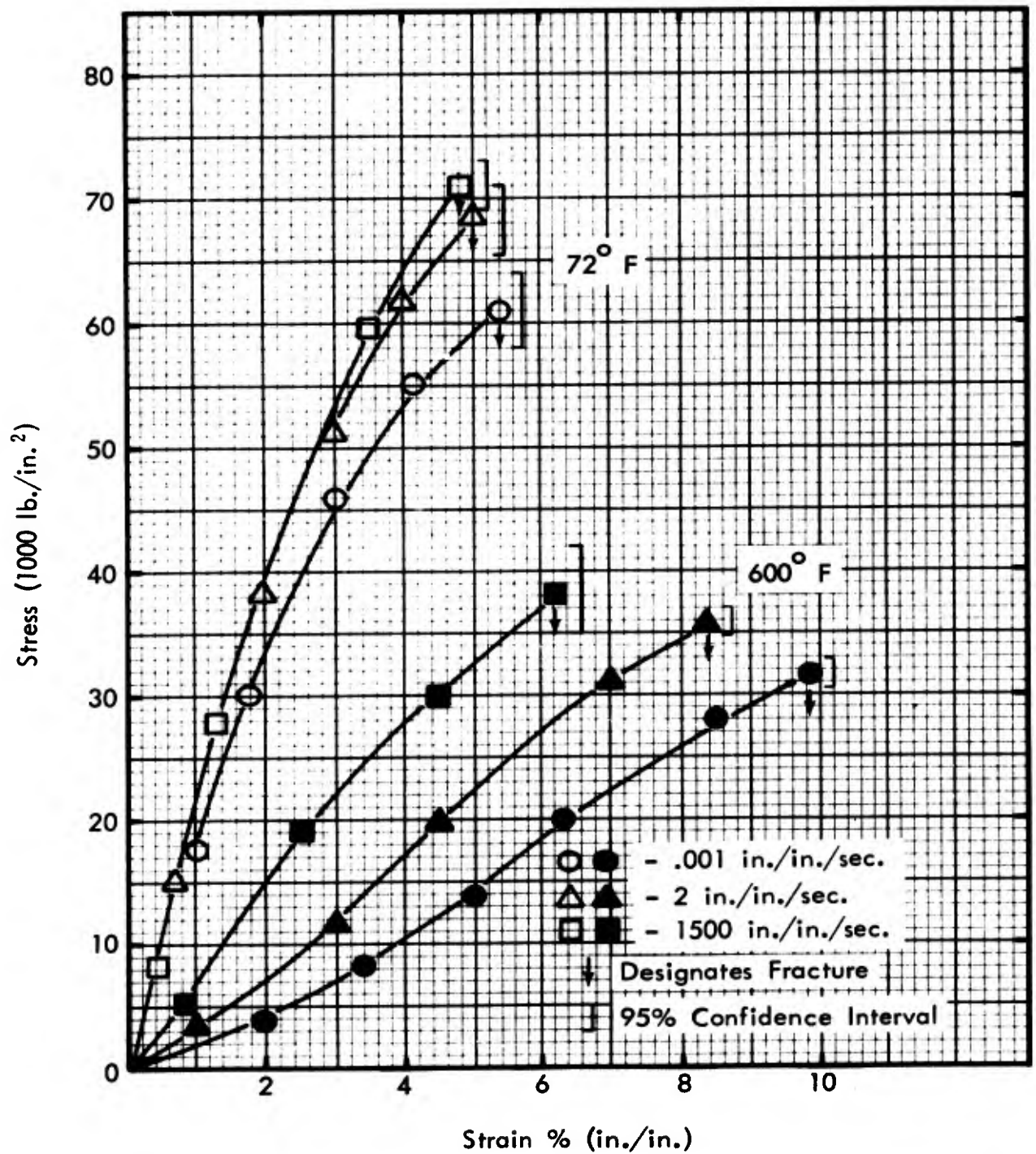


Figure 12 Compression Tests on Carbon Phenolic, Layup Normal to Loading Axis - Stress vs. Strain

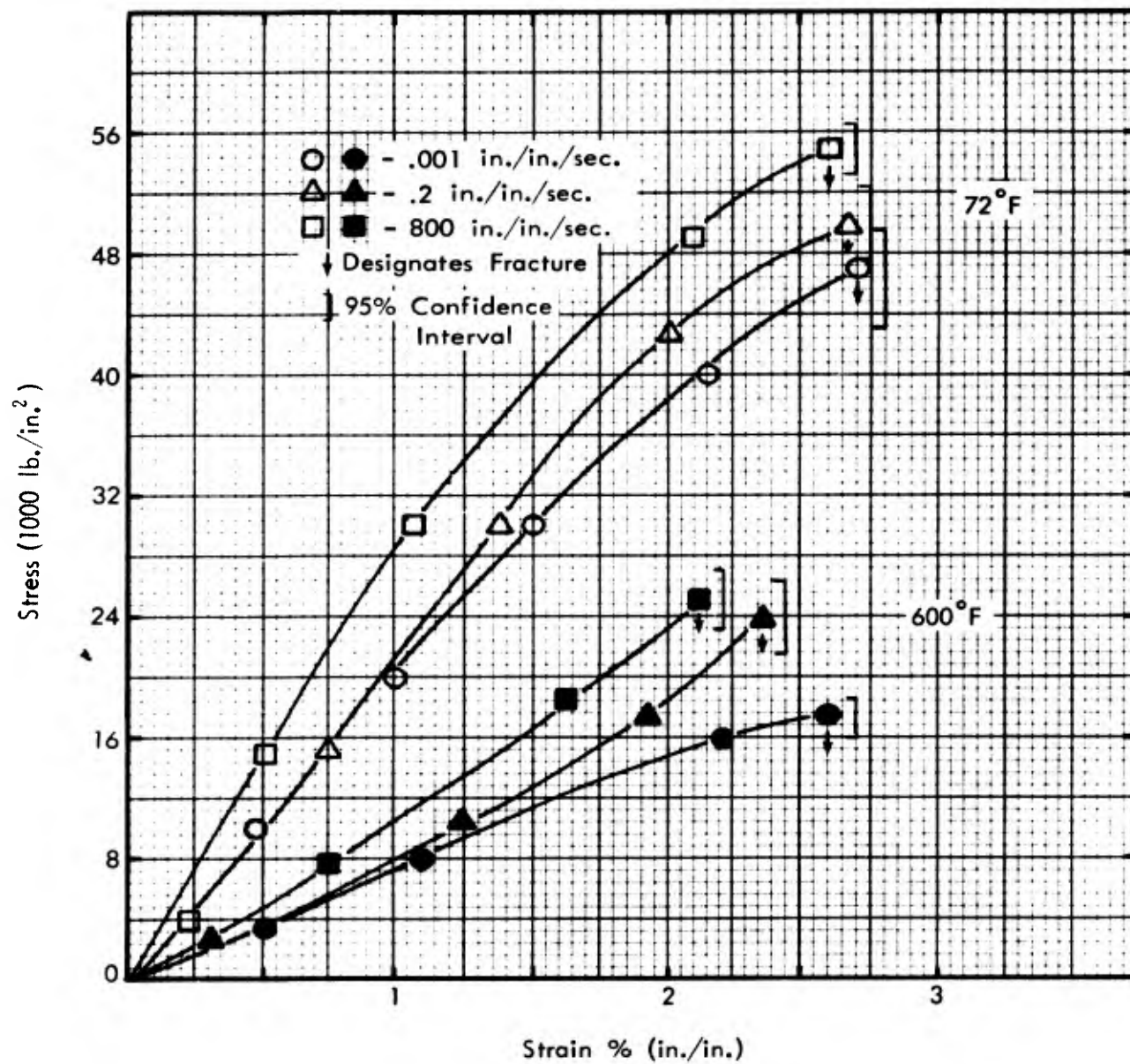


Figure 13 Compression Tests on Carbon Phenolic, Layup Parallel to Loading Axis - Stress vs. Strain

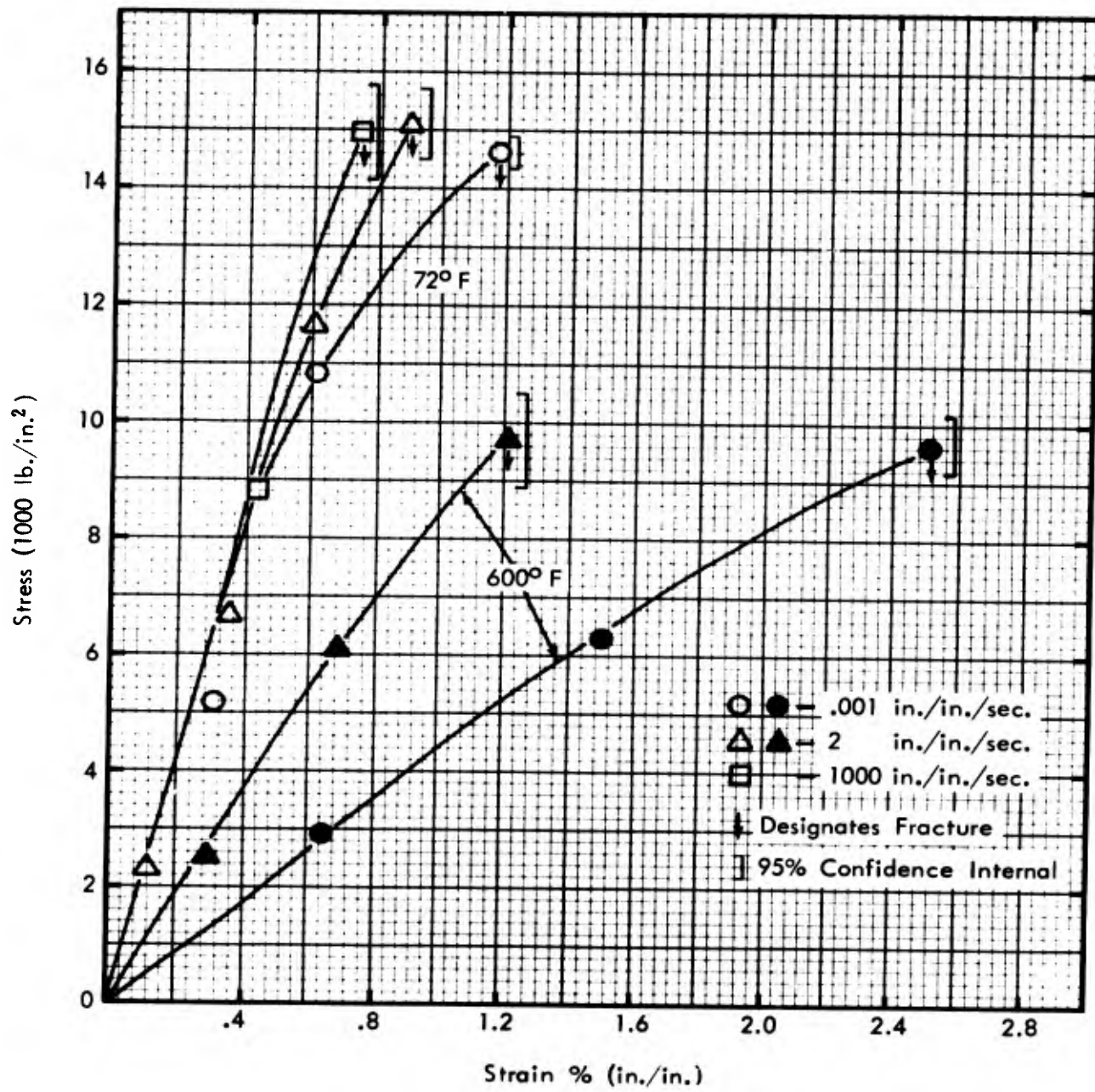


Figure 14 Tension Tests on Carbon Phenolic, Layup Parallel to Loading Axis - Stress vs. Strain

Figures 15 and 16 show the results of compression size effect studies on quartz phenolic when loaded normal to the fiber layup. Specimens 0.188 inch, 0.375 inch, and 0.500 inch in diameter were tested at three strain rates and at temperatures of 72°, 400°, and 600°F. Figure 15 shows fracture stress plotted against specimen size. The results at 72°F are taken from Reference 3. From these results it appears that elevated temperature tends to decrease the effect of specimen size for the range studied. However, large scatter was experienced in this limited study so that firm conclusions are not feasible.

Figure 16 shows stress at 4% strain (or stiffness) plotted against specimen size where the results at 72°F are taken from Reference 3.

Figures 17 and 18 show the results of tension size effect studies for loadings parallel and normal to the fiber layup. Specimen sizes from 0.10 to 0.375-inch-square all with an effective length-to-diameter ratio of 5 were used. For loadings parallel to the fiber layup on quartz phenolic (Figure 17), the same general trends are shown for 72°F and 600°F tests. While the 72°F results are taken from Reference 3, tests at 600°F were conducted at a medium strain rate only. The noticeable increase in fracture stress at 72°F up to about 0.25-inch-square is not as pronounced at 600°F. In general, no change in stiffness (stress at 1.2% strain) is observed with specimen size up to 600°F. It should be noted that the difficulty found in gripping the large 0.375-inch-square specimens (which required very high loads to fracture) at 72°F⁽³⁾ were not present at 600°F.

Figure 18 shows the results of room temperature tension tests on quartz and carbon loaded normal to the fiber layup

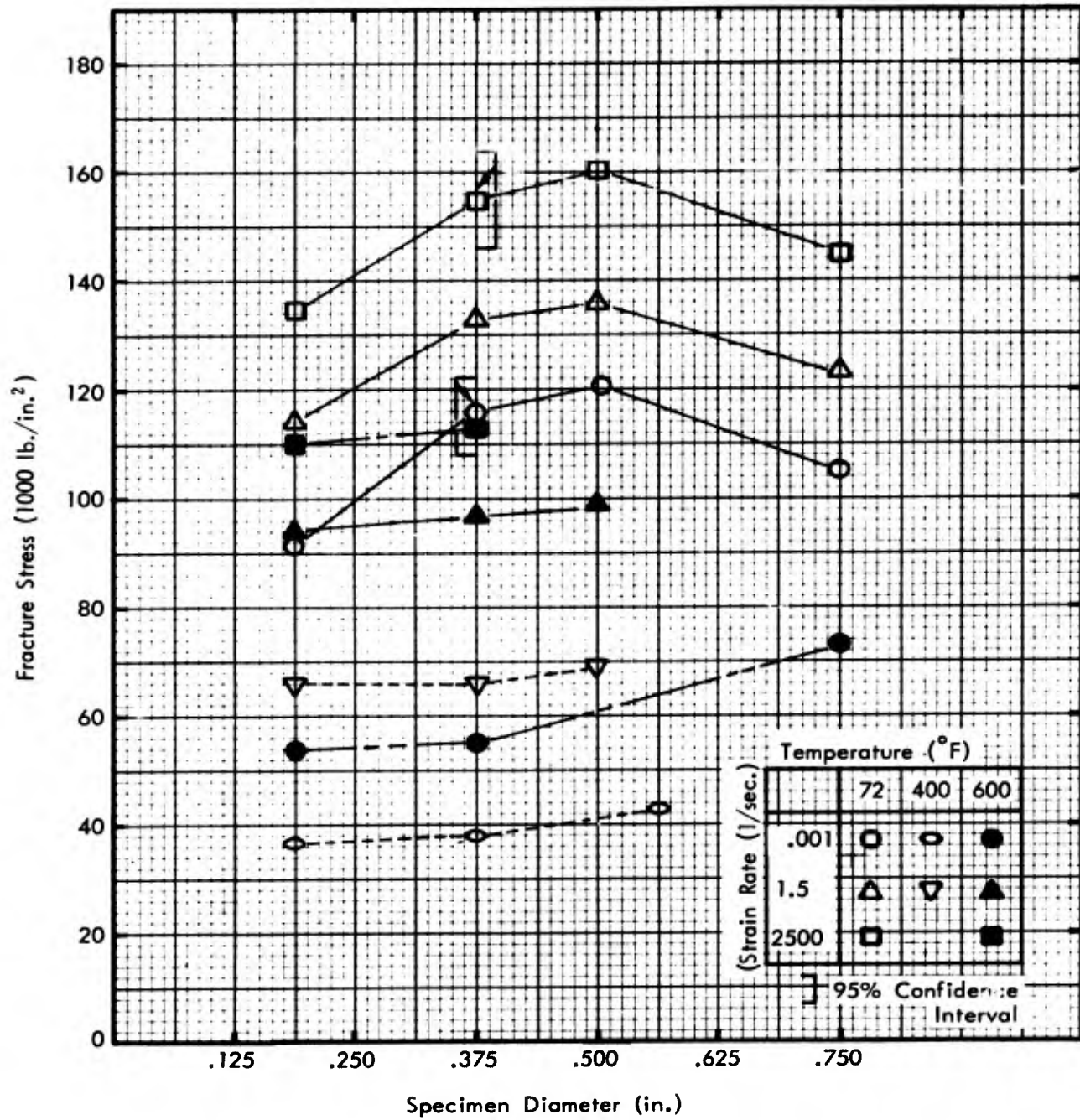


Figure 15 Size Effect Study on Quartz Phenolic in Compression, Layup Normal to Loading Axis

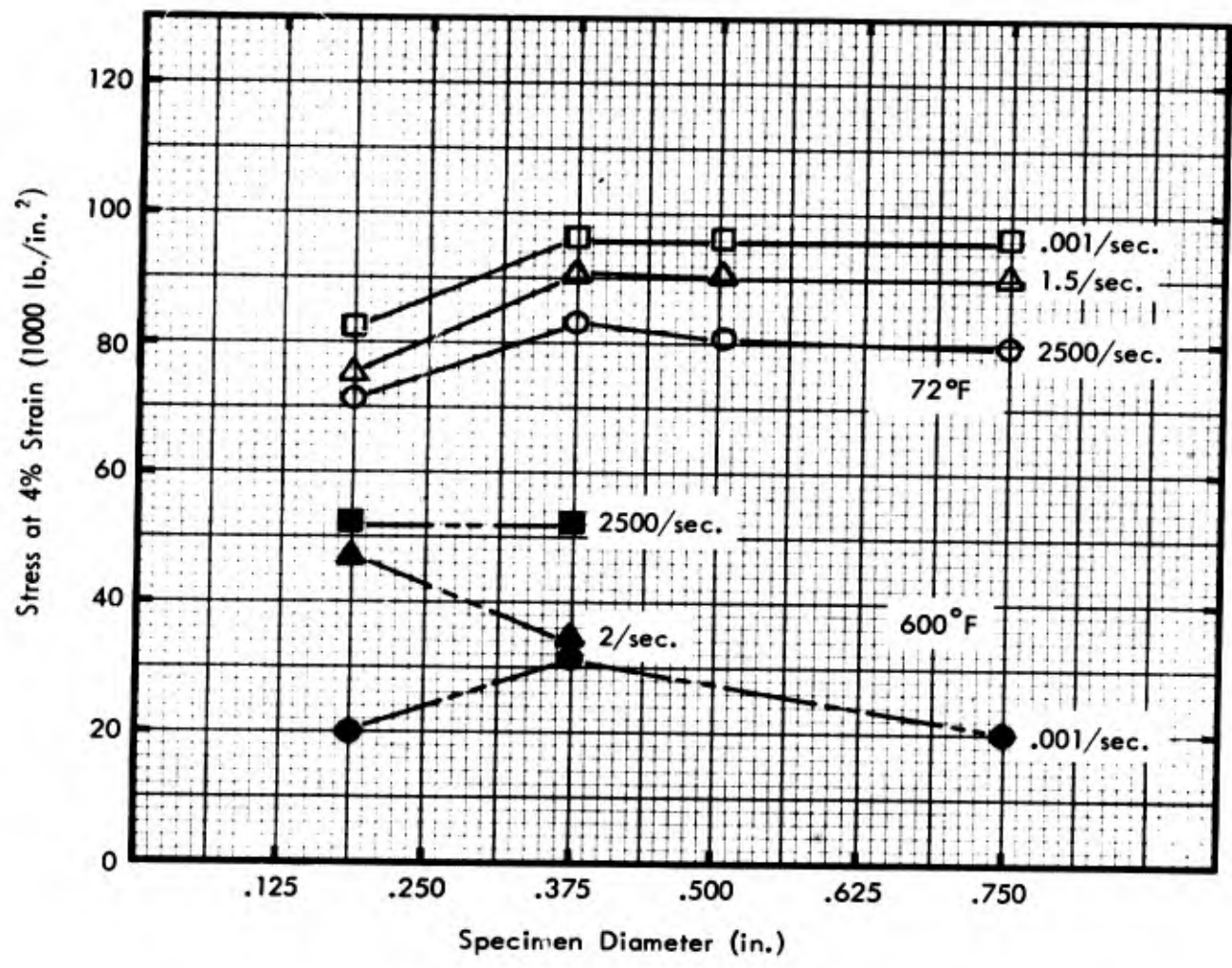


Figure 16 Size Effect Study on Quartz Phenolic in Compression, Layup Parallel to Loading Axis

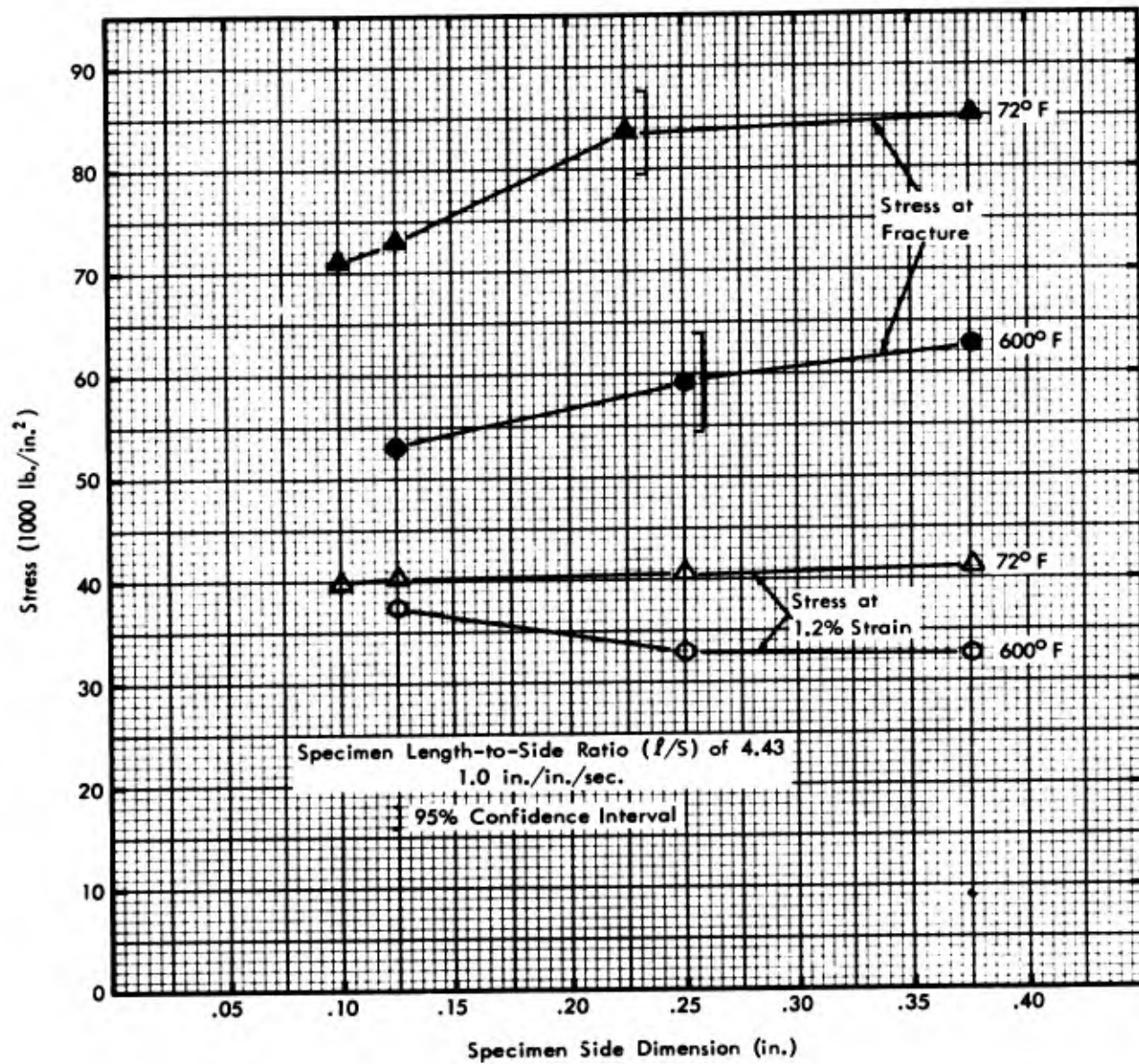


Figure 17 Size Effect Study on Quartz Phenolic in Tension, Layup Parallel to Loading Axis

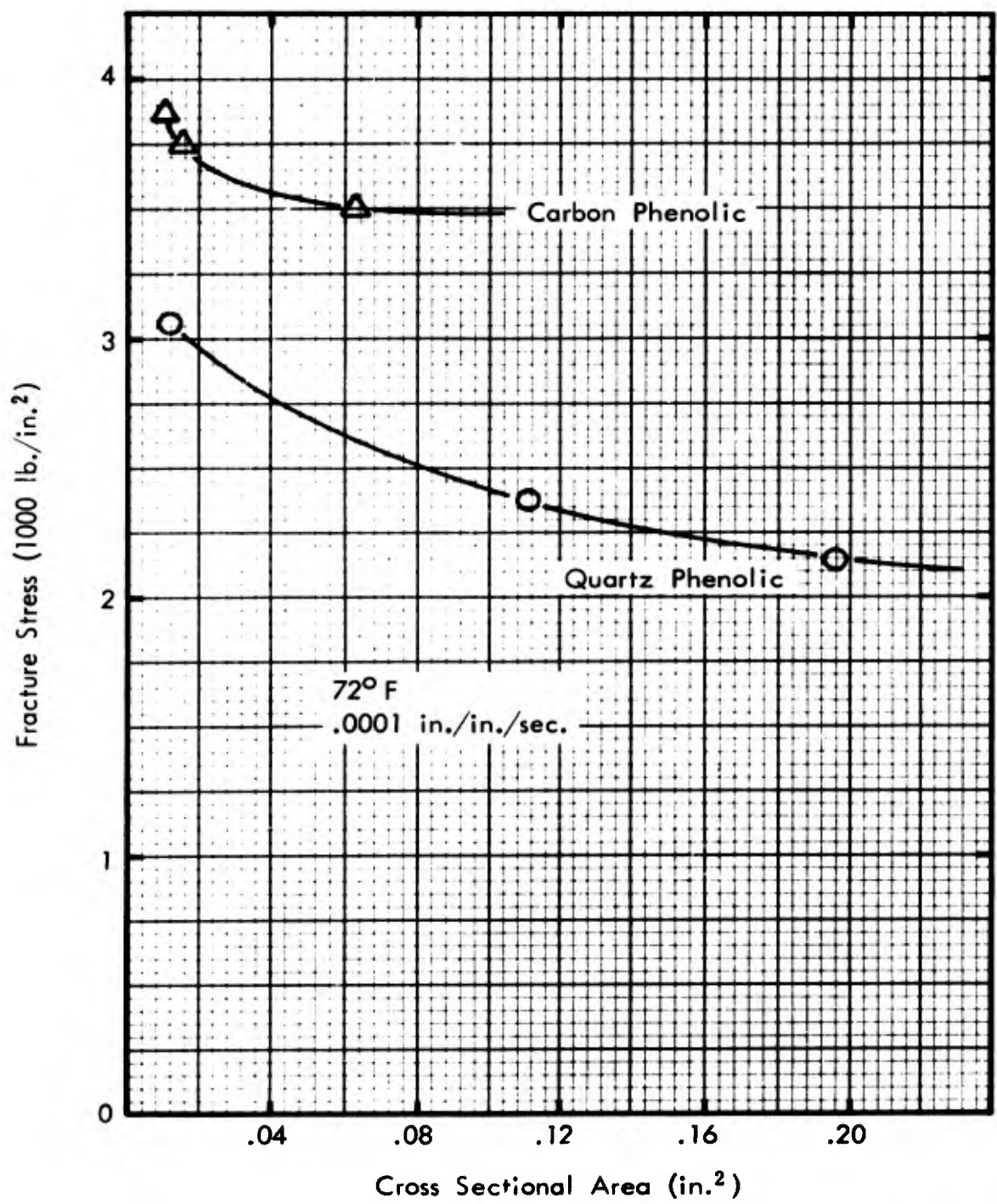


Figure 18 Size Effect Study on Quartz and Carbon Phenolic in Tension, Layup Normal to Loading Axis

at a low strain rate. Initial tests to study quartz phenolic using the standard "dog-bone" shaped specimens were unsuccessful⁽³⁾ because of the difficulty of machining these very weak samples. A new technique was developed where cylindrical-shaped specimens were bonded into metal grips (Figure 19). Figure 18 shows fracture stress plotted against cross-sectional area instead of specimen diameter because while the quartz phenolic tests used the bonded grip technique, the carbon phenolic tests used the standard "dog-bone" shaped specimens. Length-to-diameter ratios are not the same for these two techniques, but for this fiber layup end effects are essentially negligible. It is seen that fracture stress decreases with increasing cross section. Carbon phenolic exhibits an apparent minimum leveling off of fracture stress above about 0.08 inch². Quartz phenolic appears to be leveling off in fracture somewhere above about 0.20 inch².

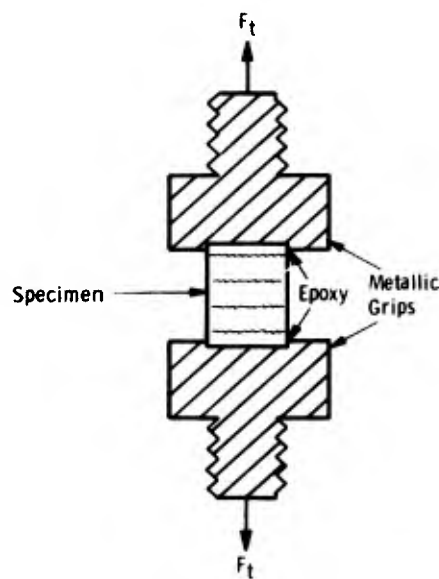


Figure 19 Tensile Specimen Schematic

A detailed explanation of the size behavior at room temperature is presented in Reference 3. However, a synopsis is pertinent to this discussion. For room temperature loadings other than tension loaded normal to the fiber layup, two criteria are observed over the range of specimen sizes studied. For the small specimens (less than about 0.375 inch diameter) strength tends to increase with size because a larger proportion of the smaller specimens have been damaged during fabrication. For specimens larger than about 0.375 to 0.500 inch diameter, strength tends to decrease with increasing size because of the increasing probability of a series of weak links (or flaws) joining to form a fault. This follows the well-known Weibull-Griffith crack theory. At elevated temperatures the phenolic matrix, from which most flaws are initiated, plays a less important role in the fracture of the composite; therefore, it is not unlikely that the size effect diminishes with increasing temperatures over the range of specimens studied here.

The exception to these criteria is for tension loading normal to the fiber layup. For this condition the "weak link" criterion predominates such that as smaller and smaller specimens are fabricated, only the strongest specimens will survive the rigors of fabrication. Therefore, the smaller specimens sampled are not truly representative of the actual material. The "weak link" plateau stress is rather easily reached because for this loading condition fracture results from a single flaw (rather than being initiated from a series of aligned flaws).

LOADING AT INTERMEDIATE FIBER LAYUP ANGLES

Since the ablative-composite materials tested in the MARS program are highly anisotropic, testing in one or two fiber layup orientations (usually parallel and normal to the loading axis) will not necessarily determine the behavior of these materials when loaded in different orientations. In general, the loading direction encountered in a structural configuration is somewhere between parallel (0°) and normal (90°) to the fiber layup. In view of this circumstance, a series of constant strain-rate tests was performed on quartz phenolic to determine the effect of fiber orientation or layup angle on the material mechanical properties.

Room temperature uniaxial compression and tension tests were conducted at various strain rates; approximately 10^{-3} /sec to 1.4×10^3 /sec in compression and 10^{-4} /sec to 3/sec in tension. Specimens with layup angles of 0, 15, 30, 45, 60, 75, and 90 degrees to the loading axis were tested. A comparison was made between the experimental test results and results predicted using the fracture conditions proposed by Hoffman. ⁽⁶⁾

Theoretical Prediction

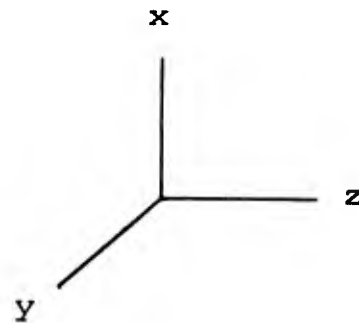
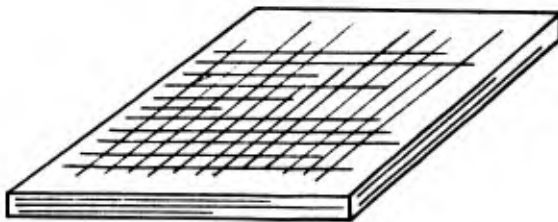
An existing phenomenological fracture condition proposed by Hoffman ⁽⁶⁾ for orthotropic brittle materials is described here. Using the assumption of transverse isotropy in the plane of the fabric and borrowing features of the Mises - Schleischer isotropic and Hill's orthotropic yield conditions, the following fracture condition was proposed:

$$\begin{aligned}
& c_1 (\sigma_y - \sigma_z)^2 + c_2 (\sigma_z - \sigma_x)^2 + c_3 (\sigma_x - \sigma_y)^2 \\
& + c_4 \sigma_x + c_5 \sigma_y + c_6 \sigma_z + c_7 T_{yz}^2 + c_8 T_{zx}^2 + c_9 T_{xy}^2 = 1 \quad (1)
\end{aligned}$$

where $c_1 \dots c_9$ are material parameters

$\sigma_x \quad \sigma_y \quad \sigma_z$ are uniaxial stresses

$T_{yz} \quad T_{zx} \quad T_{xy}$ are shear stresses



Assuming transverse isotropy in the y-z plane

$$\begin{aligned}
F_{cy} &= F_{cz} && \text{for compressive fracture strengths} \\
F_{ty} &= F_{tz} && \text{for tensile fracture strengths} \\
F_s \text{ (xy plane)} &= F_s \text{ (xz plane)} && \text{for pure shear strengths}
\end{aligned}$$

equation (1) becomes

$$\begin{aligned} & \frac{\sigma_x^2 - \sigma_x \sigma_y}{F_{cx} F_{tx}} + \frac{\sigma_y^2}{F_{cy} F_{ty}} + \frac{F_{cx} - F_{tx}}{F_{cx} F_{tx}} \cdot \sigma_x \\ & + \frac{F_{cy} - F_{ty}}{F_{cy} F_{ty}} \cdot \sigma_y + \frac{T_{yz}^2}{F_{sy}^2} = 1 \end{aligned} \quad (2)$$

where: $\sigma_z = T_{xy} = T_{xz} = 0$ for plane stress.

Simplifying the well-known stress tensor transformations,

$$\begin{aligned} \sigma_x &= \sigma_\theta \cos^2 \theta \\ \sigma_y &= \sigma_\theta \sin^2 \theta \\ T_{xy} &= \sigma_\theta \sin \theta \cos \theta \end{aligned} \quad (3)$$

where the angle θ is taken with respect to the X-axis and substituting equations (3) into (2), the following quadratic equation in σ_θ is obtained:

$$\begin{aligned} & \left[(\cos^4 \theta) \left(\frac{1}{F_{cx} F_{tx}} \right) + (\sin^2 \theta \cos^2 \theta) \left(\frac{1}{F_{sy}^2} - \frac{1}{F_{cx} F_{tx}} \right) \right. \\ & + \left. (\sin^4 \theta) \left(\frac{1}{F_{cy} F_{ty}} \right) \right] \sigma_\theta^2 + \left[(\cos^2 \theta) \left(\frac{F_{cx} - F_{tx}}{F_{cx} F_{tx}} \right) \right. \\ & + \left. (\sin^2 \theta) \left(\frac{F_{cy} - F_{ty}}{F_{cy} F_{ty}} \right) \right] \sigma_\theta = 1 \end{aligned} \quad (4)$$

Discussion of Results

Figures 20 through 22 show the results of room temperature compression and tension tests on quartz phenolic where fracture stress versus layup angle is plotted at various strain rates. The layup angle is taken with respect to the axis of loading. Included in these figures are the predicted results using Equation 4.

In Figure 20 compression test results at three rates of loading are shown with Equation 4 plotted for the low and medium rates. Equation 4 could not be used for the high strain rate (1.4×10^3 /sec) since tension tests were not conducted at this rate. Close examination shows that the largest deviation between experimental and theoretical results occurs at the medium rate between approximately 25° and 70° layup angles. The deviations shown are probably due to material scatter ($\pm 10\%$), or the fact that the layup angle does have a tolerance of about $\pm 3^\circ$, and near 15° and 75° this variation could cause the deviation shown.

Figure 21 shows room temperature tension test results at two rates of loading with Equation 4 included. Very close agreement is shown except near the 15° layup angle at the medium strain rate. It can be seen that if the layup angle was actually 18° instead of 15° , the agreement would be perfect. This change in layup angle is almost impossible to measure accurately due to the nature of the composite laminate. Figure 22 shows the fracture strain behavior of quartz phenolic in tension at various layup angles. Other than at 0° , layup angle has no effect on fracture strain. This behavior is because fracture is by interlaminar shear from 15° to 90° , while at 0° fracture is by random failure of individual fibers followed by delamination. ⁽³⁾

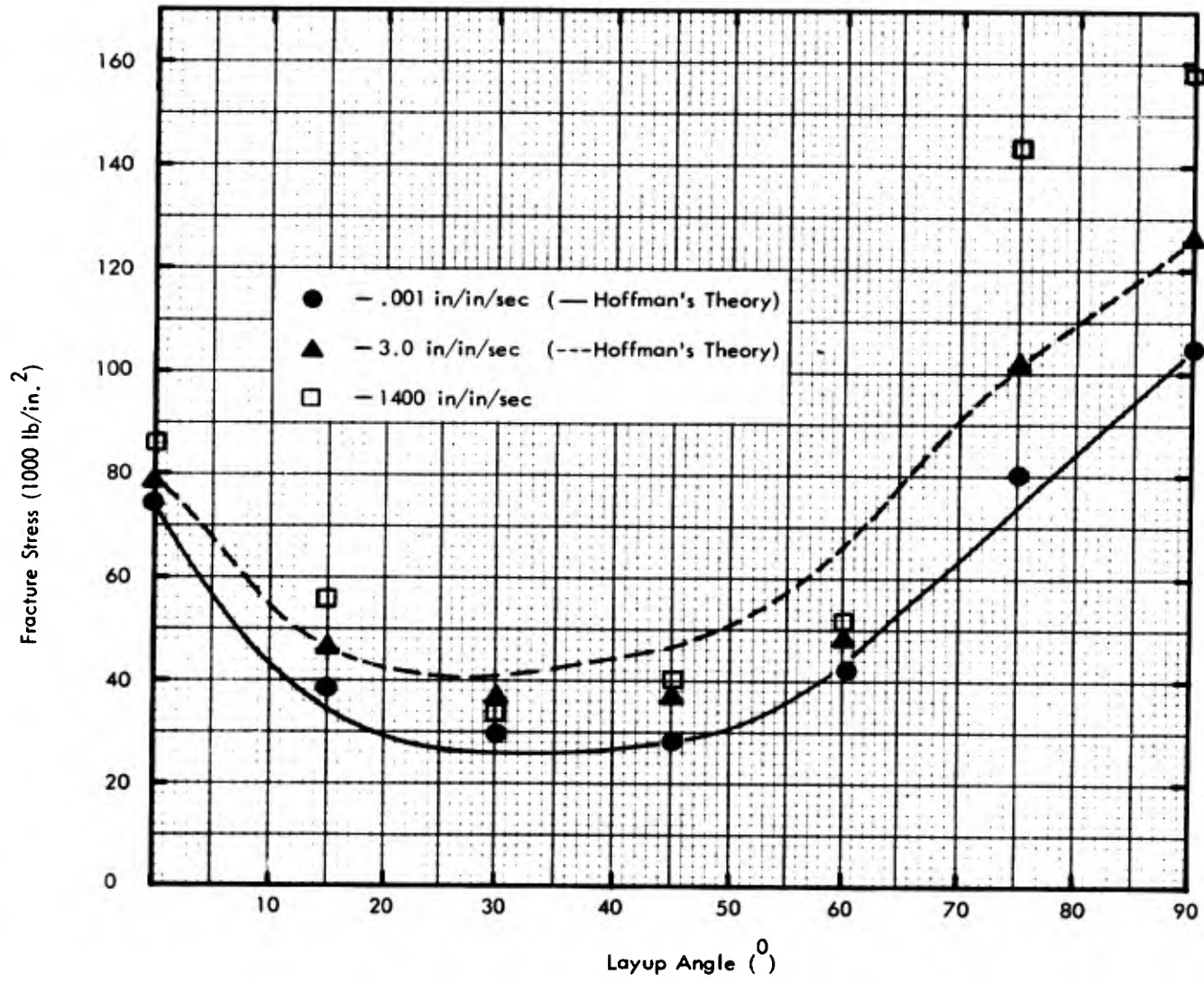


Figure 20 Compressive Behavior of Quartz Phenolic at Various Layup Angles - Fracture Stress vs. Layup Angle

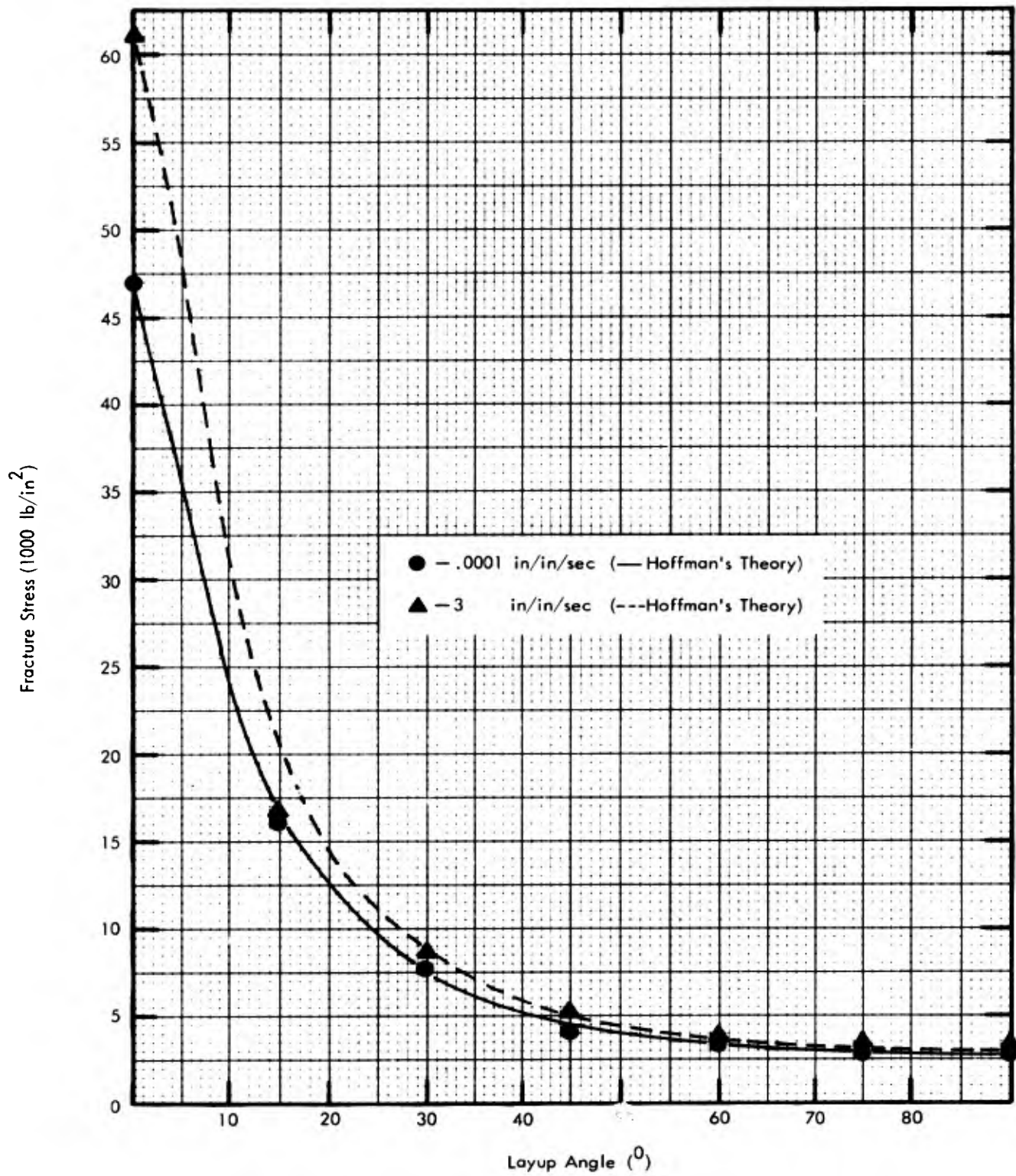


Figure 21 Tensile Behavior of Quartz Phenolic at Various Layup Angles - Fracture Stress vs. Layup Angle

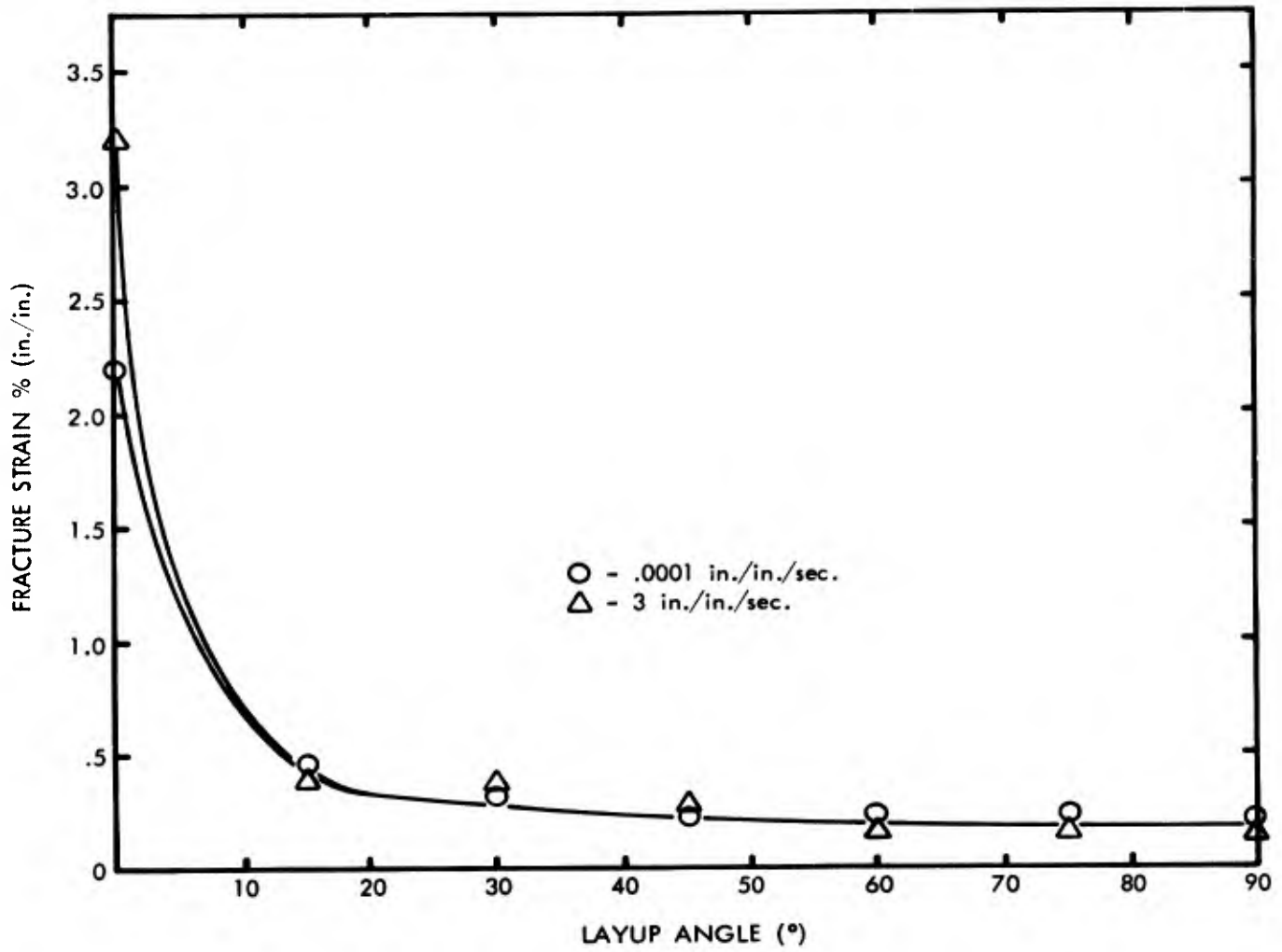


Figure 22 Tensile Behavior of Quartz Phenolic at Various Layup Angles - Fracture Strain vs. Layup Angle

There is remarkably close correlation between the test results and Hoffman's analysis. The quartz phenolic used in these tests was in the form of a laminated cloth and possessed no unidirectional properties.

Although this material is orthotropic, the assumption of transverse isotropy in the plane of the fabric (y-z plane) is not necessarily valid. The fill and warp directions possess different strengths.

Figure 23 shows the effect of layup angle on the initial modulus of quartz phenolic in compression and tension. These results are similar to those predicted by simple orthotropic elastic transformation equations. (7-10)

In order to develop an understanding of the effect of strain rate on the fracture strength of quartz phenolic at various angles of loading, cross plots of fracture stress and initial modulus versus log strain rate at several layup angles were made (Figures 24 and 25). It is seen that fracture stress strain-rate sensitivity increases with layup angle above 45°, or in other words increases with static fracture strength.

Figure 26 shows the increase in fracture stress and percent sensitivity (from 10^{-3} to 10^3 /sec) plotted against layup angle. With the exception of 0° and 90°, the general shape of both curves is similar to the plot of fracture stress versus layup angle. This is another indication that fracture stress strain-rate sensitivity increases with increasing static strength. It is not surprising that the 0° and 90° layup angles deviate from this trend as a different failure mechanism occurs at these angles. Figure 27 shows

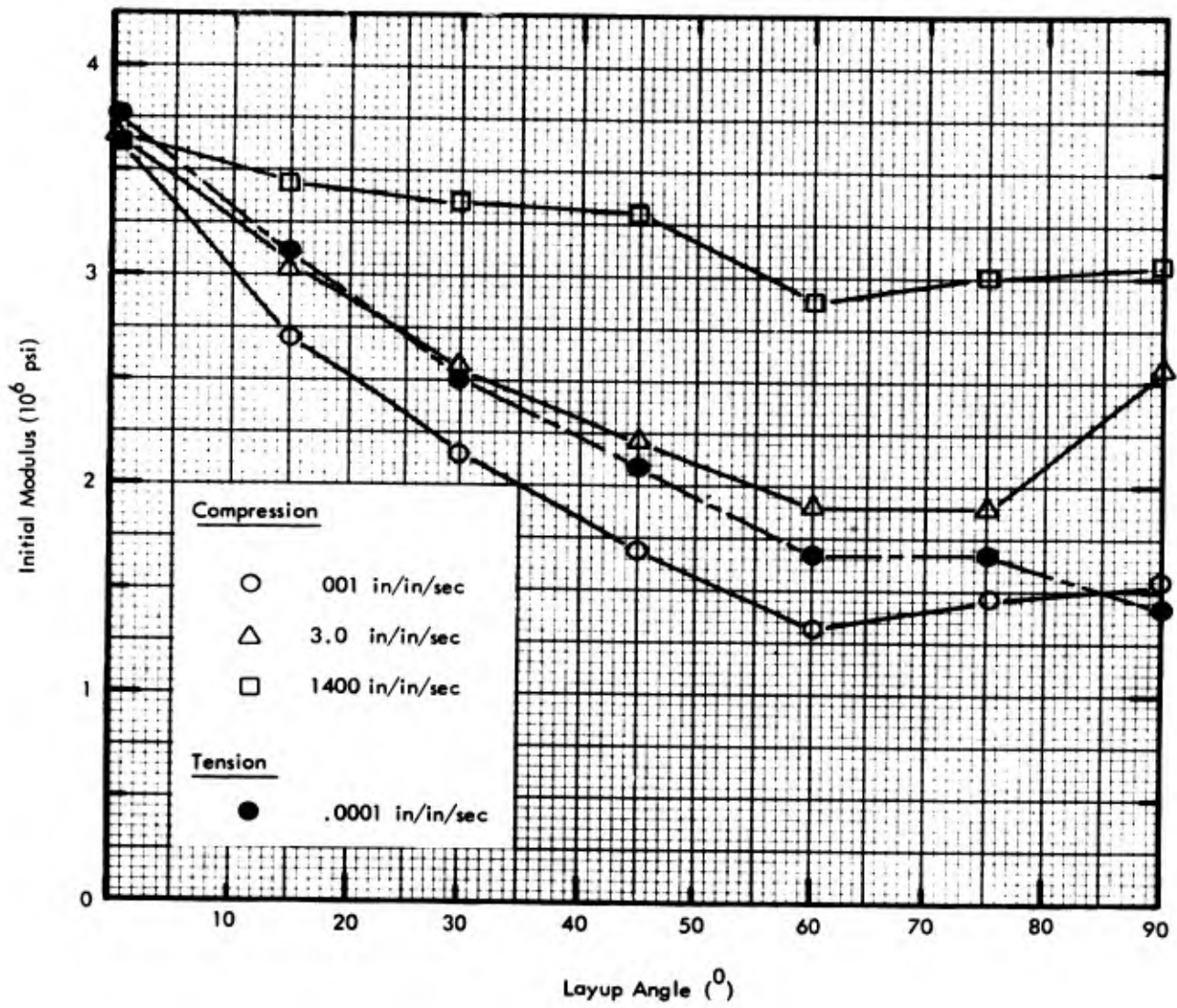


Figure 23 Stiffness Behavior of Quartz Phenolic at Various Layup Angles - Initial Modulus vs. Layup Angle

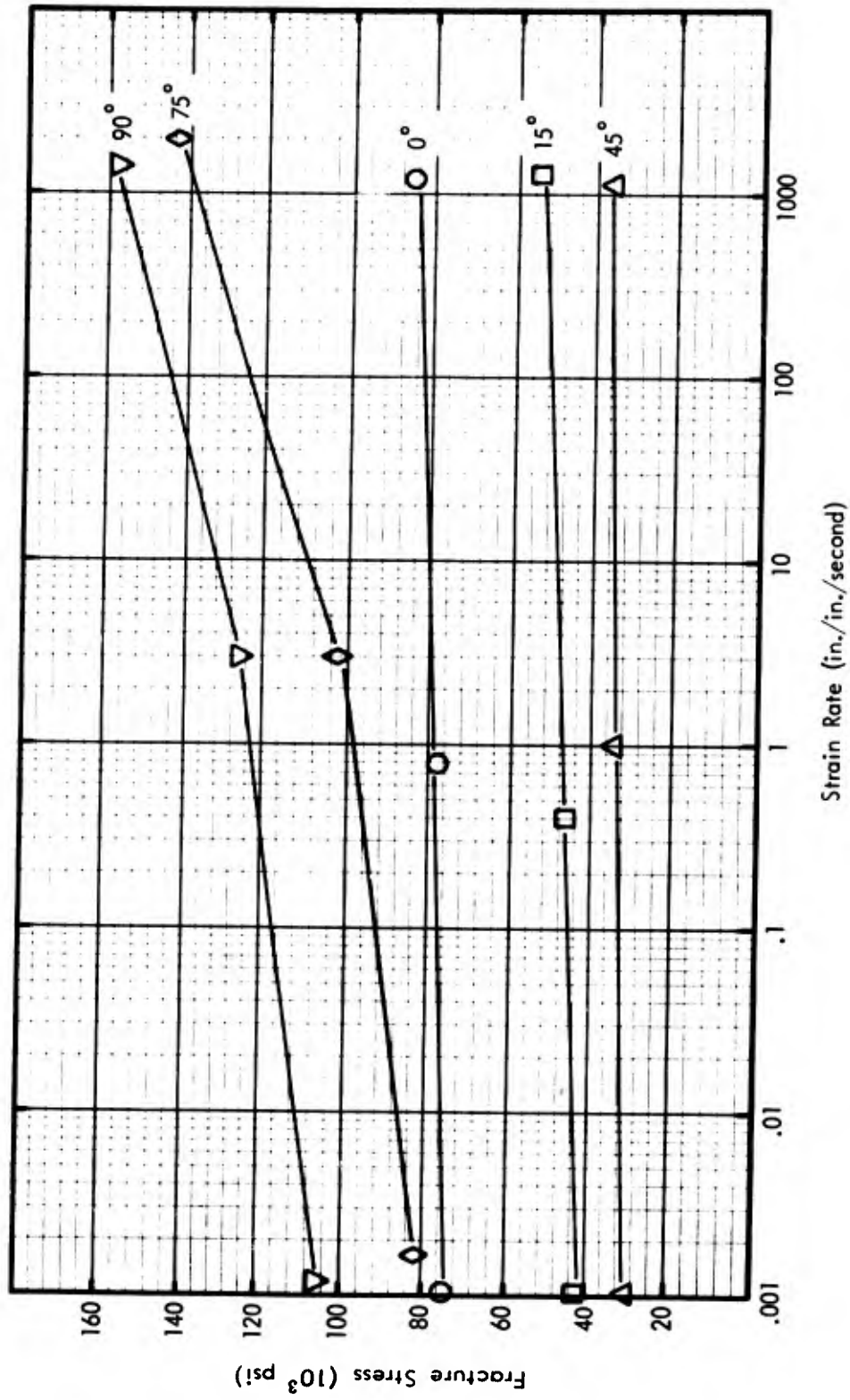


Figure 24 Compressive Behavior of Quartz Phenolic at Various Strain Rates - Fracture Stress vs. Strain Rate

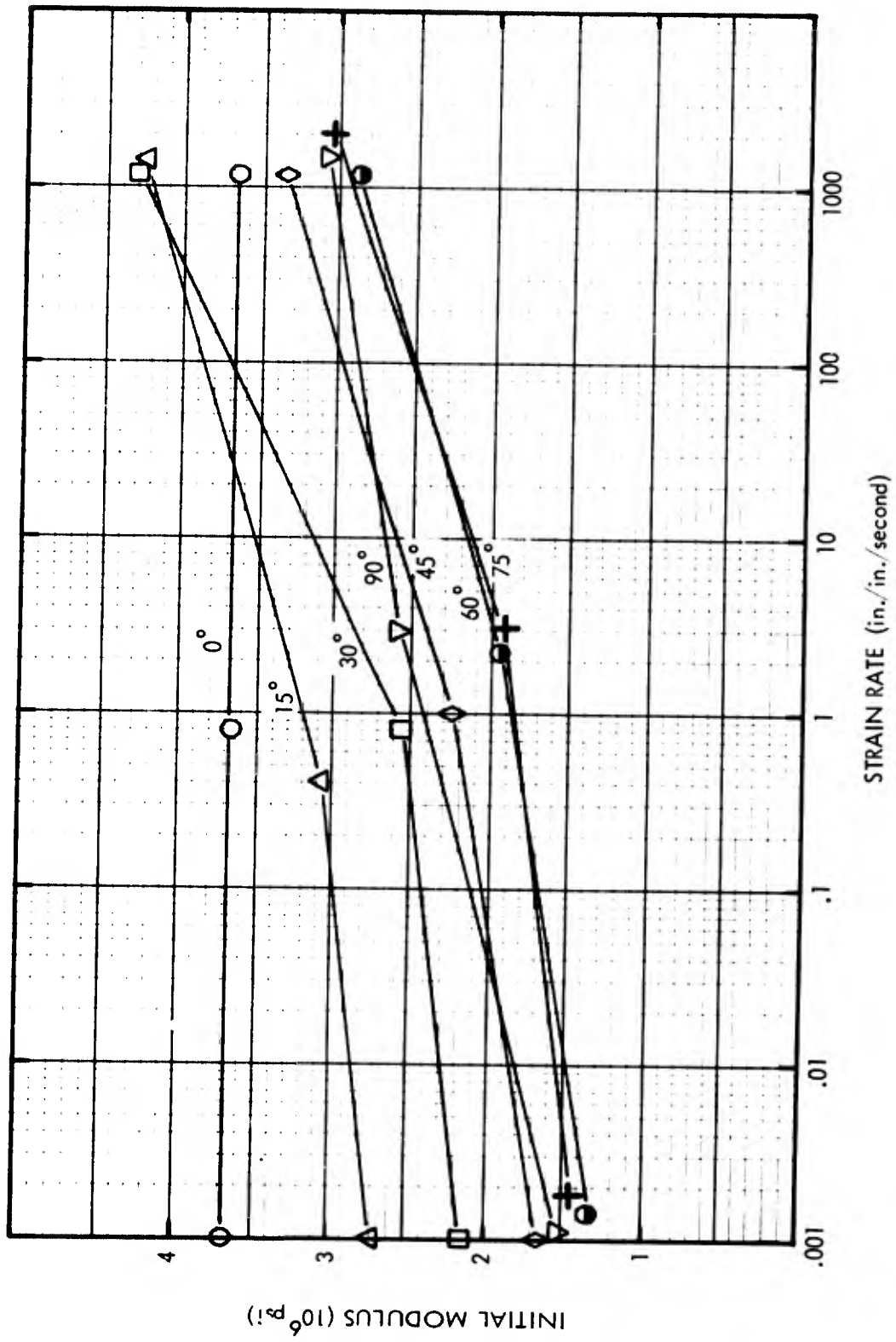


Figure 25 Compressive Behavior of Quartz Phenolic at Various Strain Rates - Initial Modulus vs. Strain Rate

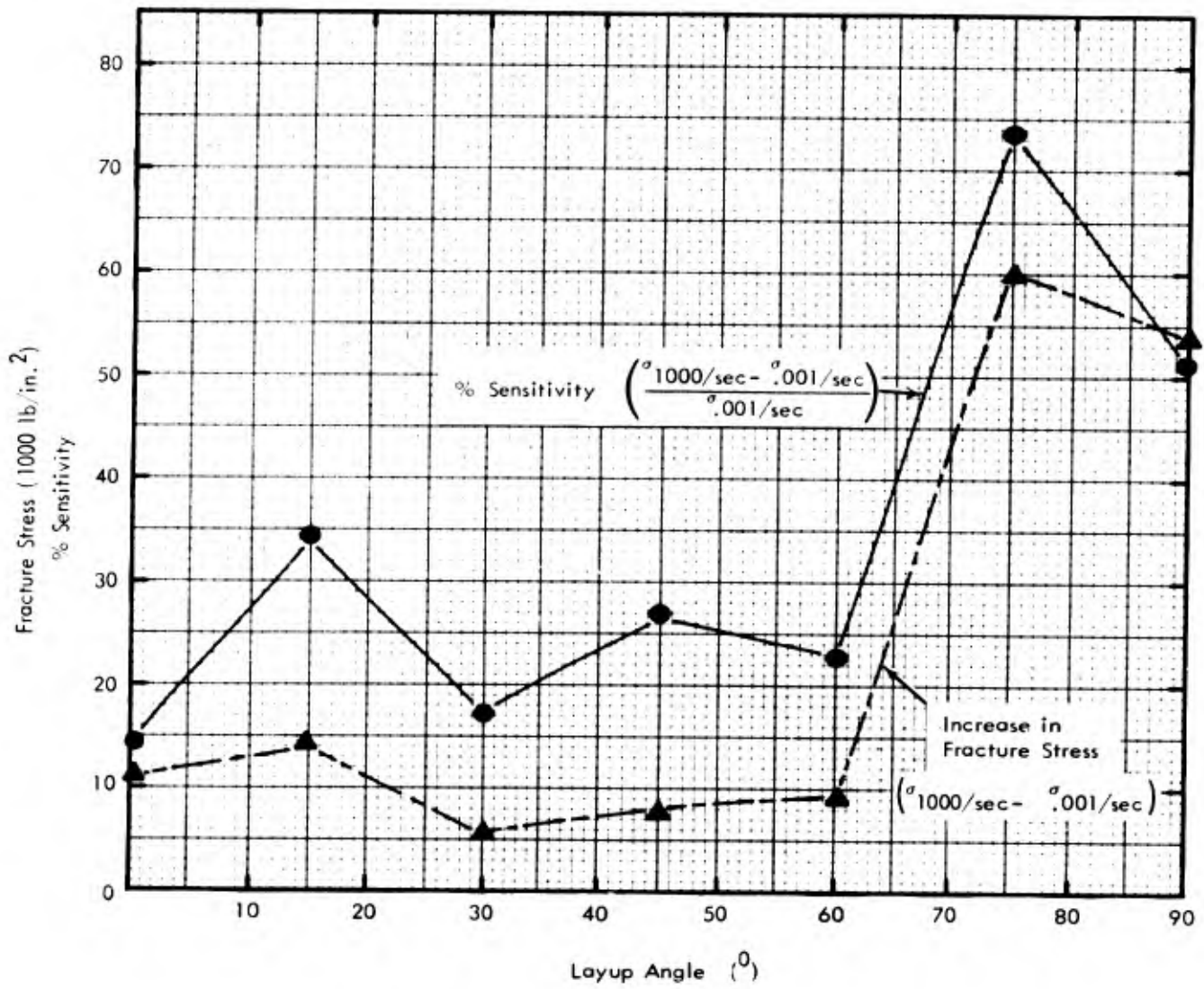


Figure 26 Compressive Strain Rate Sensitivity of Quartz Phenolic at Various Layup Angles

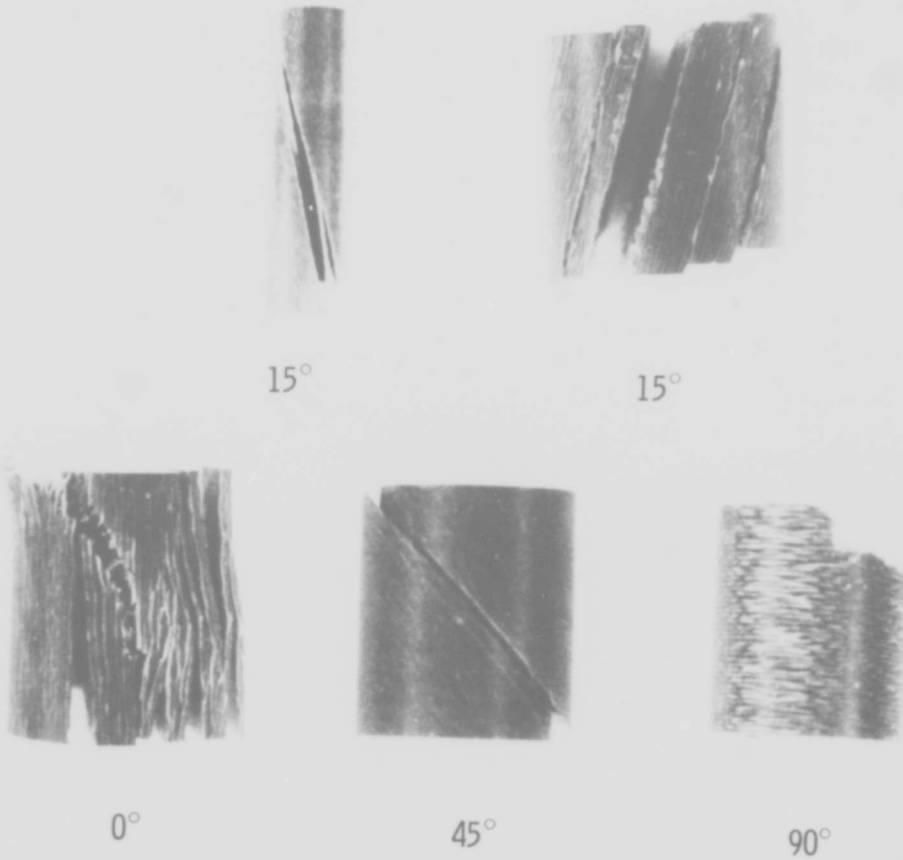


Figure 27 Photograph of Fractured Quartz Phenolic Compression Specimens

post test photographs of compression specimens at 0°, 15°, and 90°. It is clear that while failure was by interlaminar shear at angles from 15° to 75°, a different mode of shear failure occurred at 0° and 90°. A complete discussion of failure mode at various layup angles is included in Volume V of the MARS final report.⁽¹¹⁾ It should be noted that while interlaminar shear failure was predominant at angles from 15° to 75°, failure on the 15° specimen was interrupted by the specimen faces since one complete shear plane could not be made from one side of the specimen to the other, resulting in three pieces instead of two, as shown in FIGURE 27. A series of tests was conducted on 15° layup angle specimens in compression where the length was increased from 0.500 to 1.47 inches. These results indicated approximately a 15% decrease in fracture stress on the longer specimens.

SECTION II
STRAIN-RATE BEHAVIOR AFTER IMPULSIVE LOADING

Reentry vehicles are designed to respond to impulsive loads, generating strain-rate loadings from 10 to 10^8 /second, and survive to respond to subsequent similar loadings. In order to assess the effect of initial impulsive preloading on typical reentry-vehicle materials, this study was conducted. Two types of preloading were investigated; uniaxial-strain preshock and uniaxial-stress preload. The discussion to follow extends the investigation conducted at room temperature⁽³⁾ to elevated temperature. Since the room temperature behavior of quartz and carbon phenolic was similar,⁽³⁾ this study was conducted on quartz phenolic only.

UNIAXIAL-STRAIN PRESOCK

Experimental Technique

Several experimental techniques which have been developed to obtain specimens subjected to a compressive shock passage are discussed in References 3 and 5. Only the techniques used to obtain the data on quartz phenolic reported in Tables I and II will be discussed in this report.

The experimental arrangement, schematically shown in Figure 28, consists of two 0.188-inch diameter by 0.250-inch long right circular cylinders. The first is the specimen to be shocked and the second is the momentum trap to keep reflected tensile waves from entering the specimen. The edge rarefactions are trapped by placing the small cylinders within an annular ring 1 inch outside diameter and 0.188 inch inside diameter. All mating surfaces between the three

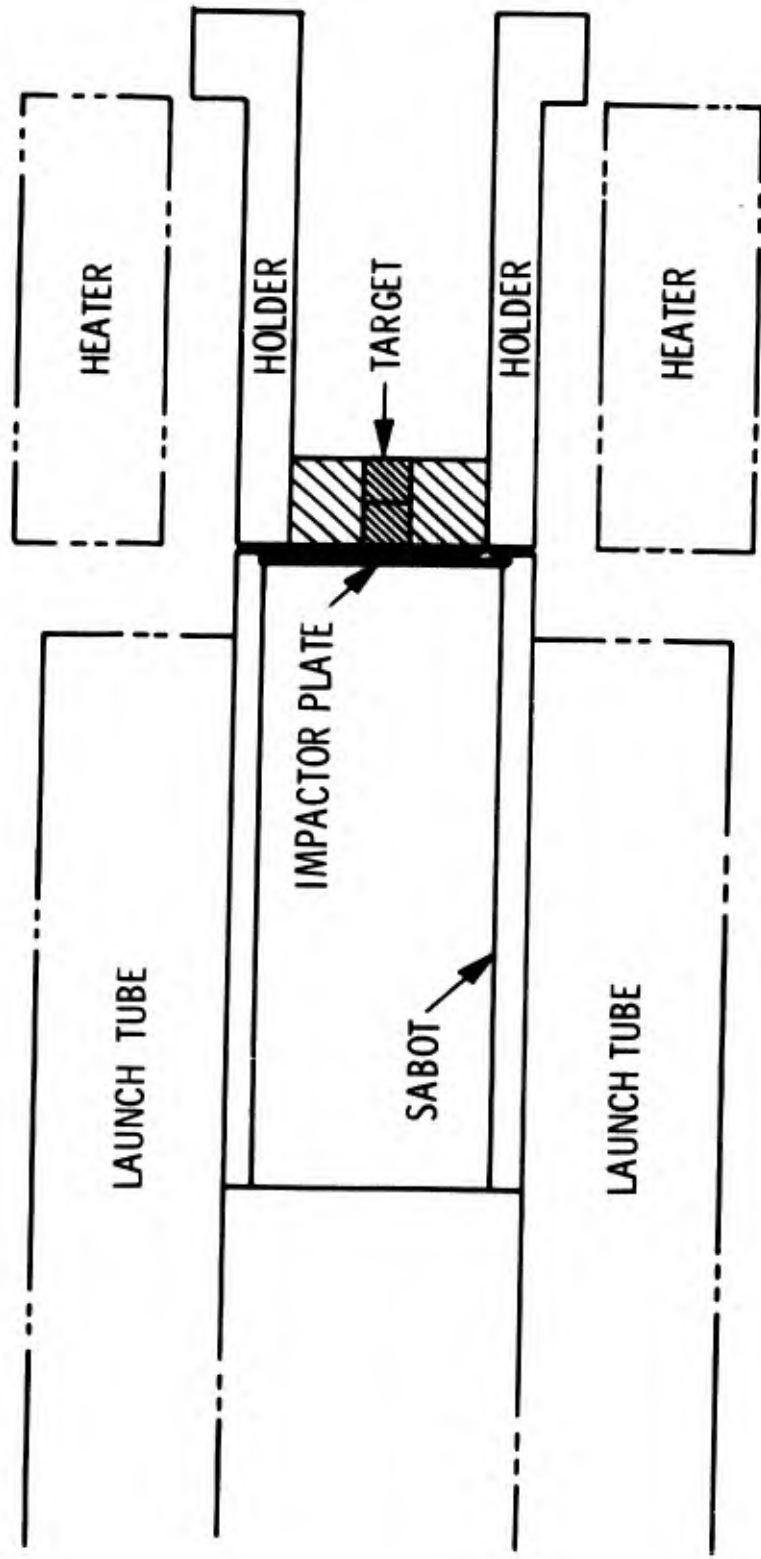


Figure 28 Schematic Diagram of Preshock Experimental Technique

parts composing the target are joined by thin epoxy layers which form a zero tensile strength interface. By using the same material for the specimen as well as the edge rarefaction and momentum traps, the material properties of modulus of elasticity, Poisson's ratio, density, and wave speed are all identical, thereby minimizing the production of unknown waves at the various interfaces.

The assembled target is mounted into a steel holder which not only provides for alignment of the target face with the impactor face but also provides for target recovery. The inside diameter of the holder is just slightly larger than the target diameter, thereby limiting the amount of tumbling of the target after preshocking.

Two types of impactors were used in this study, one of 4340 steel (R_c 38-42) and one of material identical to the target; the impactors were 1.0 inch in diameter and 0.1 inch thick. The transit time for a wave to propagate from the front face, reflect from the rear face, and return to the impact face is 0.87 microseconds for a steel impactor and about 1.5 microseconds for the composite impactor. The impactors are mounted in 1.5 inch diameter light weight plexiglass tubular sabots which are filled with very low impedance foam. The back of the sabots are closed with a plexiglass plate. Figure 29 shows the target and impactor components as used for preliminary tests on plexiglass.

The saboted impactor is launched towards the target from a 1.5 inch bore, 100 inches long, compressed gas gun. The velocities are measured by a photomultiplier velocity system during the last 6 inches of travel in the launch tube. This system is similar to the velocity system

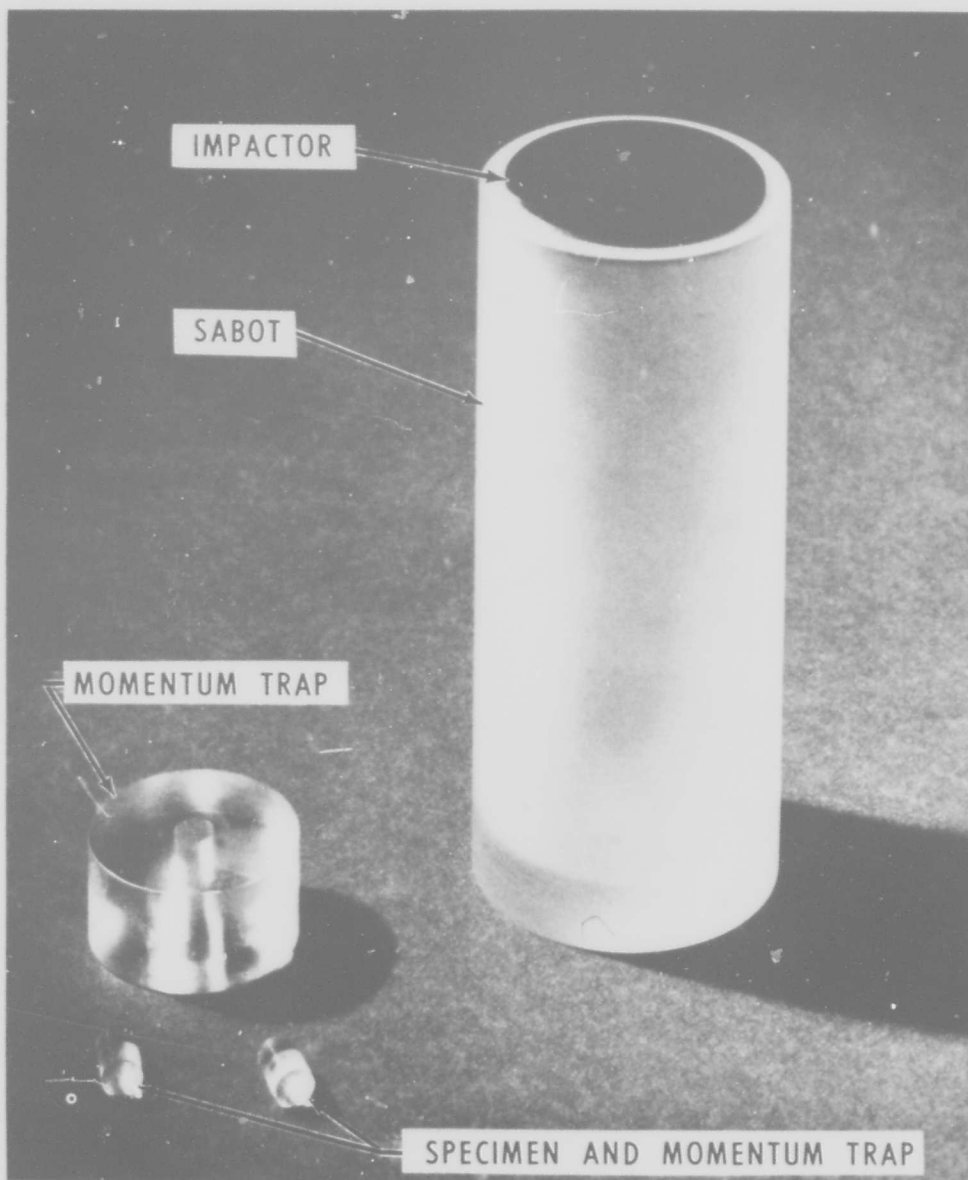


Figure 29 Preshock Target and Impactor Components

described in detail in Reference 12. The impactor chamber, which contains the specimen during impact, is evacuated to about 2 mm of mercury prior to each test.

Specimens are preshocked at elevated temperature by inserting the entire specimen and holder into a radiant heat oven. The oven uses four 500 watt quartz-iodine lamps to bring the specimen to temperature. Temperature gradients through the target were found to be quite small. Therefore the test temperature was measured by a single thermocouple mounted on the rear of the target. The specimen was brought to temperature slowly over a period of about 15 minutes; after preshock the specimen was allowed to cool in the target chamber for another 15 minutes. A photograph of the arrangement for preshock studies at elevated temperatures is shown in Figure 30.

The specimen under shock conditions is in a state of uniaxial strain. In terms of stress, the specimen is loaded in a triaxial state of stress, i.e., a hydrostatic component together with deviatoric stress components as determined by the shear strength of the material. By knowing the equation of state of the target (from Reference 13) and the impactor materials (from Reference 13 and 14) as well as the impact velocity of the impactor, the magnitude of the shock pulse may be determined through the "impedance matching" (13, 15) method. Unfortunately, no equation of state is available for quartz phenolic at elevated temperatures. Therefore, all shock pressures were calculated using the room temperature data.

After the target was shocked, the fracture strength of the material was obtained. Samples were tested in uniaxial-stress

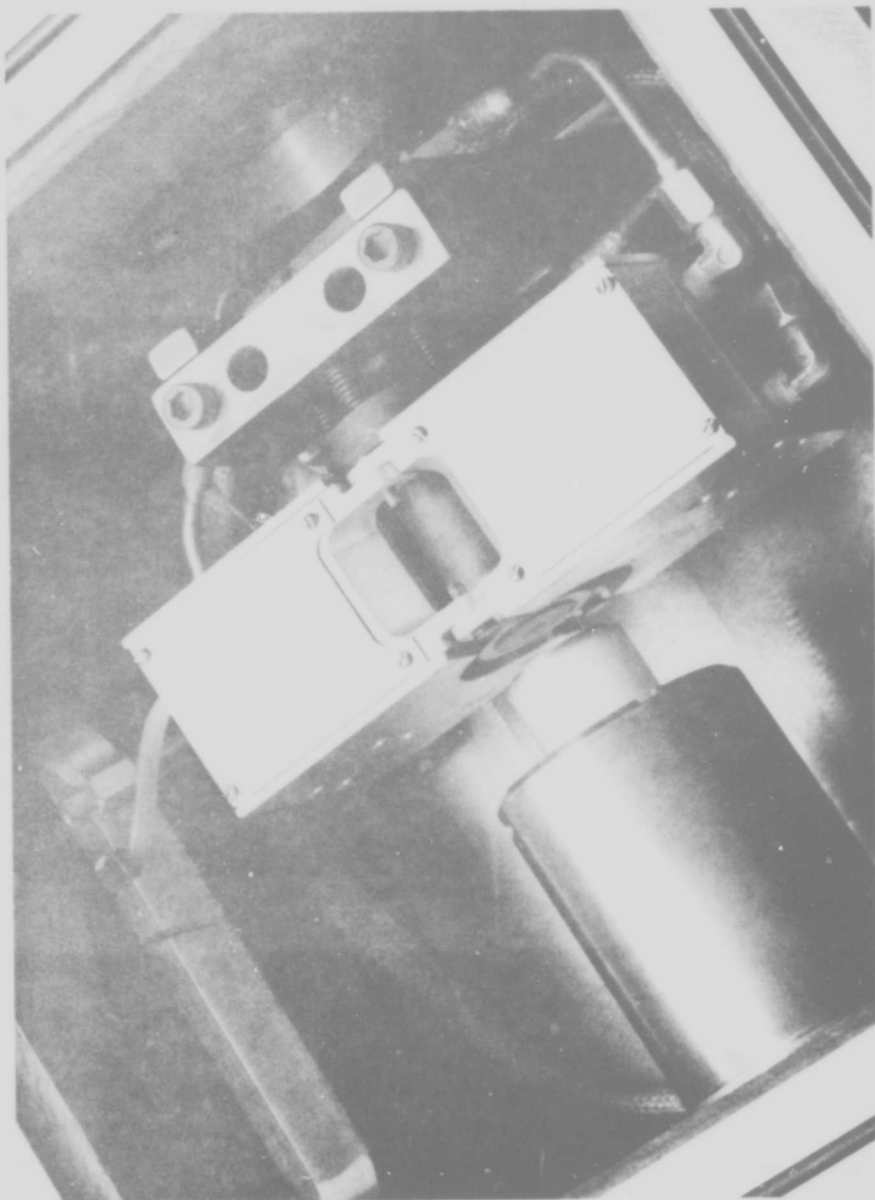


Figure 30 Photograph of Experimental Arrangement for Preshock

compression as shown in Figure 31. Samples with fiber layup perpendicular to the specimen axis were tested in uniaxial-stress tension by bonding the samples with epoxy to metallic grips as shown in Figure 31.

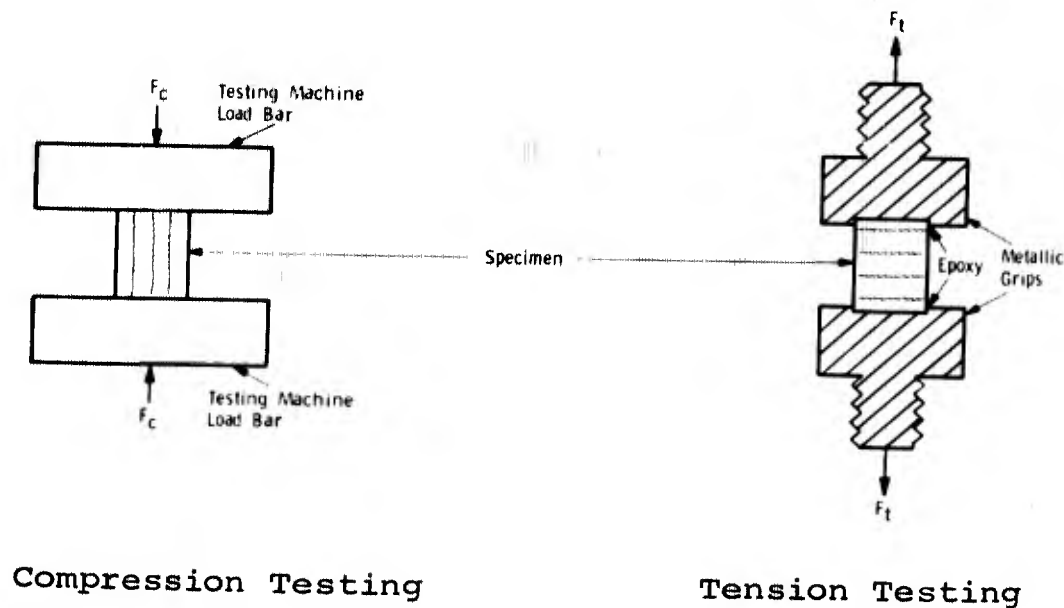


Figure 31 Testing of Preshocked Specimens

Discussion of Results

The experimental results obtained from the study of the pre-conditioning effects by shocking on quartz phenolic are shown in Tables I and II. These tables contain data from the uniaxial-stress loadings which are controlled, or at least affected, by the resin matrix. Selection of these tests resulted from earlier photomicrographic studies which showed cracking of the matrix (Figure 32), but no fiber mat damage, in shocked material. Matrix cracking was found to be independent of the shock direction with respect to the fiber layup.⁽³⁾ Therefore, the conditions in which the fiber mats, rather than the matrix, controlled the fracture

TABLE I

QUARTZ PHENOLIC - FIBER LAYUP PARALLEL TO SPECIMEN AXIS

Test No.	Test Temp °F	Impactor Material	Preshock Material (Kilobars)	Uniaxial Compressive Stress ₂ (lbs/in ²)	Avg. Stress ₂ (lbs/in ²)	Percent Difference From R.T. Norm	Group
A	72	None	None	7.04 X 10 ⁴			
B	72	None	None	5.76 X 10 ⁴			
C	72	None	None	6.10 X 10 ⁴			
D	72	None	None	7.43 X 10 ⁴			
E	72	None	None	7.44 X 10 ⁴	6.44 X 10 ⁴	0	a
F	72	None	None	6.89 X 10 ⁴			
G	72	None	None	6.13 X 10 ⁴			
H	72	None	None	5.07 X 10 ⁴			
I	72	None	None	6.14 X 10 ⁴			
J	600	None	None	5.62 X 10 ⁴			
K	600	None	None	5.49 X 10 ⁴	5.59 X 10 ⁴	-13.4	b
L	600	None	None	5.68 X 10 ⁴			
24	72	4340	13.6	2.30 X 10 ⁴			
25	72	4340	13.6	4.52 X 10 ⁴	3.45 X 10 ⁴	-46.5	c
34	72	4340	15.7	3.52 X 10 ⁴			
35	600	Quartz Phenolic	16.2*	2.11 X 10 ⁴			
36	600	Quartz Phenolic	16.8*	2.24 X 10 ⁴	2.17 X 10 ⁴	-66.5	d
32	72	Quartz Phenolic	13.5	4.81 X 10 ⁴			
33	72	Quartz Phenolic	15.7	5.11 X 10 ⁴			
26	72	Quartz Phenolic	17.1	4.82 X 10 ⁴	5.39 X 10 ⁴	-16.3	e
28	72	Quartz Phenolic	17.6	6.96 X 10 ⁴			
29	72	Quartz Phenolic	17.5	5.24 X 10 ⁴			
7	72	4340	19.1	2.77 X 10 ⁴			
8	72	4340	20.2	2.78 X 10 ⁴			
20	72	4340	20.5	2.16 X 10 ⁴	2.55 X 10 ⁴	-60.5	f
22	72	4340	22.0	2.81 X 10 ⁴			
23	72	4340	19.2	2.22 X 10 ⁴			

* Calculated from room temperature equation of state

TABLE II
 QUARTZ PHENOLIC - FIBER LAYUP PARALLEL TO SPECIMEN AXIS

Test No.	Test Temp °F	Impactor Material	Preshock Material (Kilobars)	Uniaxial Tensile Stress ₂ (lbs/in ²)	Avg. Stress ₂ (lbs/in ²)	Percent Difference From R.T. Norm	Group
M	72	None	None	3.49 X 10 ³	3.52 X 10 ³	0	a
N	72	None	None	3.54 X 10 ³			
9	72	4340	3.75	4.73 X 10 ²	4.38 X 10 ²	-87.5	b
10	72	4340	4.45	5.45 X 10 ²			
11	72	4340	4.10	3.21 X 10 ²			
12	72	4340	4.20	4.11 X 10 ²			
30	72	Quartz Phenolic	3.70	1.61 X 10 ²	1.81 X 10 ²	-94.8	c
31	72	Quartz Phenolic	3.80	2.00 X 10 ²			
15	600	4340	4.40*	6.25 X 10 ²	6.58 X 10 ²	-81.2	d
16	600	4340	4.40*	6.35 X 10 ²			
17	600	4340	4.45*	7.14 X 10 ²			

* Calculated from room temperature equation of state



Figure 32 Photomicrograph Showing Cracks in Resin Matrix in Preshocked Quartz Phenolic

strength were neglected in favor of more thorough studies of the limiting cases: (1) tension with fiber layup normal to the specimen axis where the resin determines the tensile strength; and (2) compression with fiber layup parallel to the specimen axis where the resin matrix helps distribute the load between the fiber mats. Throughout the collected data, variations in fracture stress for a given condition may be found. These variations are a result of partial failure of the wave traps, damage during recovery, material scatter, and loading variations (note that specimens were tested directly after loading without remachining of the end surfaces).

Table I contains the results on material with loading parallel to the fiber layup. For this condition, two sets of control samples were tested: one set was tested as machined from bulk material; the other set was preheated to 600°F over a period of 15 minutes, then oven cooled in order to simulate only the temperature effects on the specimens preshocked at temperature. This simulation was necessary as micrographic studies showed that this type of temperature cycling tended to crack the phenolic, thereby degrading the material's mechanical strength much like the effects of a preshock. (3)

Observing the column "Percent Difference from Room Temperature Norm," it is seen that two sets of conditions produce similar degradation; namely, elevated temperature control samples and the specimens shocked to about 17 kilobars at room temperature with a quartz phenolic impactor. The former group (b) exhibited about -13% deviation and the latter group (e) about -16%. For comparison, a second set are targets shocked at 600° to about 16 kb with a quartz

phenolic impactor and those shocked at room temperature to about 20 kb with a steel impactor. The former group (d) exhibited about -66% deviation and the latter group (f) about -60%.

For groups (b) and (e) the strength degradation is a result of the cracked matrix not being able to distribute the load between the fiber mats. Groups (d) and (f), however, show more extensive effects of preconditioning. From the above results, it appears that these groups underwent more extensive degradation of the matrix than groups (b) and (e) as well as possible fiber bundle damage. While the cracks from groups (b) and (e) were produced only by thermal cycling and compressive shock loadings, respectively, cracking from untrapped tensile waves is the probable cause for strength degradation of specimen groups (d) and (f). These tensile waves result from impedance mismatch* between the target and the impactor. For group (f) the mismatch was the result of using a higher impedance steel impactor, resulting in higher shock pressures being generated at lower impact velocities. For group (d), however, the mismatch resulted from the target being at elevated temperature and the impactor at room temperature.

When similar materials are impacted, the unloading wave from the rear surface of the impactor, which is equal in magnitude and opposite in sign to the generated wave in the target, is totally transmitted into the target thereby unloading it. However, for mismatched systems (assuming the impactor is of greater impedance than the target) the same factors which allow higher target pressures at lower impact velocities (Figure 33a) produce only partial transmittal of the unloading wave into the

* Impedance here is defined as ρc where ρ is the density and c is the wave speed. The impedance is the slope of the Hugoniot on the pressure-particle velocity plane. This definition applies to a "linearly elastic" material such as quartz phenolic.

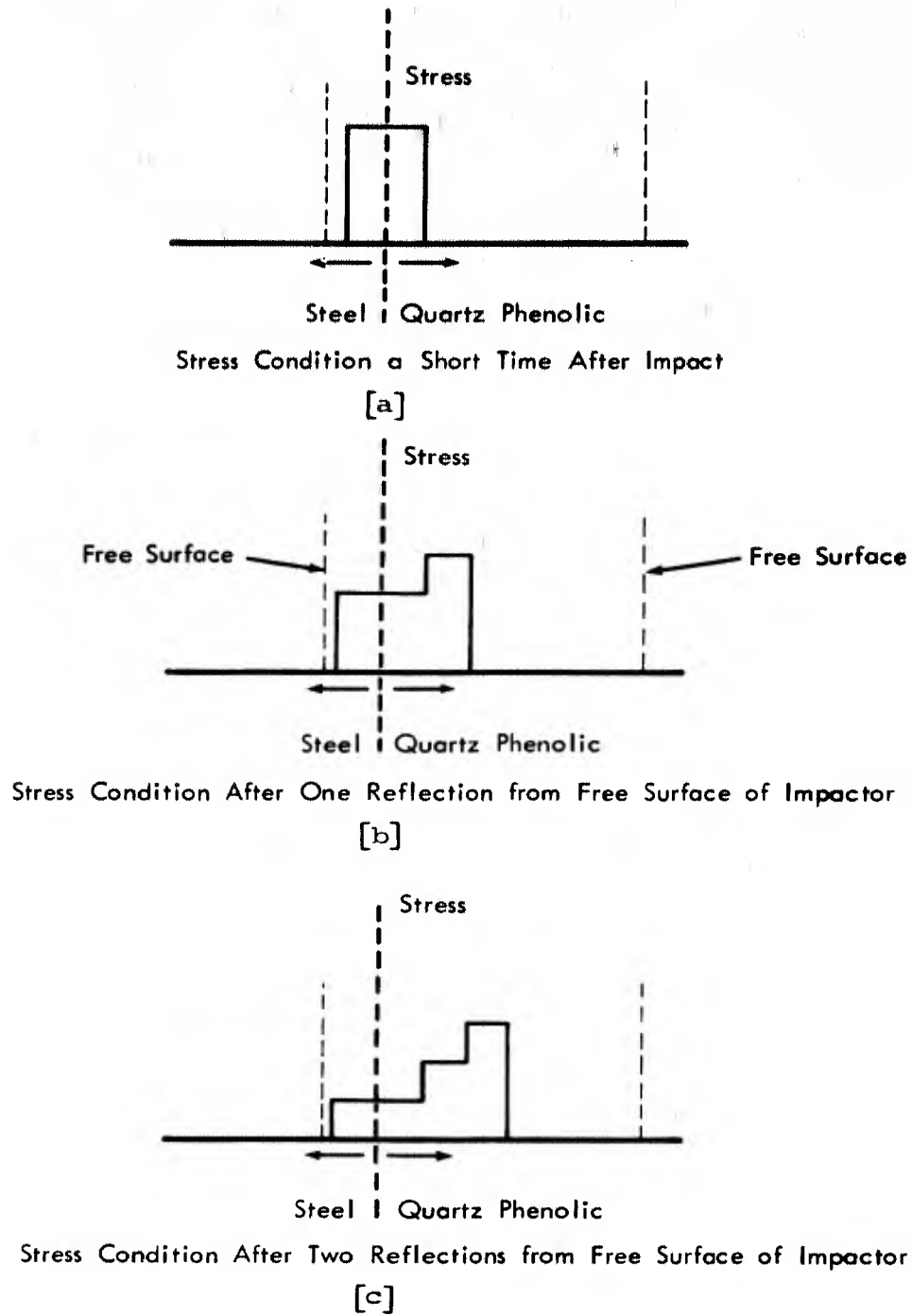


Figure 33 Diagram of Stepped Release Wave in Target - Impactor System with Mismatched Impedances

target for each reflection at the impactor-target interface (Figure 33b, 33c).

Therefore, the point in the target at which the resultant from the loading wave and the wave reflected from the rear surface become tensile may be inside the specimen and not inside the momentum trap (which is thrown off when a resultant tensile wave cannot cross the specimen-momentum trap interface). Furthermore, even if the resultant becomes tensile in the momentum trap (thereby trapping the primary source of longitudinally propagating tensile waves), trapped compressive waves from the "tail" of the loading wave will reflect from the target rear surface producing trapped waves which continue to degrade the material.

Shock-wave produced matrix cracking in quartz phenolic resulted in large tensile strength degradation when loaded normal to the fiber layup (Table II). For this condition the tensile strength is essentially dependent upon the matrix, and if this matrix is cracked extreme strength degradation occurs.

From this preshock study, it has been found that if a fiber-reinforced composite is exposed to a single compressive shock wave and subsequently completely unloaded, the uniaxial-stress compressive strength when loaded parallel to the fiber layup will be decreased by about 15 to 20%. Under shock loading with gradual stepped unloading, compressive strength degradation up to 60 to 70% will result for this layup. Regardless of the shock profile, the uniaxial tensile strength when loaded normal to the fiber layup will exhibit 80 to 90% degradation. Although compressive strengths loaded normal to the fiber layup and tensile

strength loaded parallel to the fiber layup were not determined, the strength degradation should be less than 15 to 20% because, for these layups, the material strength is primarily dependent upon the undamaged fiber mats.

UNIAXIAL-STRESS PRELOAD

Experimental Techniques

The study of material damage caused by an initial high strain-rate loading at room temperature below the fracture stress (milliseconds in duration) was reported in Reference 3. The results discussed in this report extend the study to elevated temperature.

Specimens were heated in the furnace attached to the medium strain-rate machine, described in Appendix B. In order to eliminate potential problems induced by thermal cycling and minimize the effects of time-at-temperature, specimens were heated to 600°F in approximately seven minutes, loaded to a strain level below fracture, unloaded, then reloaded to fracture without any variation in temperature. The total length of time to perform the experiment was approximately ten to twelve minutes. This technique was very difficult to perform because of the many mechanical operations involved, thus many preliminary tests were performed to perfect the procedure. Other specimens under identical conditions were fractured on the first loading. Stiffness and strength were compared for the two loading conditions to assess the preload damage.

As an assist in determining preload damage, specimens subjected to initial loadings below ultimate fracture strain, then removed from the machine without reloading, were

sectioned and photomicrographically analyzed. Correlation was then attempted between micrographic observations and data from identical specimens loaded a second time to fracture.

Discussion of Results

The initial study on uniaxial-stress compressive preload damage at room temperature⁽³⁾ determined that preloads to about 50-70% of fracture stress produced phenolic cracking but only slight degradation (maximum of about 10%). In this study, room temperature tests on quartz phenolic were extended to preloads of about 90% of fracture strength and to 600°F.

Figures 34 and 35 show the room temperature compression test results obtained for loadings normal and parallel to the fiber layup respectively. The results for this year's study are shown in addition to the results from Reference 3. In Figure 34 the results of initial loadings up to 70% of fracture stress at 1.5 to 2.5/sec are shown for two lots of quartz phenolic. Although the results differ slightly (due to different lots and manufacturers), only slight degradation in strength (about 5%), and essentially no degradation in stiffness, was obtained on the second loading to fracture. Data for initial loading to fracture at 10^{-3} /sec are shown for comparison purposes.

Figure 35 shows the results for room temperature compressive loading parallel to the fiber layup. While Reference 3 results indicated that an initial medium strain-rate loading (0.4/sec) to 77% of fracture stress produced little stiffness or strength degradation upon reloading at the same strain rate, this year's results show that an initial loading

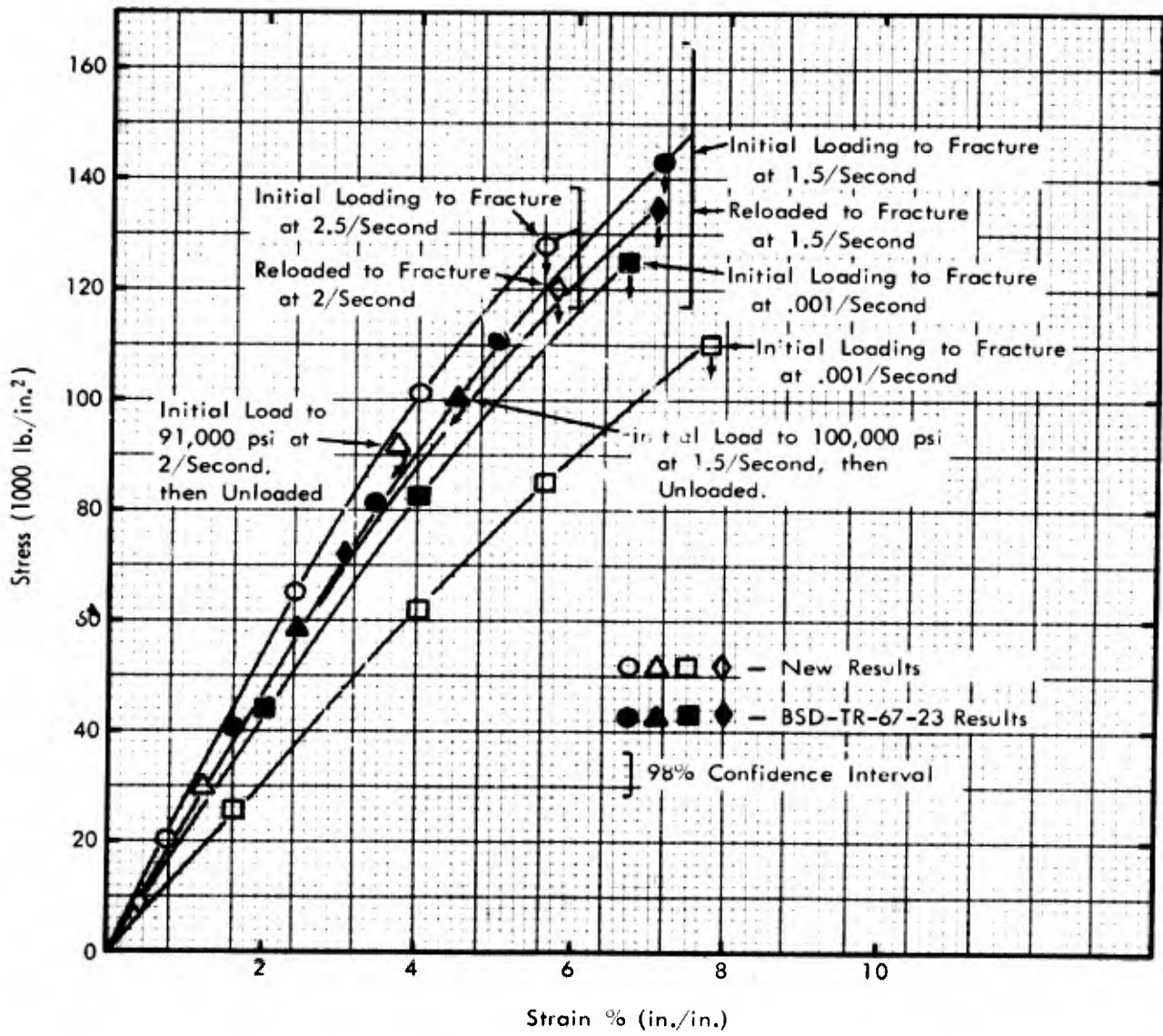


Figure 34 Prefracture Damage Study on Quartz Phenolic, Compressive Loading Normal to Layup - 72°F

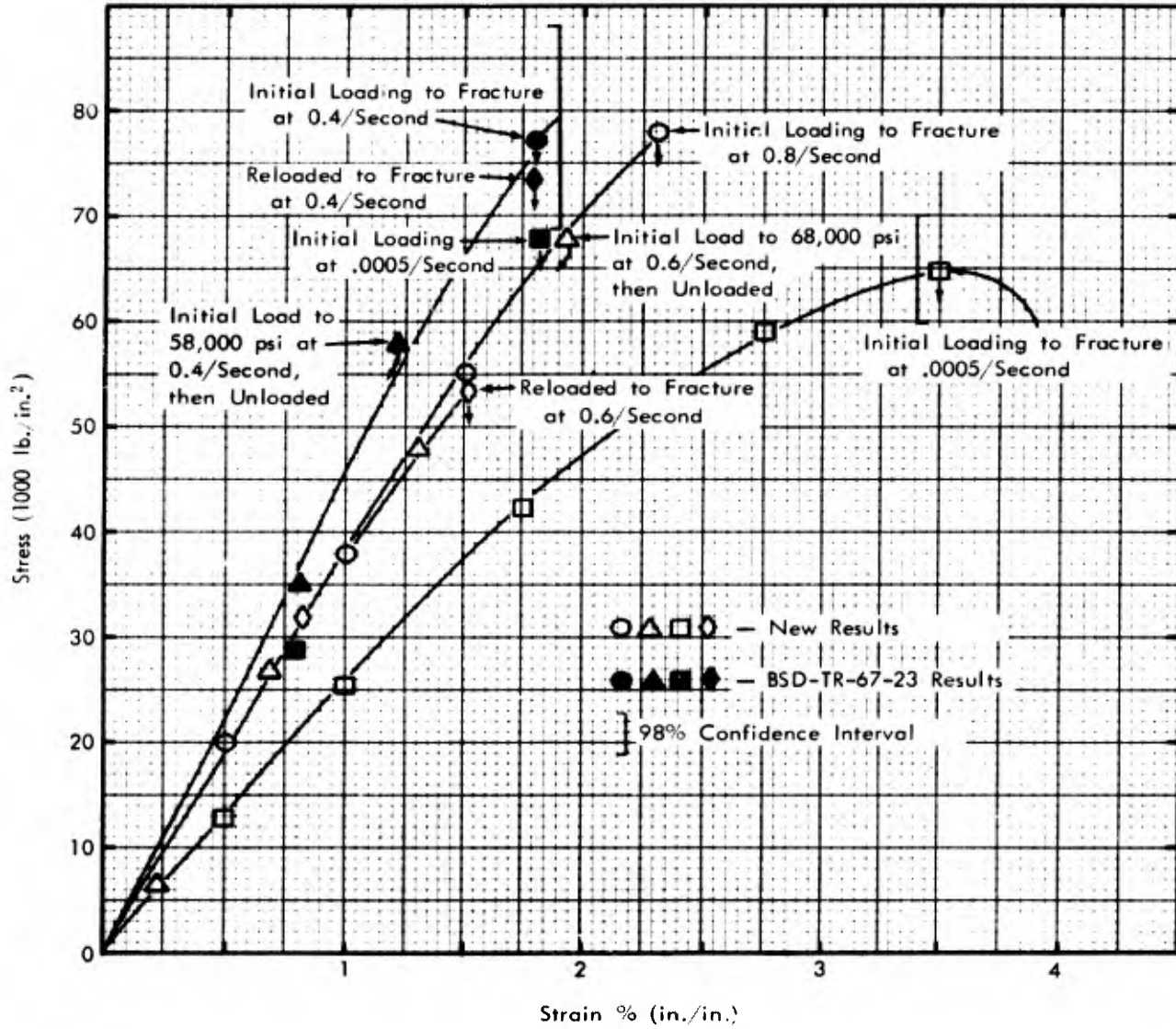


Figure 35 Prefracture Damage Study on Quartz Phenolic, Compressive Loading Parallel to Layup - 72°F

to 88% of fracture stress at 0.6/sec produces about a 30% degradation in strength on a second loading with no change in stiffness. Initial loading to fracture curves at 5×10^{-4} /sec are included in Figure 35 to show the difference in behavior between the two lots of material tested. Photomicrographs of specimens loaded to 88% of fracture stress, without reloading, show small cracks propagating across fiber bundles (Figure 40).

Figure 36 shows the results of tests on material with fiber layup normal to the axis of loading to 58% of fracture stress at a rate of 2/sec at 600°F. No degradation on second loadings to fracture was observed. Photomicrographs of a specimen loaded to 58% of fracture stress at 600°F are shown in Figure 39. In Figure 37 the results of initial loading to 62% of the compressive fracture strength at 600°F are shown for loadings parallel to the material layup. Second cycle loadings produced strength degradation of 66%. Figure 40 shows photomicrographs of a specimen loaded to 62% of fracture stress at 600°F.

The test results for loading quartz phenolic in tension at 600°F parallel to the fiber layup are shown in Figure 38. Room temperature tests for this layup⁽³⁾ showed initial loadings to 75% of fracture stress at 5×10^{-4} /sec and to 63% of fracture stress at 5×10^{-1} /sec produced no degradation on loading to fracture at the same rate. Figure 38 shows that at 600°F, initial loadings at 1/sec to 86% of fracture stress produced approximately 25% degradation in fracture strength after reloading to fracture at the same rate. No stiffness degradation was observed. As reported in Reference 3, tension tests on quartz phenolic with layup normal to the loading axis was impossible to conduct due to

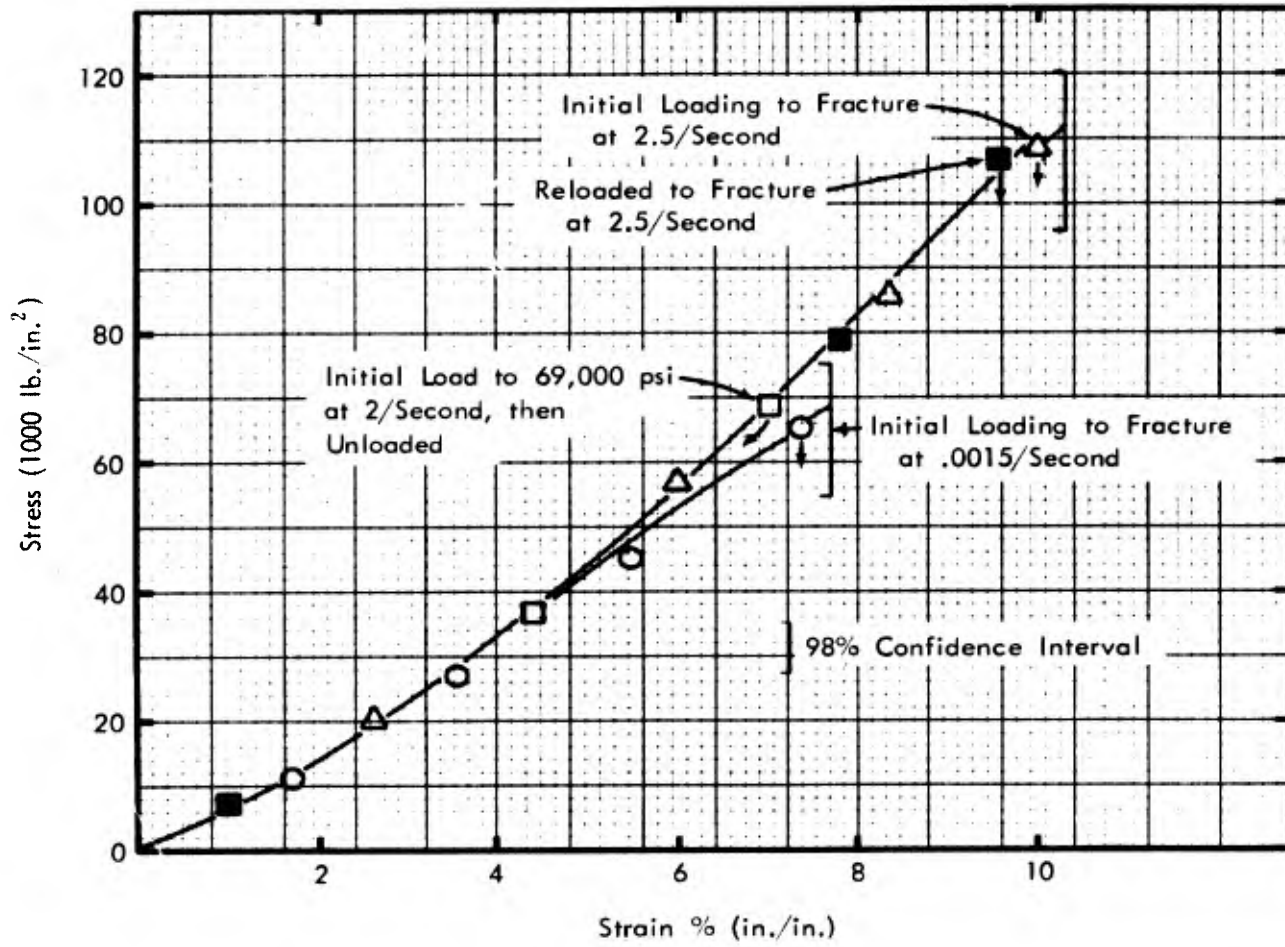


Figure 36 Prefracture Damage Study on Quartz Phenolic, Compressive Loading Normal to Layup - 600°F

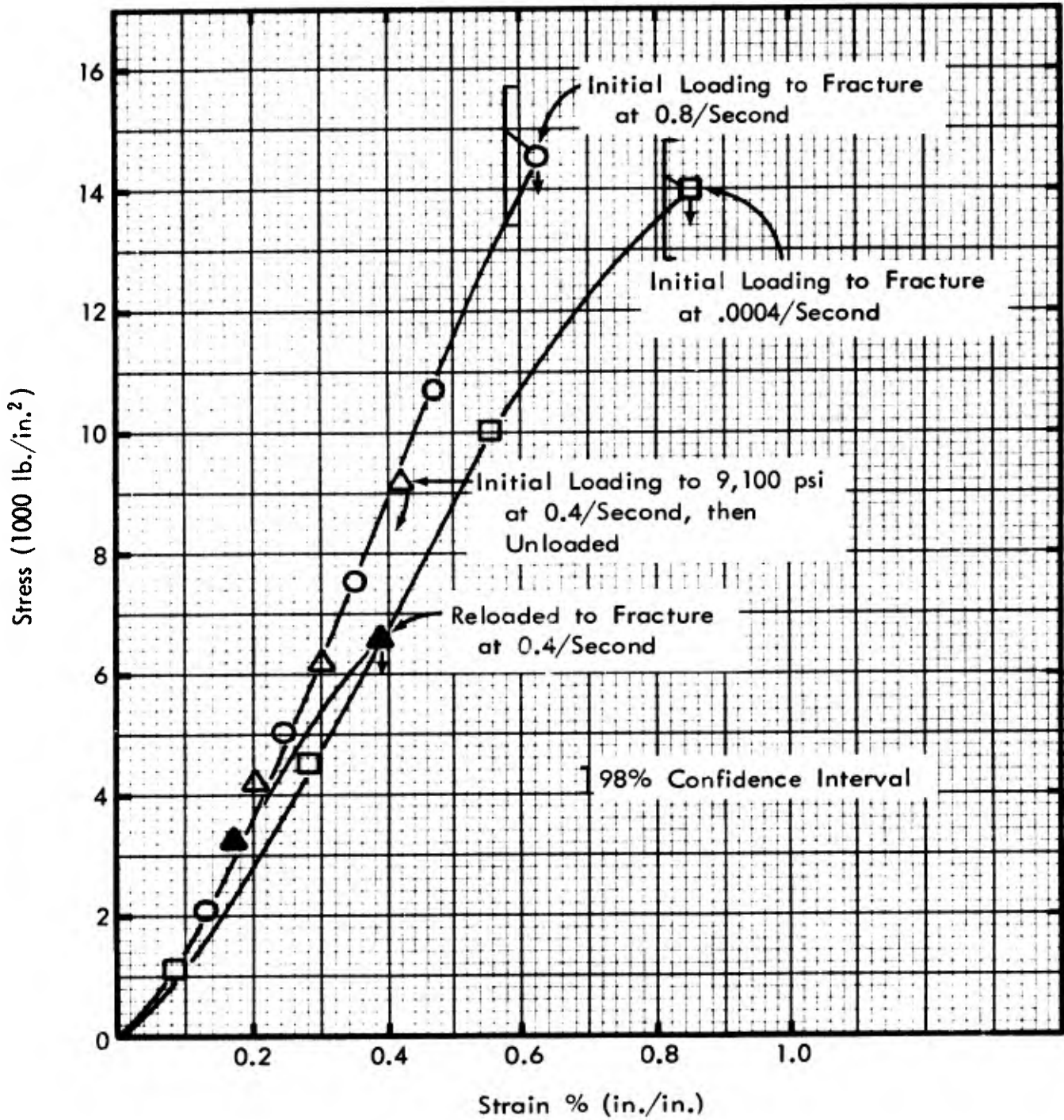


Figure 37 Prefracture Damage Study on Quartz Phenolic, Compressive Loading Parallel to Layup - 600°F

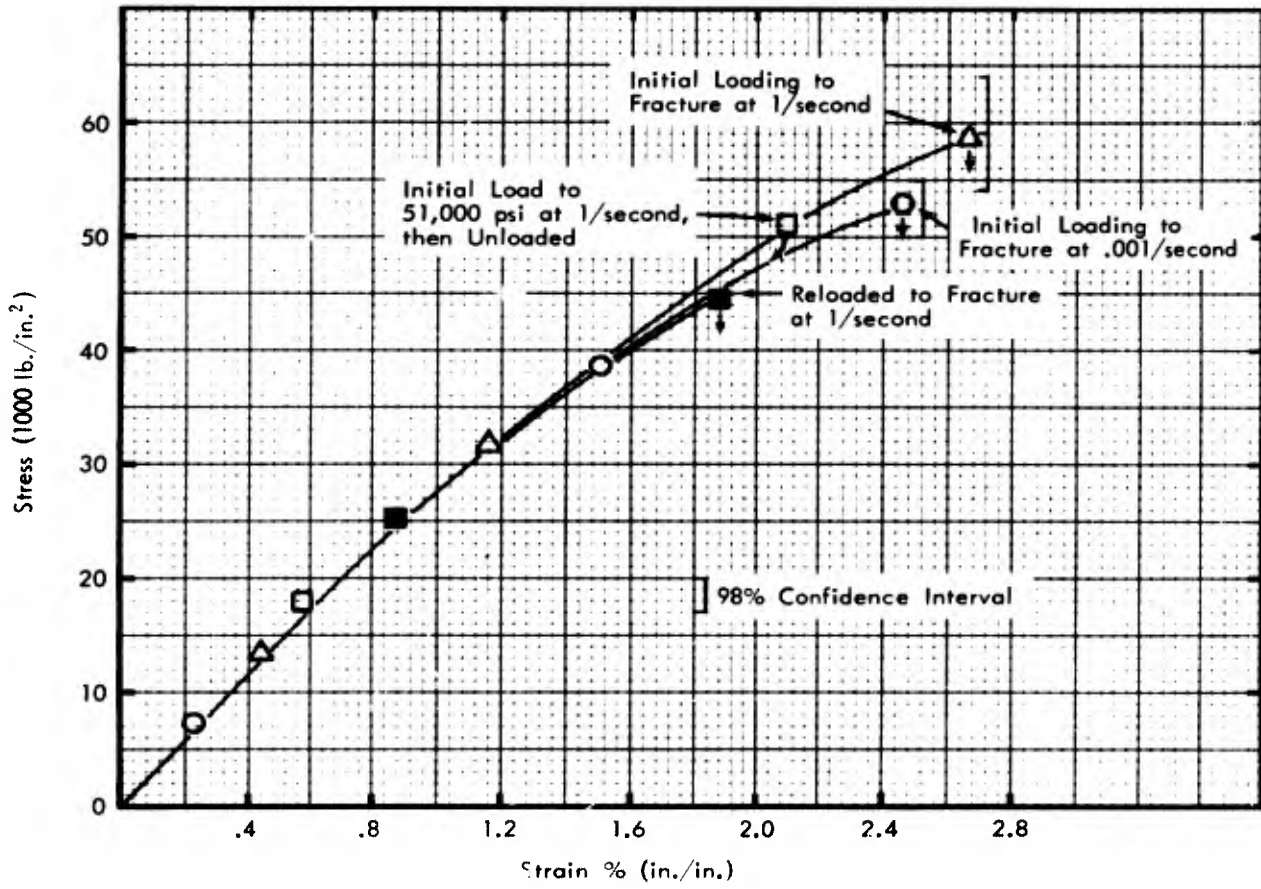


Figure 38 Prefracture Damage Study on Quartz Phenolic, Tensile Loading Parallel to Layup - 600°F



60 x

Direction of Loading
Normal to Paper



60 x

Direction of Loading



Specimen Loaded to 58% of Fracture
Stress at 2/Second - 600 °F

Figure 39 Photomicrographs of Quartz Phenolic After Loading in Compression Normal to Fiber Layup



60 x

Direction of Loading Normal To Paper



60 x



60 x

↑
Direction of Loading
↓



60 x

Specimen Loaded to 62% of Fracture Stress at 0.6/Second - 600°F

Specimen Loaded to 88% of Fracture Stress at 0.6/Second - 72°F

Figure 40 Photomicrographs of Quartz Phenolic After Loading in Compression Parallel to Fiber Layup

the very weak strength and brittleness of this layup. From previous tests and tests conducted in the preshock damage study, large degradations in strength would be expected if the phenolic matrix was damaged by preloading.

To investigate the response of composite materials to initial high strain-rate loadings below fracture, several factors must be considered. Among these factors include the effects of rate of loading and related relaxation characteristics of the material and the effect of the temperature environment on the material including heating rate and time-at-temperature.

As discussed in Reference 3, the problem of relaxation must be considered if the characteristic material relaxation times are short compared to the times of loading of the tests. Results from high strain-rate tension and compression tests on quartz phenolic indicated relaxation takes place when loading to a stress below fracture. For loading times of 30 to 45 milliseconds, relaxation times in the order of 5 to 15 milliseconds have been observed, the shorter relaxation times being associated with higher stress levels. For high strain-rate loadings both normal and parallel to the fiber layups, fracture always occurred after a finite relaxation time if the static fracture strength was exceeded. For this reason (i.e. the machine unloading time was long compared to the relaxation time of the material) no specimens were obtained which had been preloaded above the static fracture stress.

The effect of temperature environment on the observed behavior of quartz phenolic was minimized in this study by heating specimens at relatively slow rates (about 60°F/minute),

eliminating cool-down between initial loadings and subsequent reloadings to fracture, and minimizing the total time at temperature.

In general the following characteristics are observed for quartz phenolic. At room temperature, compressive high strain-rate loadings to about 88% of fracture stress produced about 30% degradation in fracture strength when loaded parallel to the fiber layup. For compressive loadings normal to the fiber layup only slight degradation in strength and no change in stiffness was observed. Tensile room temperature loadings parallel to the fiber layup below 75% of fracture stress produced no degradation. At 600°F, high strain-rate compressive loadings parallel to the fiber layup above 60% of fracture stress produced degradation of about 66% on reloading to fracture. Loadings normal to the fiber layup in compression at high strain-rate up to static fracture stress produced no degradation at temperatures up to 600°F. High strain-rate tensile loading parallel to the fiber layup at 600°F above 85% of fracture stress produced about 25% degradation. Tension tests normal to the fiber layup could not be conducted due to the weakness of the material in this direction; however, cracking of the phenolic matrix should highly degrade the tensile strength of this layup.

Throughout this study, as in the uniaxial-strain preshock study, the strengths of composite materials are most affected when the fracture mode is dependent upon the phenolic matrix; i.e., compression loadings parallel to the fiber layup and tension loadings normal to the fiber layup. For conditions which the fiber mats provide the primary strength influence, i.e. compression normal to the fiber

layup and tension parallel to the fiber layup, preload studies show little influence of the cracked phenolic. In all cases, specimens could not be preloaded to stresses above the static fracture stress because the machine unloading times were long relative to the relaxation times of the material.

Although both parts of this impulsive loading study concentrated on quartz phenolic, the basic findings may be extended to other fiber-reinforced composites. The magnitudes of strength degradation, however, will depend on the influence of the resin matrix on the strength of each composite.

SUMMARY

1. Large material scatter observed in this study points out the requirements for improved material fabrication techniques in order to reliably apply the results from these tests to design problems. Nevertheless, this study has shown that temperatures up to 600°F cause considerable degradation in heat shield structural characteristics.
2. Although not simple orthotropic composites, present candidate two-dimensional heat shield composite mechanical behavior can be predicted using existing theoretical relationships.
3. Fiber reinforced phenolic heat shield materials preconditioned by a compressive shock wave loading exhibit subsequent mechanical degradation depending on the direction and temperature of loading. Room temperature uniaxial-strain preshocks up to 20 kilobars produce 15-20% uniaxial-stress compressive strength degradation when preshocked and completely unloaded then subsequently loaded parallel to the fiber layup. When partial unloading occurs or the test temperature is increased to 600°F, 60-70% degradation can result for this loading direction. Tensile strength degradation when loaded normal to the fiber layup after 4 - 5 kilobar preshock pulses approaches 95% regardless of test temperature.
4. Room temperature uniaxial-stress loadings at strain rates near 1-10/sec up to 90% of the "static" (10^{-3} /sec)

fracture strength produces no degradation on future loadings. Higher loadings produce noticeable degradation depending on how near to the "static" fracture strength the load terminates. Elevated temperature (600°F) produces greater degradation for similar loadings only where the matrix tensile strength plays a role in failure, compression parallel to the fiber layup and tension normal to the fiber layup.

REFERENCES

1. C. J. Maiden and S. J. Green, "Response of Materials and Structures to Suddenly Applied Stress Loads," Interim Report on DASA Contract DA-49-146-XZ-322, General Motors Defense Research Laboratories TR 65-69, DASA-1716, October, 1965.
2. S. G. Babcock, A. Kumar, and S. J. Green, "High Strain-Rate Properties of Eleven Reentry-Vehicle Materials at Elevated Temperatures," Part I of Final Report for DASA Contract DA-49-146-XZ-322, AFFDL-TR-67-35, Part I (AD 813-880), April, 1967.
3. S. J. Green, S. G. Babcock, and R. D. Perkins, "Fundamental Material Behavior Study, Vol. 1: Response of Several Reentry - Vehicle Materials to Impulsive Loads," Final Report for Air Force Contract AF 04-(694)-807, BSD Report TR-67-23 (AD-822 803L), February, 1967.
4. S. J. Green and R. D. Perkins, "Material Response Studies (MARS)," Semi-annual Report on Air Force Contract FO 4794 67-C-0033 (SAMSO), General Motors Manufacturing Development Report TR-70021-1, July, 1967.
5. S. J. Green, et al., "Interim Progress Report on Fundamental Material Behavior Study," GM Defense Research Laboratories Report TR-66-61; also BSD-TR-66-398, October, 1966.
6. O. Hoffman, "The Brittle Strength of Orthotropic Materials," Journal of Composite Materials, Vol. 1, April, 1967, p. 200.
7. S. G. Lekhnitskii, Theory of Elasticity of an Anisotropic Body, San Francisco, Holden-Day, 1963.
8. R. F. S. Hearmon, Applied Anisotropic Elasticity, Oxford University Press, 1961.
9. A. E. H. Love, A Treatise on the Mathematical Theory of Elasticity, Dover Publications, 1944.
10. B. M. Lempriere, "Uniaxial Loading of Orthotropic Materials," AIAA Journal, Vol. 6, No. 2, February 1968, p. 365.

11. A. Kumar, R. D. Perkins, F. L. Schierloh, and D. L. Holt, "Dynamic Behavior of Polymers and Composites," Volume V of Material Response Studies (MARS) Final Report, SAMSO TR 68-71, January, 1968.
12. R. L. Warnica and J. A. Charest, "Final Report on Fundamental Material Behavior Study, Vol. II: Spallation Thresholds of Quartz Phenolic," GM AC Electronics-Defense Research Laboratories Report TR 67-07, Vol. II; also BSD-TR-67-24, Feb. 1967.
13. W. M. Isbell, N. Froula, and F. H. Shipman, "Final Report on Fundamental Material Behavior Study, Vol. III: Shock Wave Propagation and Equation of State Measurements of Quartz Phenolic," GM AC Electronics - Defense Research Laboratories Report TR 67-07, Vol. III; also BSD-TR-67-25, Feb. 1967.
14. B. M. Butcher and J. R. Canon, "Influence of Work-Hardening on the Dynamic Stress-Strain Curves of 4340 Steel," AIAA Journal, 2,2174, 1964.
15. G. E. Duvall and G. R. Fowles, Shock Waves, (Chapter 9), High Pressure Physics and Chemistry, Vol. 2, edited by R. S. Bradley, Academic Press, New York, 1963.
16. D. S. Clark and D. S. Wood, "The Time Delay for the Initiation of Plastic Deformation at Rapidly Applied Constant Stress," Proc. of the ASTM, Vol. 49, 1949.
17. J. D. Campbell and K. J. Marsh, "The Effect of Grain Size on the Delayed Yielding of Mild Steel," Philosophical Mag., Vol. 7, No. 78, June, 1962.
18. R. H. Cooper and J. D. Campbell, "Testing of Materials at Medium Rates of Strain," Journal of Mech. Eng. Science, Vol. 9, No. 4, 1967, p. 278.
19. H. Kolsky, "An Investigation of the Mechanical Properties of Materials at Very High Rates of Loading," Proc. of the Physical Soc., Vol. 62, 1949.
20. J. D. Campbell and J. Duby, "The Yield Behavior of Mild Steel in Dynamic Compression," Proc. of the Royal Society A, Vol. 236, 1956.
21. J. M. Krafft, A. M. Sullivan, and C. F. Tipper, "The Effect of Static and Dynamic Loading and Temperature on the Yield Stress of Iron and Mild Steel in Compression," Proc. of the Royal Society A, Vol. 221, 1954.

22. C. J. Maiden and J. D. Campbell, "The Effect of Impact Loading on the Static Yield Strength of a Medium-Carbon Steel," Philosophical Mag., Vol. 3, 1958; also C. J. Maiden, "The Strain Rate Sensitivity of α -Uranium," J. Mech. Phys. Solids, Vol. 7, 1959.
23. F. E. Hauser, J. A. Simmons, and J. E. Dorn, "Strain Rate Effects in Plastic Wave Propagation," Proc. of Met. Society Conferences, Vol. 9, 1960.
24. E. D. H. Davies and S. C. Hunter, "The Dynamic Compression Testing of Solids by the Method of the Split Hopkinson Bar," J. Mech. Phys. of Solids, Vol. 11, 1963.
25. J. L. Chiddister and L. E. Malvern, "Compression-Impact Testing of Aluminum at Elevated Temperatures," Experimental Mechanics, Vol. 3, 1963.
26. C. H. Karnes and E. A. Ripperger, "Strain Rate Effect in Cold Worked High-Purity Aluminum," Jour. of Mech. and Physics of Solids, Vol. XIV, 1966.
27. C. J. Maiden and S. J. Green, "Compressive Strain-Rate Tests on Six Selected Materials at Strain Rates from 10^{-3} to 10^4 in./in./second," J. of Applied Mechanics, Vol. 33, Sept. 1966.
28. A. Hald, Statistical Theory with Engineering Applications, John Wiley and Sons, 1952.
29. A. H. Bowker and G. J. Lieberman, Engineering Statistics, Prentice-Hall, 1959.
30. D. L. Holt, S. G. Babcock, S. J. Green, and C. J. Maiden, "The Strain Rate Dependence of Flow Stress in Some Aluminum Alloys," A.S.M. Transaction Quarterly, Vol. 60, No. 2, June, 1967.
31. S. J. Green, S. G. Babcock, and C. J. Maiden, "Tensile and Compressive Strain Rate Tests on Aluminum and Aluminum Alloys from Rates of 10^{-3} in./in./sec. to 10^4 in./in./sec.," Proceedings of the Fifth U. S. National Congress of Applied Mechanics, ASME, June 1966 (Abstract only).
32. S. J. Green, S. G. Babcock, and C. J. Maiden, "High Temperature Compression Strain-Rate Tests on Six Engineering Materials," Presented at Annual SESA Conference, Pittsburg, Penn., November, 1966.

APPENDIX A
MATERIAL DESCRIPTION

The following is a description of the materials that were tested in this program:

1. Quartz Phenolic

This two-dimensional laminated composite material was made by Reflective Laminates Incorporated from J. P. Stevens Company Astro-quartz 581 fabric and Monsanto Chemical Company SC-1008 phenolic resin. The resin volume fraction was 31%, giving a material bulk density of 1.79 gm/cm^3 nominal.

2. Silica Phenolic

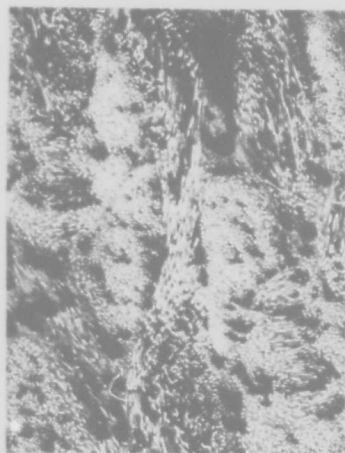
This two-dimensional laminated composite material was made by Reflective Laminates Incorporated from J. P. Stevens Company Astrosil 84 ultrapure fabric and Monsanto Chemical Company SC-1008 phenolic resin. Resin volume fraction was 37%, giving a bulk laminate density of 1.65 gm/cm^3 nominal.

3. Carbon Phenolic

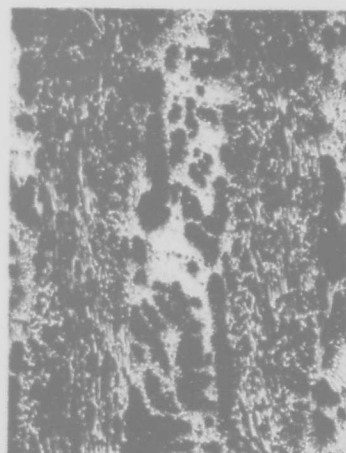
This material was manufactured by AVCO as RAD 6300 HP carbon phenolic. The component materials were 3M two-dimensional weave Pluton B-1 carbon fabric and Monsanto Chemical SC-1008 phenolic resin. Resin volume fraction was 50%, giving a nominal laminate bulk density of 1.40 gm/cm^3 .

This material is the same lot as that used in Reference 3. A new lot of the same material was purchased this year from Reflective Laminates Incorporated. Even though the same

specifications and processes were supposedly used by Reflective as were used by AVCO, the material received from Reflective did not meet the AVCO specifications. Laminate bulk density varied from 1.18 to 1.40 gm/cm³. Figure A-1 shows photomicrographs of several samples, including samples from AVCO, Reflective, and Fiberite Corporation, who supplied the prepreged material to Reflective. These photos clearly show that samples from Reflective and Fiberite contain large voids that are not present in the AVCO sample.



FIBERITE SAMPLE
(1.41 GM/CM³)
60X



PANEL NO. 3
(1.18 GM/CM³)
60X



PANEL NO. 4
(1.40 GM/CM³)
60X



LAST YEAR'S
AVCO MATERIAL
(1.41 GM/CM³)
60X

PHOTOMICROGRAPHS OF CARBON PHENOLIC

APPENDIX B
EQUIPMENT DESCRIPTION

INSTRON UNIVERSAL TESTING MACHINE

The Instron is a commercial testing machine (Figure B-1) with a screw-driven cross head. This machine is capable of performing quasistatic to medium strain-rate tests (10^{-5} to about 10^{-1} /sec) in either tension or compression. Maximum load capability is 20,000 lbs. Test temperatures may be varied from -250° to $+2000^{\circ}$ F.

MEDIUM STRAIN-RATE MACHINE

The Medium Strain-Rate Machine (Figure B-2) was developed at General Motors to enable the testing of various materials from ductile plastics to brittle ceramics as well as high-strength metals and composites. This device is similar in principle to machines developed by Clark and Wood⁽¹⁶⁾ and Campbell and Marsh⁽¹⁷⁾; however, the present device has undergone extensive modifications in order to improve the accuracy of the experimental techniques as well as to accommodate a wide variety of materials. Depending upon the size and strength of the specimen, strain rates from 10^{-3} to about 10^2 /second are achievable with this device. (References 2 and 26 discuss the above device in more detail than presented here.)

Basically, this medium rate machine is a gas operated device capable of either upward or downward piston motion for compression or tension testing, respectively. Gas is loaded at equal pressure into the upper and lower chambers, and upon initiation by a specially-designed fast-acting valve the gas



Figure B-1 Quasi-Static Testing Machine

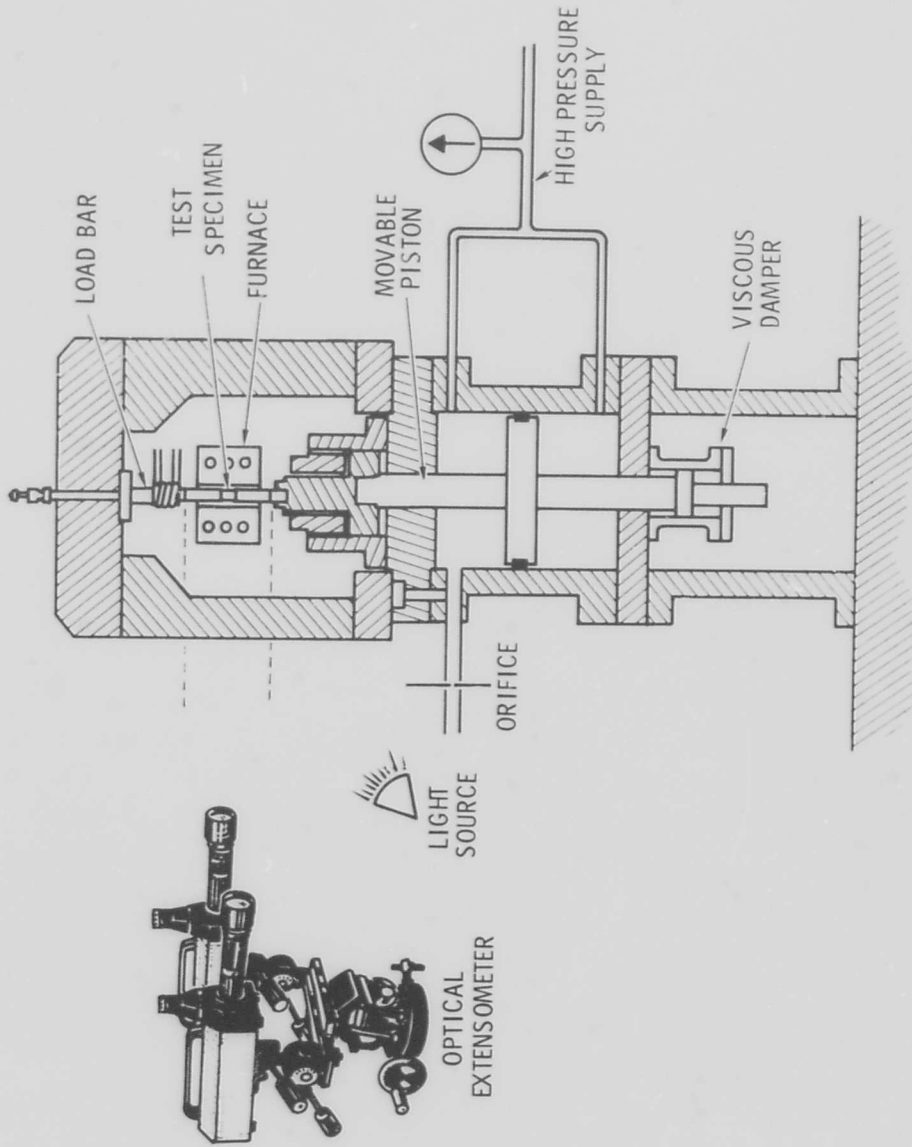


Figure B-2 Medium Strain-Rate Machine

is discharged from one chamber (dependent upon the desired direction of motion) through an orifice. Piston motion is determined by the type and pressure of the working gas, the size of the discharge orifice, and to some extent upon the specimen. Being designed as a constant strain-rate device, great care was taken to "stiffen" the machine. Cooper and Campbell⁽¹⁸⁾ discuss the requirement for a "stiff" machine in order to achieve constant strain rate. The total displacement of the piston (or strain in the specimen) is adjusted by a rigid stop arrangement on the top of the piston rod. This rigid stop was absolutely necessary in the preloading studies. Undesirable piston oscillations are damped by an adjustable viscous damper attached to the bottom of the piston rod.

Specimen load is measured by a calibrated load cell mounted directly above the specimen. Strain is determined by measuring piston displacement, by mounting strain gages on the specimen, or by using an optical extensometer. The Physitech* optical extensometer measures strain by dynamically tracking marks placed on the specimen well inside the gage section for tension specimens and on the load bars for compression specimens. At elevated temperatures a special reflective paint capable of withstanding 600°F without burning was used to mark the target.

The optics of the extensometer were improved in order to more accurately measure the very small strains (approximately 1%) encountered in testing some layup orientations of the fiber-reinforced composites. In conjunction with the

* Physitech Inc., Elkin Park, Pennsylvania

development of the high resolution optical system an improved mounting system was devised in order to reduce the mechanical "noise level" from extraneous random system vibrations. This system eliminated most of the noise which could not be filtered out electronically due to the frequency response requirements associated with high strain-rate testing.

Two system improvements were made for the room temperature work conducted in this study. First is the improved mounting system described above. Second is improved target lighting consisting of a special General Electric lamp (model 300 PAP) which reflects almost all infrared-frequency light allowing the target to remain cool during the test while providing sufficient illumination to use the extensometers.

Although tests at temperatures below 72°F may be conducted on this device, the present capabilities are restricted to the range of 72°F to 1000°F. Elevated temperatures are achieved with a three-zone quartz-lamp-powered radiant heat furnace, previously described, ⁽²⁾ which was modified to allow observation of the specimen with the optical extensometer by enlarging the furnace and installing a quartz viewing window.

HOPKINSON BAR DEVICE

To perform the high strain-rate tests ($5 \times 10^2 - 10^3$ /sec) a split-Hopkinson bar device is used. The compression device (Figure B-3) is similar to those used by Kolsky, ⁽¹⁹⁾ Campbell, and others ⁽²⁰⁻²⁶⁾. The tension device (Figure B-4) is the same in principle but not as straight forward in operation as the compression device.

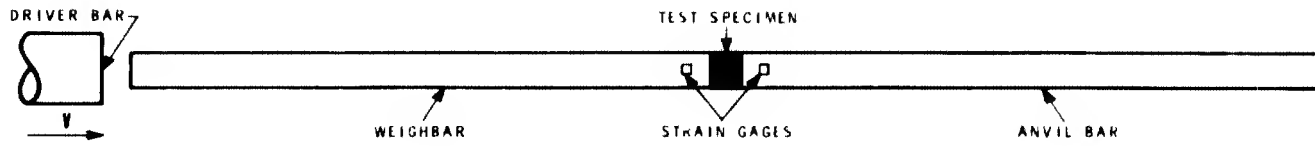


Figure B-3 Hopkinson Bar Setup

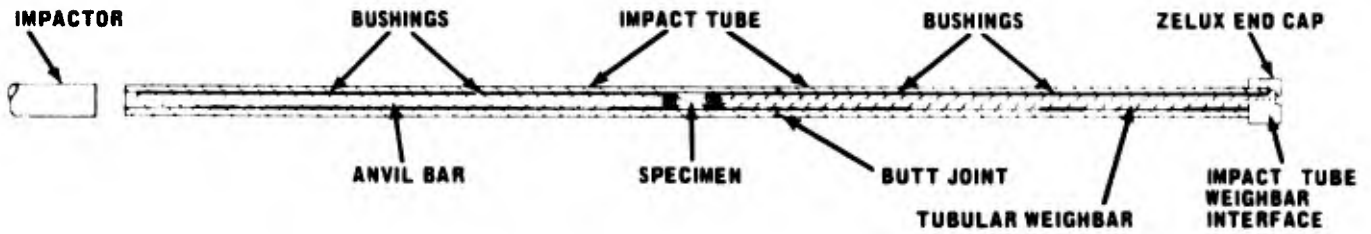


Figure B-4 Hopkinson Bar Tension Device

The operation of the Hopkinson bar technique is based upon the theory of one-dimensional elastic wave propagation. Using this theory, the deformation of a specimen sandwiched between two elastic bars and subjected to a stress wave may be calculated. For these devices stress waves are initiated by the impact of a driver bar, launched to velocity by a small gas gun, upon the "weighbar" in the compression device and the "impact tube" in the tension device. The specimen behavior is obtained by measuring the response of the load bars on both sides of the specimen and applying the one-dimensional elastic wave theory mentioned above. References 2 and 27 contain additional information on the compression technique and the wave analysis.

For elevated temperature compression operation, the device was modified to eliminate temperature gradients in the load bars. These gradients must be eliminated because they produce extraneous wave reflections, similar to those normally obtained at the specimen/bar interface, which cannot easily be accounted for in the data reduction.⁽²⁵⁾ Therefore, a technique was developed to bring a specimen up to temperature in a radiant-heat furnace, such as the one described for the medium strain-rate machine, with the load bars isolated outside the furnace. Once the test temperature is obtained, a pneumatically-operated device quickly moves the bars into contact with the specimen and triggers the acceleration of the driver bar down the launch tube to impact the "weighbar". The specimen is mounted in a firebrick sleeve which is aligned with the bars. The procedure eliminates any temperature increase at a distance of 0.050 inch from the specimen/bar interface for about 3 seconds - much longer than the time for the stress wave to be initiated and the 160 microsecond stress pulse to propagate through the specimen.

High strain rate tension results are obtained at room temperature on a newly-developed device also based on the Hopkinson bar principle (Figure B-4). The design of this device is completely discussed in Reference 4, although a short description of the operation of the device is included here. Because of the compactness and complicity of this device, the effects of temperature gradients could not be circumvented as for the compression device. Therefore, only room temperature testing is discussed. A tensile stress wave is generated in the weighbar by virtue of the free surface interface between the impact tube (carrying a compression wave generated by the driver bar impact) and the weighbar. Due to the area impedance mismatch of this free surface, only a portion of the compression wave is converted to a tension wave. The tension weighbar and anvil bars are mounted inside the annular impact tube. The "elastic" wave, i.e. the wave uneffected by the presence of the specimen, is measured with strain gages mounted near the front of the "weighbar" (very near the "weighbar"--impact tube interface). The behavior of both bars is determined from strain gages mounted close to the specimen-bar interfaces. From these three measurements and assuming one-dimensional wave theory, the stress-strain behavior of the specimen may be calculated as for the compression device. (27)

Special grips were designed to test the composite materials in this program. Basically, these grips consist of a tapered collet arrangement which grip the specimen with a mechanical interlock. Epoxy is used in place of the mechanical interlock for very weak materials. Metallic specimens for this device are simply of a threaded "dog bone" configuration. Due to the variation in specimen size between the

specimens tested at the high rates and those tested at the low and medium strain rates, the data appearing in the material characterization have been corrected for size effects.

APPENDIX C
STATISTICAL TREATMENT

To use the test results presented in this report for design purposes, a method had to be found to attach a level of reliability, or confidence, to the data. The method chosen represents the well known "standard normal" distribution, modified to account for the fact that the sample taken from the universe is very small (less than 30 samples). This modified distribution is called the "student t distribution." (28)

Mean curves were established for a given material at each average strain rate by taking several values of strain and computing the mean value of stress at each strain point by the following formula:

$$\bar{X} = \frac{\sum_{i=1}^n x_i}{n} \quad (C-1)$$

where: \bar{X} = mean value
 x_i = one value of stress at a given value of strain
 n = number of values of stress taken

The standard deviation of the sample points was calculated by the formula:

$$\sigma_x = \sqrt{\frac{n \sum_{i=1}^n x_i^2 - \left(\sum_{i=1}^n x_i \right)^2}{n(n-1)}} \quad (C-2)$$

To interpret the results of this statistical approach, a $1-2\alpha$ confidence level, or probability, was calculated using the following formula: (29)

$$\text{Confidence interval} = \bar{X} \pm t_{\alpha} \frac{\sigma_x}{\sqrt{n}} \quad (\text{C-3})$$

where: \bar{X} = mean value (stress)

σ_x = standard deviation

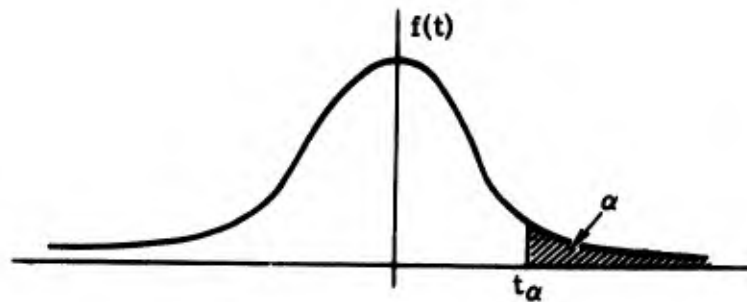
n = number of sample points (stress values)

t_a = a number taken from the student t distribution
(See Table C-I)

$$\text{Student t distribution} = f(t)c \left(1 + \frac{t^2}{v}\right)^{-\frac{(v+1)}{2}} \quad (\text{C-4})$$

where: c = constant

v = parameter called the degree of freedom of t
= $n-1$



Note that as v approaches infinity (>30), the "student t distribution" approaches the "standard normal distribution."

The significance of a confidence interval means simply that, on the average, the statement that \bar{X} will lie in the interval $\left[\bar{X} \pm t_{\alpha} \frac{\sigma_x}{\sqrt{n}}\right]$ will be correct $(1-2\alpha) \times 100$ percent of the time.

This means that "by chance" any other material of the same type as that tested will behave in the same manner. This confidence level accounts for the random errors encountered during the tests but not for predictable errors. As the number of samples of each material tested is increased, the confidence interval at one given confidence level will decrease.

TABLE C-I
"STUDENT T DISTRIBUTION"

v	t .100	t .050	t .025	t .010	t .005
1	3.078	6.314	12.706	31.021	63.657
2	1.886	2.920	4.303	6.965	9.985
3	1.638	2.353	3.182	4.541	5.851
4	1.533	2.132	2.776	3.747	4.604
5	1.476	2.015	2.571	3.365	4.032
6	1.440	1.943	2.447	3.143	3.707
7	1.415	1.895	2.365	2.998	3.499
8	1.397	1.860	2.306	2.896	3.355
9	1.383	1.833	2.262	2.821	3.250
10	1.372	1.812	2.228	2.764	3.169
11	1.363	1.796	2.201	2.718	3.106
12	1.356	1.782	2.179	2.681	3.055
13	1.350	1.771	2.160	2.650	3.012
14	1.345	1.761	2.145	2.624	2.977
15	1.341	1.753	2.131	2.602	2.947
16	1.337	1.746	2.120	2.583	2.921
17	1.333	1.740	2.110	2.567	2.898
18	1.330	1.734	2.101	2.552	2.878
19	1.328	1.729	2.093	2.539	2.861
20	1.325	1.725	2.086	2.528	2.845
21	1.323	1.721	2.080	2.518	2.831
22	1.321	1.717	2.074	2.508	2.819
23	1.319	1.714	2.069	2.500	2.807
24	1.318	1.711	2.064	2.492	2.797
25	1.316	1.708	2.060	2.485	2.787
26	1.315	1.706	2.056	2.479	2.779
27	1.314	1.703	2.052	2.473	2.771
28	1.313	1.701	2.048	2.467	2.763
29	1.311	1.699	2.045	2.462	2.756
Inf.	1.282	1.645	1.960	2.326	2.576

APPENDIX F

PRELIMINARY DATA ON TWO "3-D" QUARTZ ANTENNA-WINDOW MATERIALS

INTRODUCTION

This Appendix describes the test results for two (2) three dimensional weave reentry-vehicle antenna-window materials (developed under Air Force RESEP Task 6) and presents the results from room temperature uniaxial stress compression high strain-rate tests. The two materials tested in this program were as follows:

1. 3-D quartz/ethyl silicate binder
2. 3-D quartz/teflon binder

Approximately ten square inches of each material was supplied by Aeronutronics Division of Philco-Ford in the form of approximately 3 x 5 x 1/2 inch blocks. To perform initial tests, two blocks of each material were chosen at random from the delivered lots and 0.375 inch diameter by 0.500 inch long specimens were machined. Approximately ten specimens were machined, with axis parallel to the warp and fill directions, from each of the four blocks (80 total).

In the process of machining the compression specimens, the following observations were made:

1. Both the ethyl silicate blocks had dry porous areas near the center of the blocks. Figure D-1 is a photo of one of these blocks. Since machining time is quite expensive and several specimens had already been completed prior to discovering the porous areas, test specimens were taken from the least porous areas of each block.

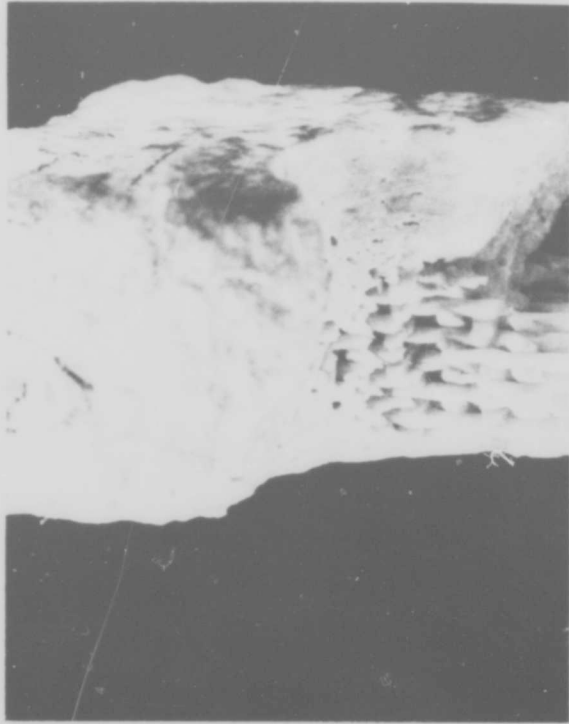


Figure D-1 Photograph of 3-D Quartz/Ethyl Silicate

2. When the teflon material was cut in the center, a dark spongy area was noticed. This dark area is caused by contamination left during the teflon impregnation cycles. Specimens were machined as far away from this dark area as possible.

The following is a discussion of the test results obtained on two materials.

EXPERIMENTAL RESULTS

3-D Quartz/Ethyl Silicate

Figure D-2 shows the results of room temperature uniaxial stress compression tests at strain rates from 10^{-3} to 10^3 /second. Two directions of loading are shown, parallel to the warp and parallel to the fill. Information noted on each curve includes block number, number of tests, strain rate, and maximum scatter in fracture stress and strain to fracture.

This material exhibits a large degree of scatter, more from block-to-block than within one block. It is extremely strain rate sensitive, exhibiting a 62% increase in fracture stress over six orders of magnitude of strain rate when loaded parallel to the fill and 100% increase in fracture stress when loaded parallel to the warp. Strain to fracture also shows strain rate dependence varying from 64% for loading parallel to the fill to 26% for loading parallel to the warp over six orders of magnitude of strain rate. Weight density measurements were made on all specimens, the average density being $1.75 \pm .05$ gm/cm³. No correlation was found between the density of the individual specimen and the observed test results.

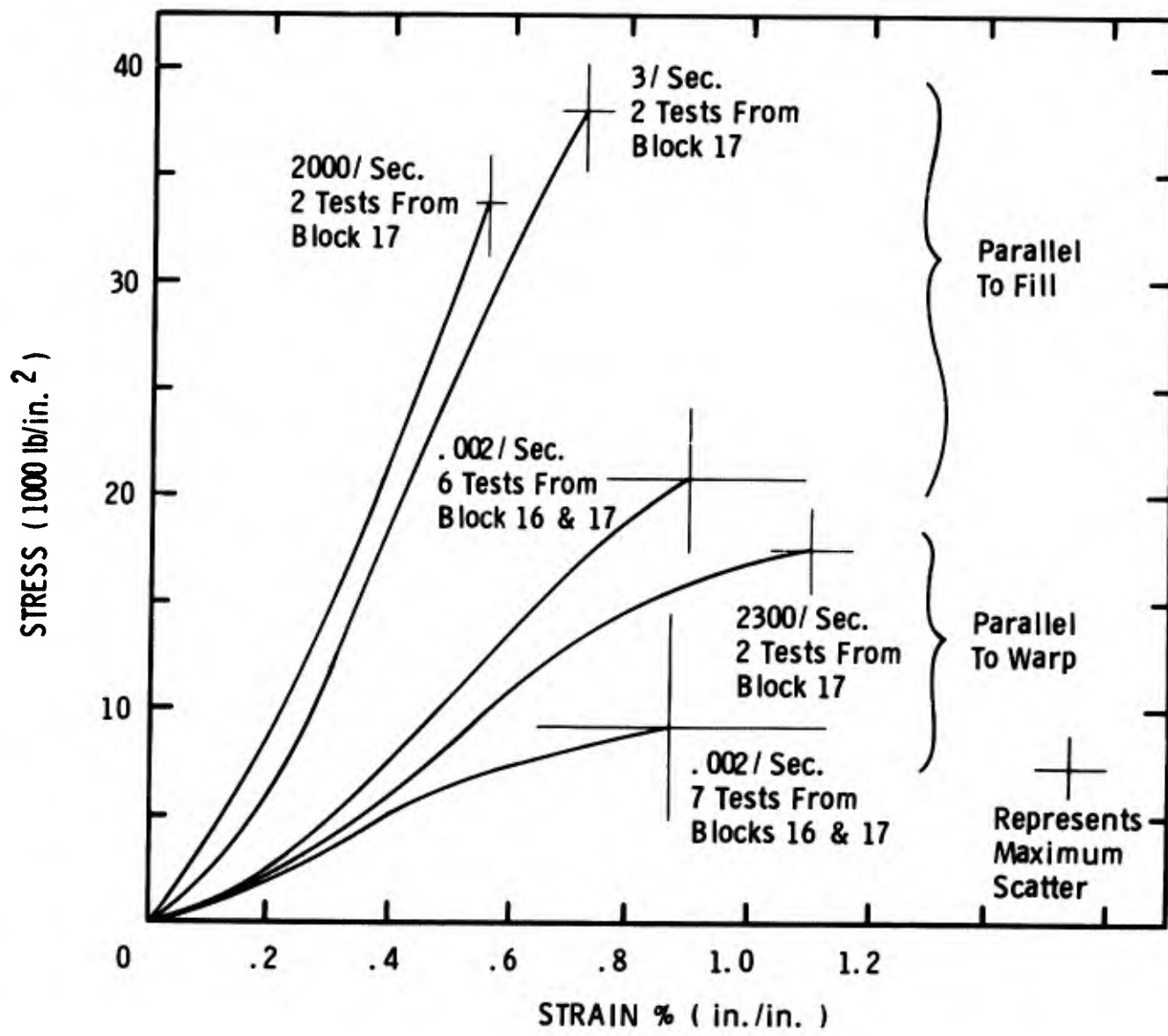


Figure D-2 Compression Tests on 3-D Quartz/Ethyl Silicate - 72°F

3-D Quartz/Teflon

Figure D-3 is the dynamic response of 3-D quartz/teflon under room temperature uniaxial stress compressive loading at rates from .001 to 12 in./in./second. Due to the dark spongy area mentioned in the introduction appearing on many of the test specimens, tests were performed on block 12 only. This block contained a small dark area, but specimens were machined as far from this area as possible. Density variations on this block were from 1.56 to 1.79 gm/cm³. The observed behavior of this material was interesting. When loaded parallel to the fill, the material behaved similar to that observed in some foams when loaded in compression. The stress-strain curves rise from zero up to about 1/2% strain and then fall to a steady stress level out to a strain beyond 10%. Although not shown in the figure, this material when loaded parallel to the fill just continued to crush with no noticeable cracking up to 60% strain. When loaded parallel to the warp, the stress-strain behavior is typically viscoelastic with no stress relaxation behavior found when loaded parallel to the fill. Initial modulus ranged from 3×10^5 psi when loaded parallel to the fill to 8×10^3 psi when loaded parallel to the warp at .001/sec. Some strain rate sensitivity was observed although only five orders of magnitude were covered. The stress-strain results obtained from the Hopkinson bar were questionable, therefore, no results are reported. Since this material is very porous and possesses a low speed of sound, typical of foam-like materials, uniform stress conditions in specimens with dimensions used for these experiments are not reached until the specimens have undergone several percent strain. Material scatter in the one block tested was very large and is noted in the figure.

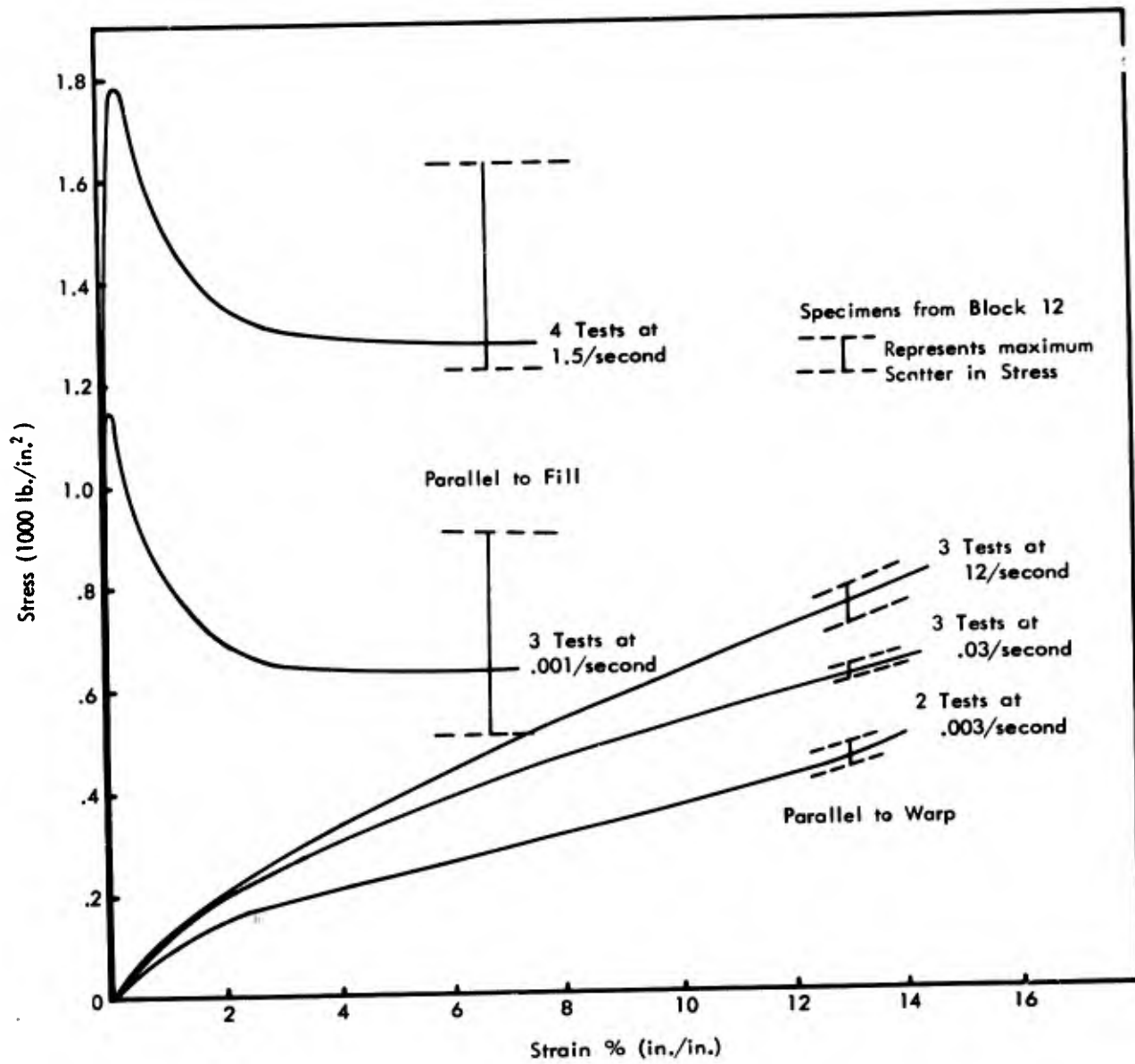


Figure D-3 Compression Tests on 3-D Quartz/Teflon - 72°F

DISCUSSION OF EXPERIMENTAL RESULTS

The two 3-D quartz fiber material test results show markedly different characteristics. Although these materials appeared to possess less than superior quality, the results do show general trends.

The observed anisotropy in both materials can be explained by observing the peculiar behavior of the quartz/teflon when loaded in compression parallel to the fill. The insertion of the fill fibers perpendicular to the warp fiber mats (see Figure D-4) is what makes the weave three dimensional. The initial stiffness of the composite is governed by the fill fibers. When the bond shear strength between the teflon matrix and the fill fibers is reached, slippage between the fill fibers and the matrix occurs causing the stress to relax while strain continues. The stress relaxation continues until the warp mats and matrix have compressed. Once the voids or gaps have been closed, the material continues to compress with a different modulus. The maximum strain before fracture is governed by the teflon matrix. Although no tests were conducted in tension, it is expected that the ultimate strain when loaded parallel to the fill would be governed by the fill fiber to teflon matrix bond shear strength. This strength should be considerably more than if the fill fibers were not present, which is the condition in a two-dimensional weave composite. In other words, the shear bond strength between the fill fibers and the matrix determines the ultimate strength in tension or compression when loaded parallel to the fill. This would be true for the ethyl silicate material also.

When loaded parallel to the warp, the fill fiber plays no role in the stiffness or fracture strength. Loading in this direction is similar to loading a two dimensional weave composite

where the fiber mats have been "nested" or oriented in the same direction and loading is at 45° to the fiber directions. The observed strain-rate sensitivity in both materials cannot be totally explained at the present time. There appears to be more sensitivity in stiffness when loaded parallel to the fill than when loaded parallel to the warp. This is not what might be expected since the fill fibers appear to govern the stiffness, and in general fibers do not exhibit strain-rate sensitivity. Therefore, a more complex interaction occurs between the fibers and matrix.

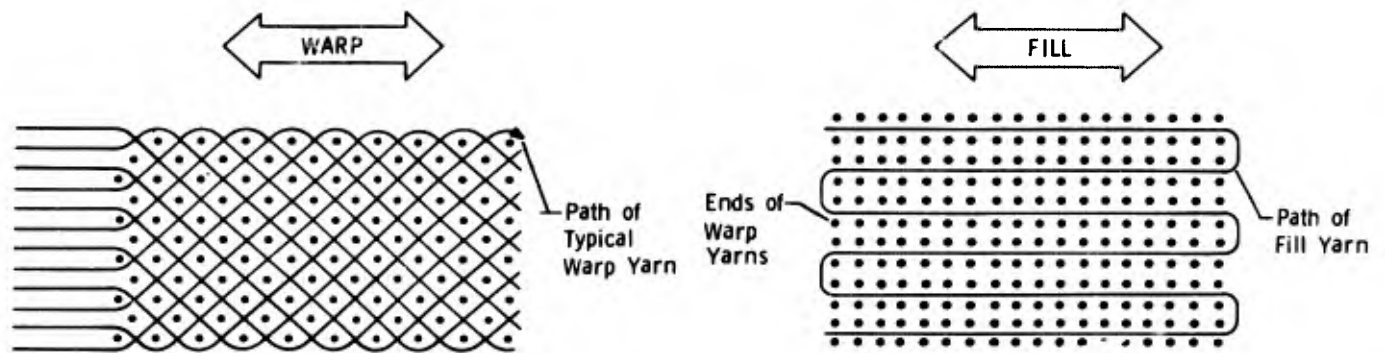


Figure D-4 Schematic of 3-D Weave

CONCLUSIONS

Both antenna-window materials exhibited strain rate sensitivity over five to six orders of magnitude strain rate depending on the direction of loading in compression under room temperature uniaxial stress. Large material scatter was observed due to the porosity and contamination found in the materials tested. While the 3-D quartz/ethyl silicate material initial modulus varied from about one to five million psi with strain to fracture from .55 to 1.1 percent, a .008 to .3 million psi initial modulus was observed on 3-D quartz/teflon with essentially no fracture up to 60% strain.

KEY WORDS	LINK A		LINK B		LINK C	
	ROLE	WT	ROLE	WT	ROLE	WT
Strain Rate Composites Quartz Phenolic Carbon Phenolic Silica Phenolic Anisotropy Size Effect Preshock Fracture Uniaxial Stress Layup Angle						

INSTRUCTIONS

1. **ORIGINATING ACTIVITY:** Enter the name and address of the contractor, subcontractor, grantee, Department of Defense activity or other organization (*corporate author*) issuing the report.

2a. **REPORT SECURITY CLASSIFICATION:** Enter the overall security classification of the report. Indicate whether "Restricted Data" is included. Marking is to be in accordance with appropriate security regulations.

2b. **GROUP:** Automatic downgrading is specified in DoD Directive 5200.10 and Armed Forces Industrial Manual. Enter the group number. Also, when applicable, show that optional markings have been used for Group 3 and Group 4 as authorized.

3. **REPORT TITLE:** Enter the complete report title in all capital letters. Titles in all cases should be unclassified. If a meaningful title cannot be selected without classification, show title classification in all capitals in parenthesis immediately following the title.

4. **DESCRIPTIVE NOTES:** If appropriate, enter the type of report, e.g., interim, progress, summary, annual, or final. Give the inclusive dates when a specific reporting period is covered.

5. **AUTHOR(S):** Enter the name(s) of author(s) as shown on or in the report. Enter last name, first name, middle initial. If military, show rank and branch of service. The name of the principal author is an absolute minimum requirement.

6. **REPORT DATE:** Enter the date of the report as day, month, year, or month, year. If more than one date appears on the report, use date of publication.

7a. **TOTAL NUMBER OF PAGES:** The total page count should follow normal pagination procedures, i.e., enter the number of pages containing information.

7b. **NUMBER OF REFERENCES:** Enter the total number of references cited in the report.

8a. **CONTRACT OR GRANT NUMBER:** If appropriate, enter the applicable number of the contract or grant under which the report was written.

8b, 8c, & 8d. **PROJECT NUMBER:** Enter the appropriate military department identification, such as project number, subproject number, system numbers, task number, etc.

9a. **ORIGINATOR'S REPORT NUMBER(S):** Enter the official report number by which the document will be identified and controlled by the originating activity. This number must be unique to this report.

9b. **OTHER REPORT NUMBER(S):** If the report has been assigned any other report numbers (*either by the originator or by the sponsor*), also enter this number(s).

10. **AVAILABILITY/LIMITATION NOTICES:** Enter any limitations on further dissemination of the report, other than those imposed by security classification, using standard statements such as:

- (1) "Qualified requesters may obtain copies of this report from DDC."
- (2) "Foreign announcement and dissemination of this report by DDC is not authorized."
- (3) "U. S. Government agencies may obtain copies of this report directly from DDC. Other qualified DDC users shall request through _____."
- (4) "U. S. military agencies may obtain copies of this report directly from DDC. Other qualified users shall request through _____."
- (5) "All distribution of this report is controlled. Qualified DDC users shall request through _____."

If the report has been furnished to the Office of Technical Services, Department of Commerce, for sale to the public, indicate this fact and enter the price, if known.

11. **SUPPLEMENTARY NOTES:** Use for additional explanatory notes.

12. **SPONSORING MILITARY ACTIVITY:** Enter the name of the departmental project office or laboratory sponsoring (*paying for*) the research and development. Include address.

13. **ABSTRACT:** Enter an abstract giving a brief and factual summary of the document indicative of the report, even though it may also appear elsewhere in the body of the technical report. If additional space is required, a continuation sheet shall be attached.

It is highly desirable that the abstract of classified reports be unclassified. Each paragraph of the abstract shall end with an indication of the military security classification of the information in the paragraph, represented as (TS), (S), (C), or (U).

There is no limitation on the length of the abstract. However, the suggested length is from 150 to 225 words.

14. **KEY WORDS:** Key words are technically meaningful terms or short phrases that characterize a report and may be used as index entries for cataloging the report. Key words must be selected so that no security classification is required. Identifiers, such as equipment model designation, trade name, military project code name, geographic location, may be used as key words but will be followed by an indication of technical context. The assignment of links, rules, and weights is optional.